

NASA CR-185238

LEWIS
GRANT
INT 33



279013
928

HOLLOW CATHODE OPERATION AT HIGH DISCHARGE CURRENTS

Prepared for
LEWIS RESEARCH CENTER
NATIONAL AERONAUTICS AND SPACE ADMINISTRATION
Grant NGR-06-002-112

by

Verlin Joe Friedly

April 1990

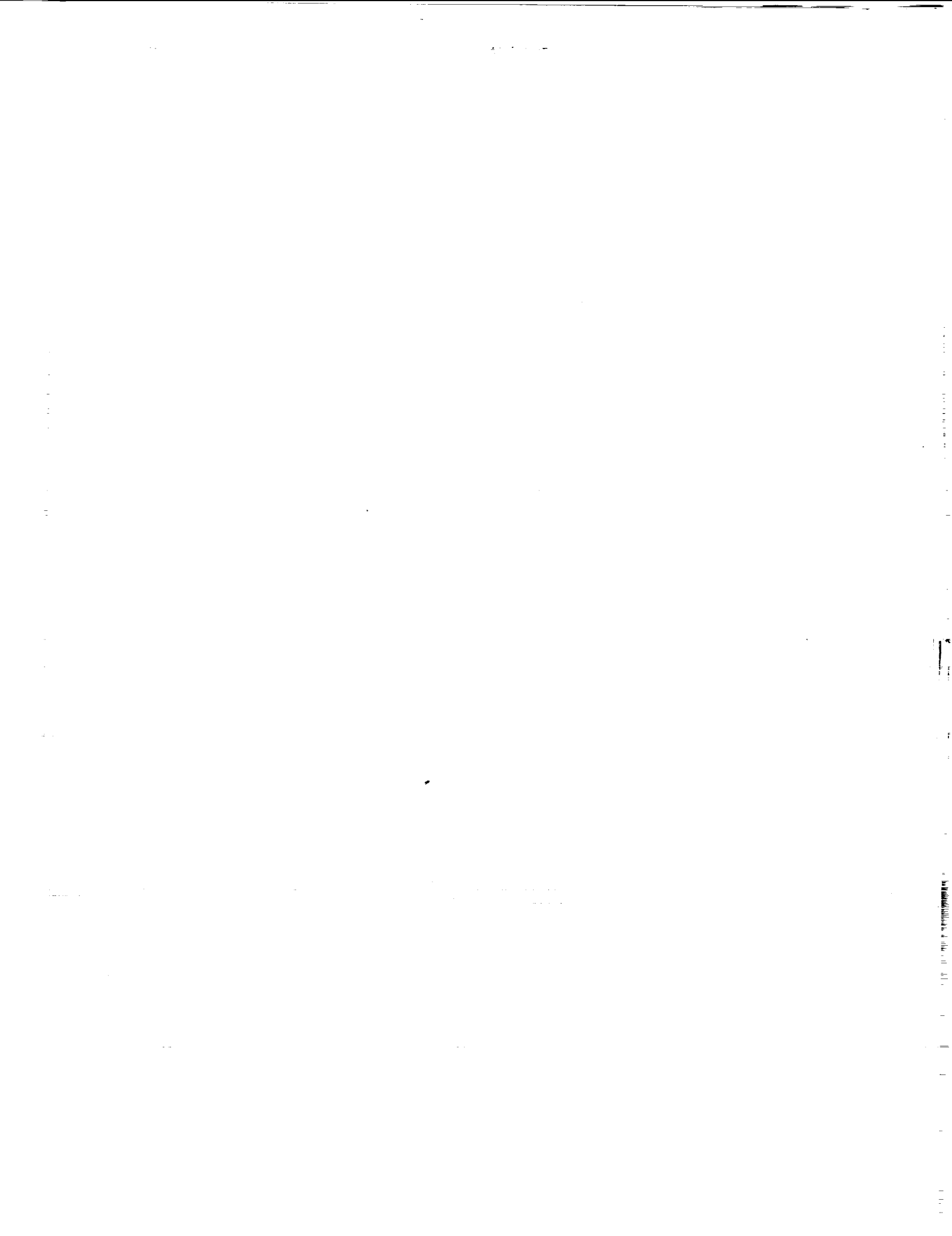
Approved by

Paul J. Wilbur
Department of Mechanical Engineering
Colorado State University
Fort Collins, Colorado 80523

(NASA-CR-185238) HOLLOW CATHODE OPERATION
AT HIGH DISCHARGE CURRENTS M.S. Thesis
(Colorado State Univ.) 92 p CSCL 09A

N90-21953

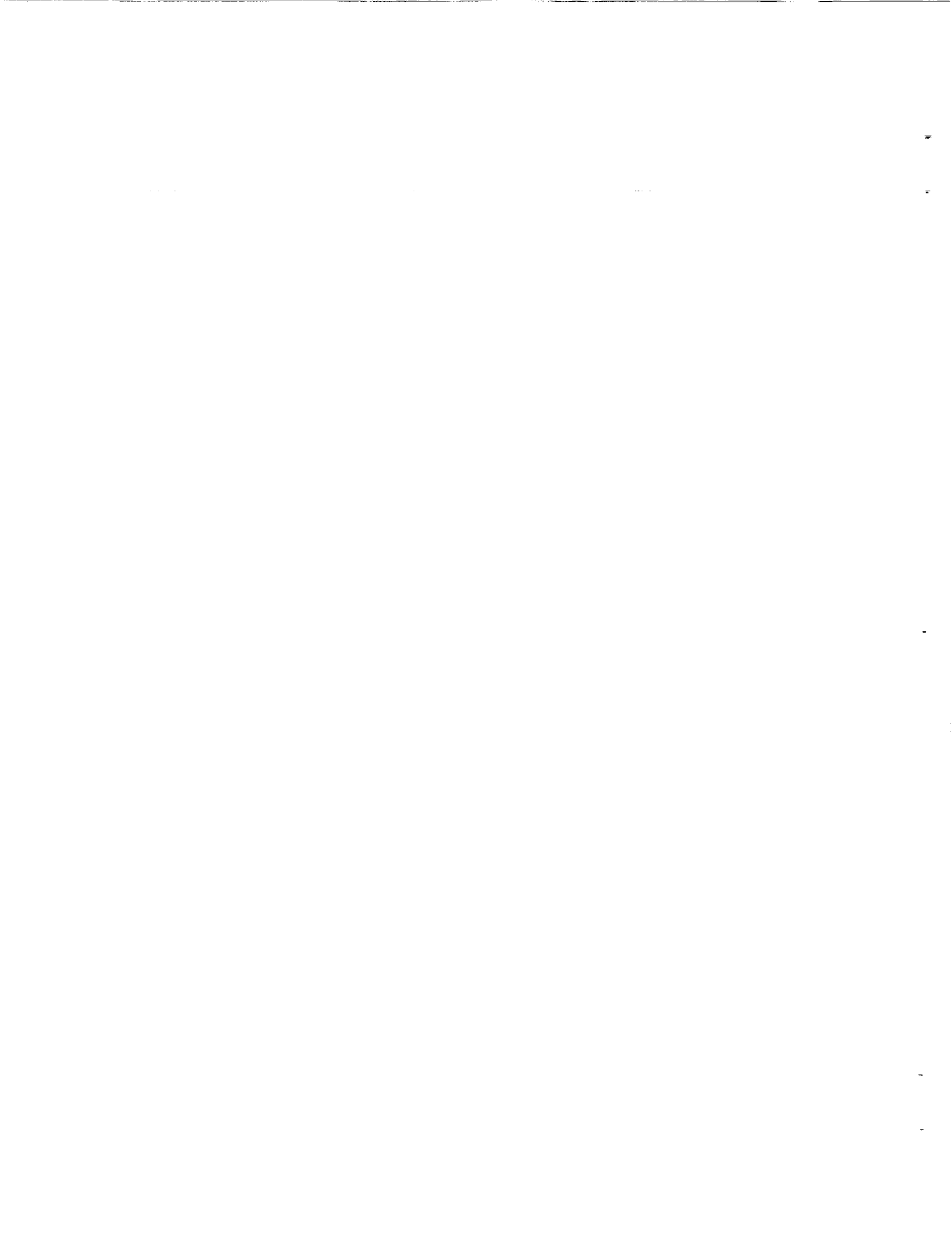
Unclas
G3/33 0279013



1. Report No. NASA CR-185238		2. Government Accession No.		3. Recipient's Catalog No.	
4. Title and Subtitle HOLLOW CATHODE OPERATION AT HIGH DISCHARGE CURRENTS				5. Report Date April 1990	
				6. Performing Organization Code	
7. Author(s) Verlin Joe Friedly				8. Performing Organization Report No.	
				10. Work Unit No.	
9. Performing Organization Name and Address Department of Mechanical Engineering Colorado State University Fort Collins, CO 80523				11. Contract or Grant No. NGR-06-002-112	
				13. Type of Report and Period Covered	
12. Sponsoring Agency Name and Address National Aeronautics and Space Administration Washington, D.C. 20546				14. Sponsoring Agency Code	
15. Supplementary Notes Grant Monitor - Vincent K. Rawlin, NASA Lewis Research Center, Cleveland, OH 44135 This report is a reproduction of the M.S. Thesis of Verlin Friedly. It is submitted to the sponsor and the distribution list in this form both as a presentation of the technical material and as an indication of the academic program supported by the grant.					
16. Abstract It has been shown that ion thruster hollow cathode operation at high discharge current levels can induce reduced thruster lifetimes by causing cathode insert overheating and/or erosion of surfaces located downstream of the cathode. The erosion problem has been particularly baffling because the mechanism by which it occurs has not been understood. The experimental investigation described herein reveals the energies of ions produced close to the cathode orifice can be several times the anode-to-cathode potential difference generally considered available to accelerate them. These energies (of order 50 eV) are sufficient to cause the observed erosion rates. The effects of discharge current (to 60 A), magnetic field configuration and the cathode flowrate, orifice diameter and insert design on the energies and current densities of these jet ions are examined. A model describing the mechanism by which the high energy ions could be produced when the anode-to-cathode potential difference is insufficient is proposed. The effects of discharge current on cathode temperature and internal pressure are also examined experimentally and described phenomenologically.					
17. Key Words (Suggested by Author(s)) Electrostatic Ion Thruster Hollow Cathode			18. Distribution Statement Unclassified - Unlimited		
19. Security Classif. (of this report) Unclassified		20. Security Classif. (of this page) Unclassified		21. No of pages 91	22. Price*

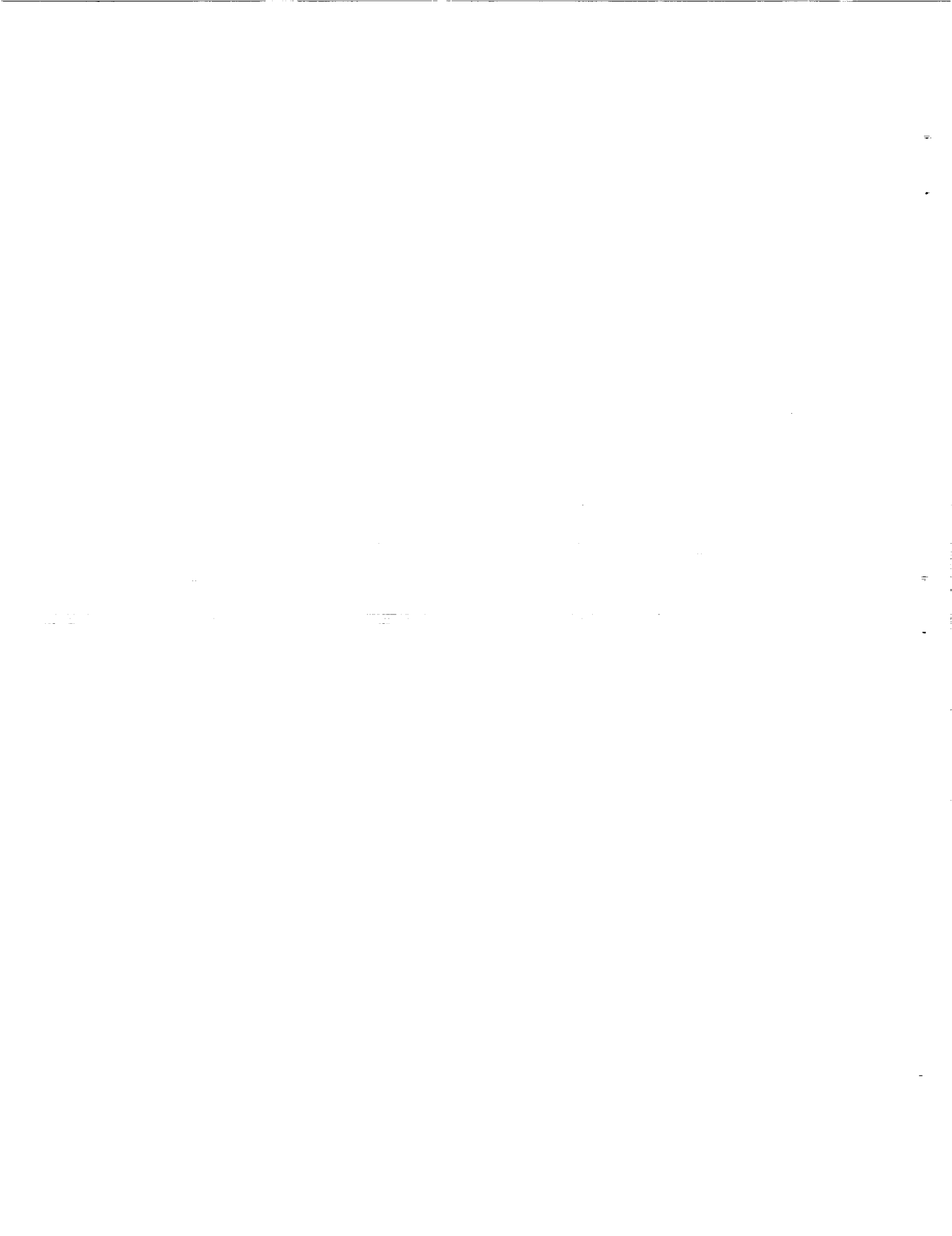
TABLE OF CONTENTS

	<u>Page</u>
I. INTRODUCTION	1
II. APPARATUS AND PROCEDURE	7
Magnetic Field Control	12
Typical Operating Procedure	12
Plasma Property Measurements	14
Measurement of the Spatial Distribution of High Energy Electrons	16
Measurement of the Characteristics of Ions	16
Erosion Testing	25
III. RESULTS	26
Basic Energy Considerations	28
Visual and Random Electron Current Density Observations .	32
Downstream Plasma Properties	37
Direct Measurements of Ion Energy Characteristics	41
Effect of the Cathode Insert	51
Effects of the Ambient Magnetic Field	57
Plasma Noise Considerations	63
Temperature Effects	64
Flowrate/Pressure Correlation Study	67
IV. THEORY	74
A Model of High Energy Ion Creation	74
Orifice Pressure Drop Considerations	77
V. CONCLUSIONS	79
VI. REFERENCES	81
APPENDIX A: Analysis of Retarding Potential Analyzer Data ..	83



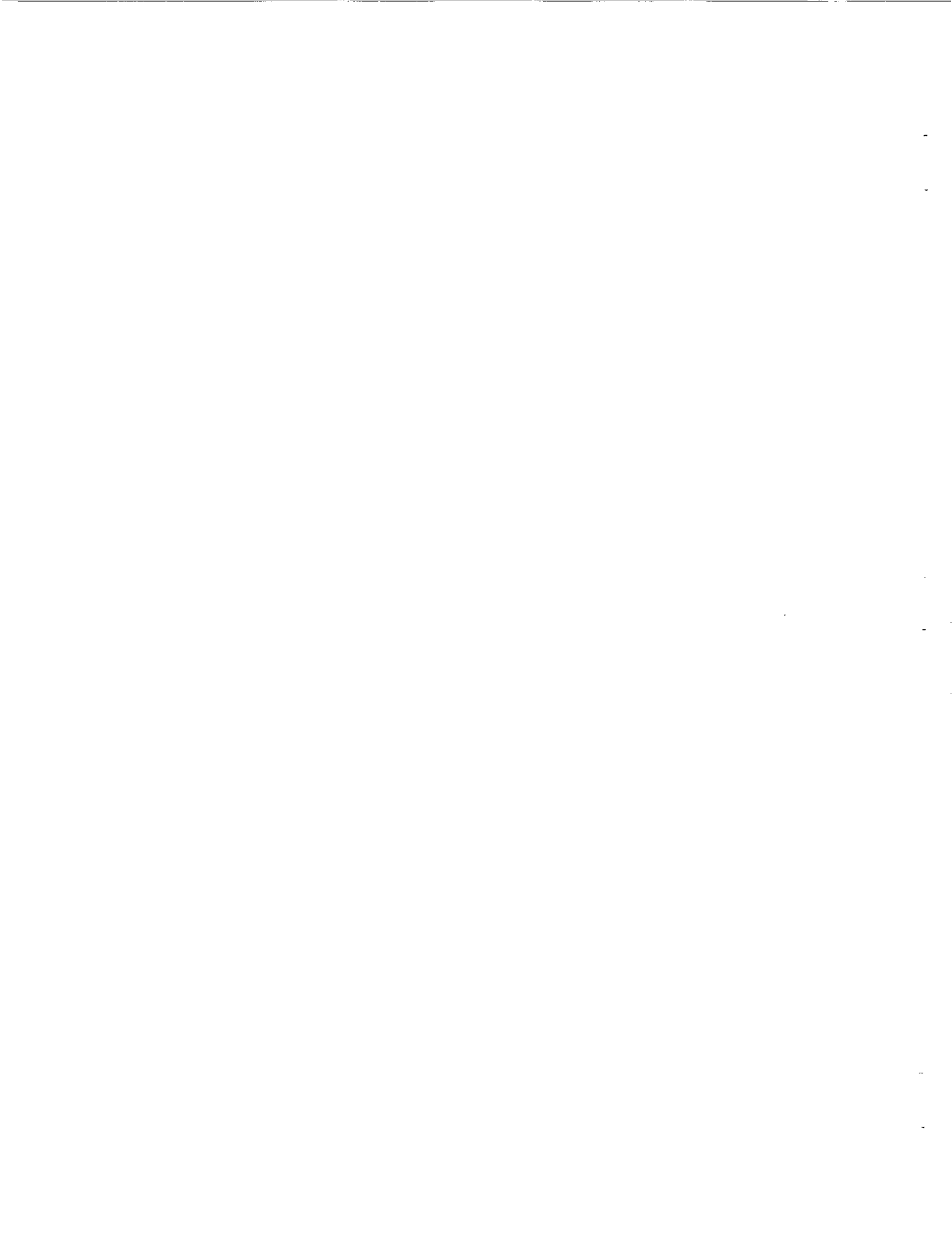
LIST OF FIGURES

<u>Figure</u>	<u>Title</u>	<u>Page</u>
1	Hollow Cathode Schematic showing Keeper and Anode	2
2	Hollow Cathode Test Apparatus	9
3	Magnetic Flux Density Profiles Induced by Solenoid along the Cathode Centerline	13
4	Retarding Potential Analyzer	18
5	Typical RPA Trace Sensed Downstream of a Hollow Cathode	20
6	Data from a Typical RPA Trace	22
7	Centerline Erosion Rate Profile	27
8	Effect of Propellant Flowrate on Discharge and Keeper Voltages	30
9	Effect of Discharge Current on Discharge and Keeper Voltages with Orifice Diameter as a Parameter ..	31
10	Hollow Cathode Operating at 60 A Discharge Current in Nulled Magnetic Field Environment	33
11	Constant Current Density Contours Associated with High Energy Electrons at 60 A Discharge Current	35
12	High Discharge Current Electron Jet in 0.4 G Transverse Magnetic Field	36
13	Effect of Discharge Current on Constant Current Density Contours Associated with High Energy Electrons	38
14	Effect of Discharge Current on Centerline Plasma Property Profiles	39
15	Effect of Discharge Current on Centerline RPA Data	42
16	The Effect of a Shield Obscuring the Orifice of an Operating Hollow Cathode from the RPA	44
17	Effect of RPA Axial Position on its Output Trace	45
18	Effects of Discharge Current and Flowrate on the Energy Characteristics of Jet Ions	47
19	Effects of Discharge Current and Flowrate on the Current Density of Jet Ions	48



List of Figures (continued)

<u>Figure</u>	<u>Title</u>	<u>Page</u>
20	Effects of Flowrate and Orifice Diameter on the Energy Characteristics of Jet Ions	49
21	Effect of Keeper Position on Jet Ion Current Density ..	52
22	Effect of Insert Type on Current/Voltage Characteristics	53
23	Effect of Insert Type on Plasma Property Profiles	54
24	Effect of Insert Type on Energy Characteristics of Jet Ions	55
25	Effect of Insert Type on Jet Ion Current Density Data .	56
26	Effect of Magnetic Field Environment on the Properties of the Plasma Downstream of a Cathode	58
27	Effect of Magnetic Field Environment on the Energy Characteristics of Jet Ions.....	60
28	Effect of Magnetic Field Environment on Jet Ion Current Density Data	61
29	Effect of Magnetic Field Environment on the Jet-to-Total Ion Current Density Ratio	62
30	Effects of Discharge Current and Cathode Configuration on Cathode Wall Temperature	65
31	Effect of Orifice Diameter on Cathode Wall Temperature	66
32	Effect of Insert Type on Cathode Wall Temperature	68
33	Effects of Discharge Current and Propellant Flowrate on Cathode Internal Pressure	69
34	Effect of Cathode Orifice Diameter on Normalized Pressure Parameter Data	73
35	Conceptual Model of Jet Ion Production	75



I. INTRODUCTION

Hollow cathodes serve as electron sources in a variety of applications. In an ion thruster, for example, one is typically used to supply the electrons that bombard propellant atoms and produce ions and another supplies the electrons that neutralize the charge and current associated with the extraction of these ions into a thrust-inducing beam [1]. Since hollow cathodes actually produce both ions and electrons, they have also been used as simple plasma sources. For example, they have been proposed as plasma sources suitable to establish electrical contact between an object in space and the ambient space plasma, thereby preventing undesirable spacecraft charging events [2]. The work described in this thesis is directed at understanding phenomena that have been observed by researchers using hollow cathodes as the electron sources that supply ionizing electrons within ion thrusters, but the results observed and conclusions reached are considered to be applicable to hollow cathodes in general.

This work will focus on orificed hollow cathodes [3] having the basic features shown in the schematic diagram of Figure 1. As the figure suggests, the cathode consists of a refractory metal tube and an orifice plate electron-beam welded together. The low work function insert shown within this assembly serves as the surface from which electrons are emitted--its low work function character facilitates substantial emission at reasonably low insert surface temperatures. The resistive heater shown is used to heat the insert via the cathode tube to the point where it can begin to emit electrons thermionically.

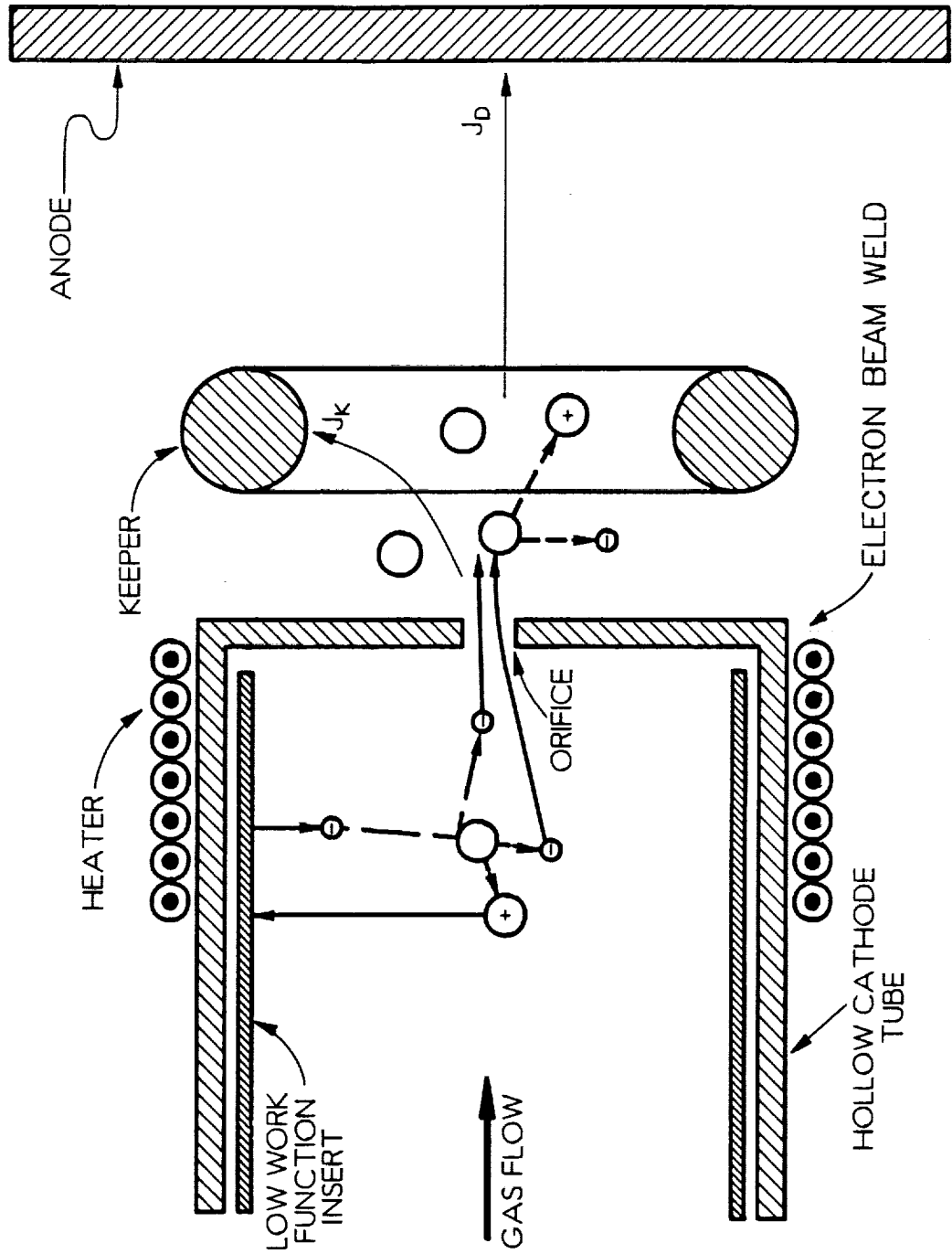


Fig. 1 Hollow Cathode Schematic showing Keeper and Anode

The keeper and anode shown downstream of the cathode are actually both anodes. The keeper is typically biased at a high positive potential (of order 100 V) to facilitate an initial, significant current flow to the keeper and the generation of a plasma within and downstream of the cathode (initiation of the cathode discharge). After the cathode discharge is initiated, the keeper voltage drops and is then adjusted to establish a modest keeper current (typically < 1 A). This current helps to sustain a plasma discharge under conditions where plasma-induced voltage fluctuations might otherwise cause it to extinguish. The electrode designated the "anode" in Fig. 1 collects the "discharge current" (J_D) which is substantially greater than the keeper current (J_K). The keeper and anode (or discharge) voltages (V_K and V_D) are both measured relative to cathode potential.

Hollow cathode discharges are initiated by flowing a neutral gas (propellant) through a heated cathode while applying a high keeper voltage. Electrons are emitted thermionically from the insert during the early phases of discharge initiation, and these electrons are typically accelerated to kinetic energies that are sufficient to induce propellant ionization and hence the generation of a high density plasma within the cathode tube. Once this plasma forms, its potential becomes quite uniform at values of order 10 V positive of the cathode except at sheaths that form at the plasma/cathode and plasma/insert boundaries. Strong electric fields exist in these sheaths and the ones at the plasma/insert interface facilitate field-enhancement of the thermionic electron emission process [4]. Under this condition, electrons emitted from the insert gain the energy they need to continue to ionize propellant gas as they pass through the sheath located there. Both the emitted and ionization-produced

electrons will, in the potential environment of the cathode plasma, find it difficult to reach a cathode potential surface. They will, therefore, tend to flow through the cathode orifice possibly inducing additional ionization downstream of it, but eventually being collected at the keeper or anode shown in Fig. 1.

The ions that are created inside the hollow cathode will, on the other hand, tend to flow toward the cathode and insert surfaces because these surfaces are at a potential below that of the plasma. The ions will collide with these surfaces and give up their kinetic and ionization energies to them. The ion heating power associated with this process will typically be sufficiently large so the resistive heater power can be reduced (possibly to zero) and field-enhanced thermionic electron emission will continue to occur.

Early ion thruster applications of hollow cathodes [5] involved electron emission currents of order 10 A or less. Cathodes operating at these current levels were studied by Siegfried [4,6] and models describing their operation were proposed and verified experimentally. Since his work was completed, discharge chamber powers and electron emission current requirements have grown as efforts to extract greater beam currents and produce greater thrust levels from single thrusters have been pursued [7]. Future applications that involve still greater discharge powers and electron emission current levels are being considered [8]. Preliminary tests conducted at these higher current levels have suggested that phenomena not observed in previous cathode tests become important as discharge current is increased [9]. The objective of the research described in this thesis has been to investigate hollow cathode operation at discharge currents extending to ~60 A and to identify phenomena that become increasingly important

as discharge current is increased. These phenomena have been examined within the context of the model proposed by Siegfried [4] in an effort to evolve a comprehensive theory of hollow cathode operation.

The low discharge current cathode tests conducted by Siegfried focused primarily on phenomena that occur upstream of the cathode orifice plate. Initially, it was hoped this study could involve phenomena occurring both upstream and downstream of the orifice plate. It was found, however, that the plasma environment upstream of the orifice plate was so hostile at high discharge currents that probes placed in it failed before useful data could be collected. Consequently, the research was focused on phenomena occurring downstream of the orifice, particularly those that could limit the lifetimes of various thruster components including that of the cathode itself.

Long thruster component lifetimes (on the order of 10,000 hr) are required to accomplish typical space propulsion missions because ion thrusters tend to operate at low thrust levels. Over such time intervals, even components in thrusters that operate at low discharge currents have shown substantial erosion. For example, severe erosion of the cathode and cathode potential components located downstream of it were observed during ~10,000 hr life tests of the J-series 30 cm and 5 cm dia mercury ion thrusters [10-12]. This erosion in turn resulted in both performance changes and the formation of metallic flakes that could under some conditions become detached and cause electrical shorts.

More recently, Rawlin [9] increased the discharge current of the J-series thruster from 15 to 35 A and operated it on xenon rather than mercury; he observed a substantial increase in component erosion

rates. For example, a tantalum baffle located between the keeper and the anode was observed to erode at rates as high as $0.9 \mu\text{m/hr}$. Rawlin observed a reduction in erosion rates as the cathode orifice diameter was increased [9] and these tests as well as ones conducted at even higher currents by Brophy and Garner [13] indicated it was probably the increase in discharge current rather than the propellant change that caused the increased erosion rates. A mechanism by which this erosion could be occurring was, however, not apparent. It had been suggested that such erosion could be caused by doubly charged ions striking cathode potential surfaces at twice the energy of singly charged ones [11], but substantial doubly charged ion concentrations were not expected near these components.

Although erosion-limited lifetime phenomena represent a major focus of this thesis, two other effects that can affect cathode lifetime were also investigated. One concerns the operating temperature of a hollow cathode. If the insert temperature increases above $-1200 \text{ }^\circ\text{C}$ [14] the low work function material applied to it begins to migrate at a rate that can cause it to deplete to the point where still higher temperatures will be required to induce the desired emission current. Eventually, this sequence of events can cause an increase in the plasma potential within the cathode and a degradation in cathode performance.

The final effect investigated is related to the cathode interior pressure. If it becomes excessive, the regions of electron emission and ion-induced heating of the insert become too localized. Under this condition, low work function material migration and subsequent insert performance degradation can also occur.

In an effort to gain additional understanding of high-current hollow cathode operation and address the areas of concern identified in the preceding paragraphs, tests were conducted on hollow cathodes of standard design [3]. The operating characteristics of these cathodes, the erosion rates induced on surfaces located downstream of them and the nature of the plasma created in this downstream region were measured. The effects of discharge current (up to 60 A), gas flowrate and cathode geometrical factors on cathode performance and downstream plasma conditions were measured and interpreted. These data will be presented and elementary models illustrating the physical mechanisms believed to induce observed phenomena will be proposed in this thesis.

II. APPARATUS AND PROCEDURE

The schematic diagram in Fig. 2 illustrates the test apparatus used to conduct the experiments described herein. The configuration shown was selected to model configurations typical of ion thruster discharge chambers that utilize hollow cathodes, although the tests were conducted in a 30 cm dia by 45 cm glass vacuum bell jar. Most of the hollow cathodes used for these tests were constructed using a 6.4 mm outside diameter, tantalum tube with a thoriated tungsten orifice plate electron beam welded to one end. One cathode was constructed from the same materials using a 12.8 mm outside diameter tube. The cathode orifices and orifice plates used, which were all different, were configured as shown in Table 1.

Table 1. Hollow Cathode Test Configurations

Minimum Orifice Diameter [d _o]	Orifice Bore Configuration	Maximum Outside Diameter	Cathode Tube Diameter
0.74 mm	chamfered	6.4 mm	6.4 mm
0.82	chamfered	16.8	6.4
0.99	straight	6.4	6.4
1.27	straight	12.8	12.8
1.70	straight	6.4	6.4

Because each cathode has a different orifice diameter, this diameter will be used to identify the particular cathode being used in a test. The chamfered orifices had their minimum diameters upstream and they were chamfered at an angle of about 45°. It should be noted that the

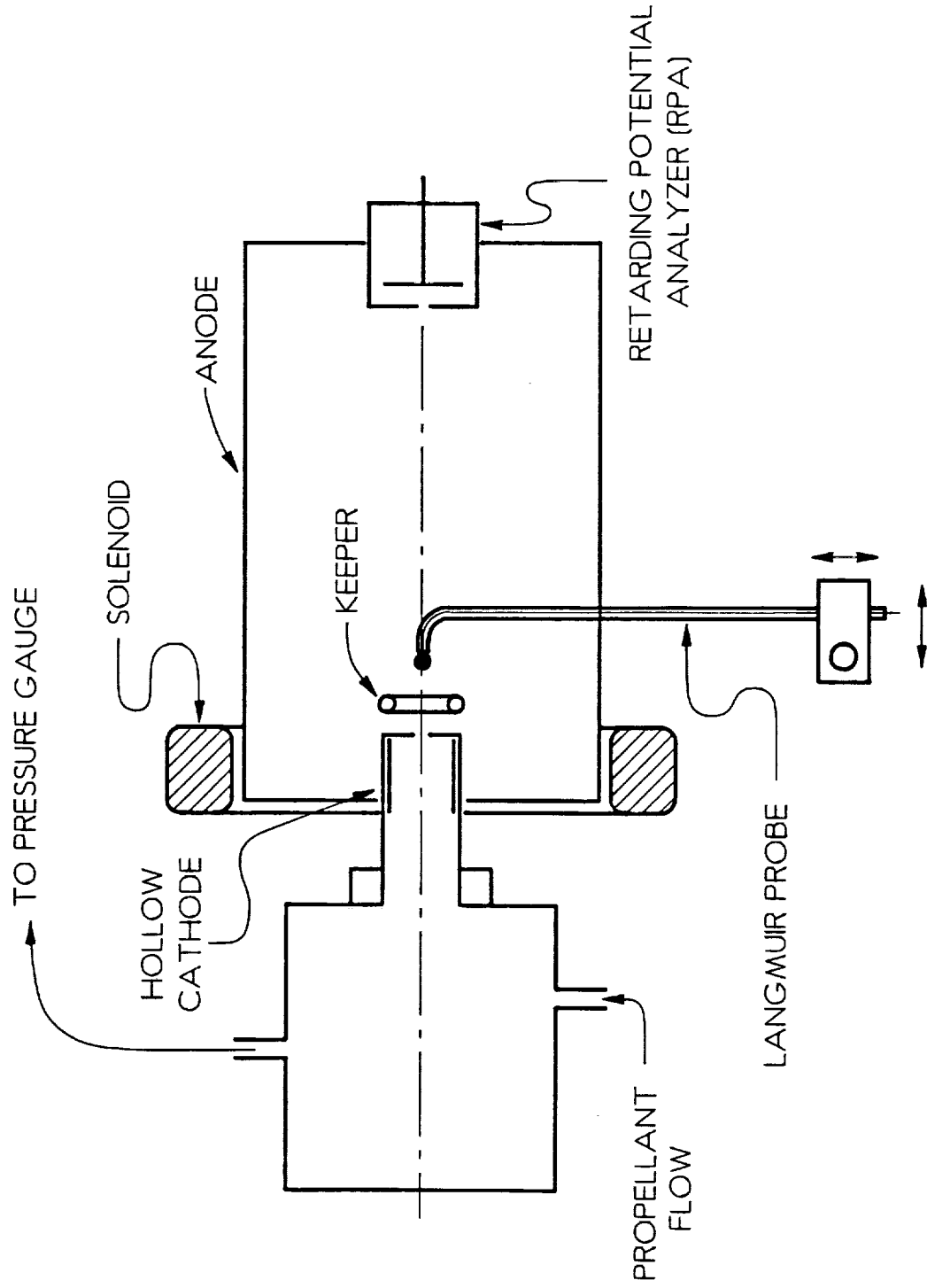


Fig. 2 Hollow Cathode Test Apparatus

fin that extended beyond the tube was welded to the second cathode identified above. This fin provided additional thermal radiation surface area and served to cool the cathode.

The inserts (low work function electron emitters) used during the tests, were generally constructed from four tight wraps of 0.03 mm thick tantalum foil rolled into a 13 mm long cylinder with an inner diameter of 4.7 mm (for the 6.4 mm dia. cathode tubes) or 10.7 mm (for the 12.8 mm dia. cathode tube). This cylinder was spot welded to two 0.25 mm thick, 2 mm wide tantalum ribbons. The rolled foil cylinders were coated with Chemical R-500¹ after fabrication so they would have a low work function. Each insert was placed into its cathode tube, next to the orifice plate, and the tantalum ribbons were spot-welded to the tube so good mechanical and electrical connection between the tube and insert could be assured. In one test series, which will be clearly identified, a barium aluminate impregnated, sintered tungsten insert like those used in most ion thruster applications was installed so performance comparisons could be made between the two types of inserts.

The hollow, cylindrical copper anode shown in Fig. 2 was 1.7 mm thick, 100 mm in length and 64 mm in dia. It had a 25 mm wide slot in one side to facilitate probing and visual observation of the plasma within it. The anode was water cooled so it would not melt at high discharge current levels. A tantalum torus, positioned 1 mm downstream of the cathode orifice plate with a 1.5 mm minor diameter

¹Chemical R-500 is a double carbonate (BaCO_3 , SrCO_3) mixture that has been manufactured by the J. R. Baker Chemical Co., Phillipsburg, NJ, but is no longer being made.

and a 5 mm major diameter, was used as the keeper electrode. The axes of the cathode, anode and keeper were all colinear. A swaged, resistive heater covered with a tantalum foil radiation shield was placed on the cathode at the location of the insert.

Two 35 A, 60 V DC power supplies, connected in parallel so a 60 A discharge current could be supplied, were used to bias the anode. These high quality power supplies with SCR voltage pre-regulation and series-pass, transistorized current-regulated outputs were used because they operate stably when they are driving a plasma discharge (noisy) load. A 2 A, 160 V DC power supply was used to bias the keeper. Its 160 V output voltage was generally sufficient to initiate the keeper discharge once the proper conditions of cathode temperature and propellant flow had been established. A 10 A, 20 V AC supply was used to power the cathode heater. All power supply biases were established and potentials were measured with respect to cathode potential. The cathode itself was allowed to float with respect to earth ground so discharges to grounded surfaces within the vacuum chamber would be eliminated.

Tests were conducted by first evacuating the vacuum chamber to $\sim 3 \times 10^{-5}$ Torr. The cathode was heated with the resistive heater for 30 to 60 minutes before the 160 V startup voltage was applied to the keeper. The keeper discharge was then started by briefly admitting the xenon gas, used for all tests, through the cathode at a rate that ranged as high as 12 sccm but was generally ~ 5 sccm. Once the discharge had started the flow was reduced and the anode voltage was increased until a discharge (anode) current of ~ 5 A was established. The keeper supply was then reduced to ~ 0.5 A and the heater was turned off. The discharge was allowed to stabilize for ~ 1 hr before tests

were conducted. During typical tests, the bell jar (ambient) pressure was on the order of 10^{-3} Torr. This pressure is probably somewhat higher than typical ion thruster discharge chamber pressures, but may be close to values observed in the keeper discharge region of a cathode that employs a baffle.

Magnetic Field Control

The magnetic environment near a hollow cathode might be expected to influence its performance, so this environmental factor was controlled during the conduct of the tests. If a magnetic field was not applied, an ambient magnetic field of ~ 0.4 gauss transverse to the cathode centerline was present (transverse field case). This field could be nulled out by positioning a magnet outside of the bell jar (null field case). In addition, an axial magnetic field could be applied using the 7.5 cm dia solenoid shown in Fig. 2. Two solenoidal fields having the centerline flux density profiles shown in Fig. 3 were applied in this study. These profiles, which were measured using a gaussmeter, are designated by the flux densities produced near the cathode orifice (30 and 60 gauss cases). Cathode placement relative to the peak flux density has been selected so it is similar to that used in typical thruster applications. Unless noted otherwise, tests were conducted in the natural, transverse field environment. Tests conducted in other magnetic field environments were used to determine the extent to which these fields affected the operation of the hollow cathode and the downstream plasma it produced.

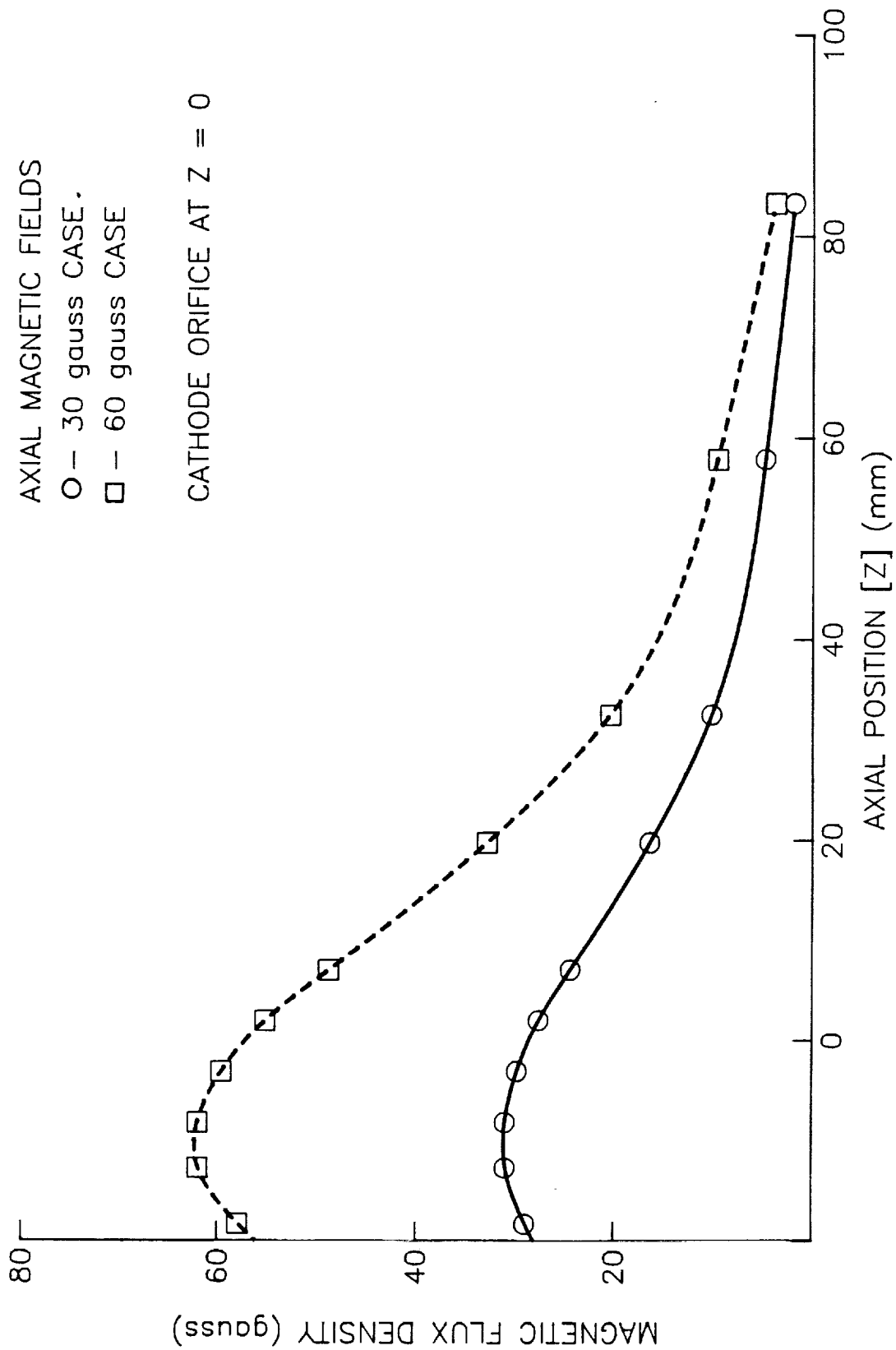


Fig. 3 Magnetic Flux Density Profiles Induced by Solenoid along Cathode Centerline

Typical Operating Procedure

Tests were generally conducted by increasing the discharge current from 5 to 60 A in 5 A increments. At each current level, measurements of cathode internal pressure, cathode temperature and anode and keeper voltages were made. Subsequently, measurements of plasma properties, high energy ion and electron characteristics and/or erosion rates in the plasma downstream of the cathode were made.

The pressure within the cathode was measured using a capacitance gauge, accurate to within ± 1 Torr. Because pressure measurements were made in the plenum chamber upstream of the cathode tube, as suggested in Fig. 2, and because the flowrates involved were low ($< 7 \times 10^{-7}$ kg/s), it is argued that these measured pressures were close to the stagnation pressures in the active region of the cathode just upstream of the orifice. Cathode wall temperatures were measured by viewing the surface of the weld between the orifice plate and cathode tube using a micro-optical pyrometer located outside of the glass bell jar. Measurements were corrected for surface emissivity errors and absorption losses through the glass using a calibration curve developed for this facility by Siegfried [15]. This was accomplished by making simultaneous temperature measurements on a heated tantalum surface using a thermocouple and the optical pyrometer. After the calibration had been completed, significant coating of the bell jar could have changed the calibration curve. No evidence of such a coating has been detected and it is believed the initial calibration has remained valid and temperatures are accurate to about ± 20 °C.

Plasma Property Measurements

The Langmuir probe shown downstream of the orifice plate in Fig. 2 was used to collect plasma property data in this region. The probe was constructed using a 0.25 mm dia tantalum conductor with one end melted to form the ~0.8 mm dia spherical surface on which current was collected. The conductor was insulated with a quartz tube which had a 2.2 mm outside dia and was reduced in size near the spherical collector to minimize the extent to which the insulator masked the collection surface. The probe could be swept both radially and axially throughout the region downstream of the cathode. Typically, however, it was positioned no closer than about 4 mm from the orifice to keep it from perturbing the orifice flow pattern and altering the cathode operating conditions. Keeping it at least 4 mm from the orifice also prevented probe failure due to overheating. A tungsten probe, biased even a few volts above cathode potential will melt if it is too close to the orifice, because of the very hostile environment (plasma densities above 10^{14} cm^{-3}) that can exist there. The probe was biased using a simple battery-driven circuit [16] and the resulting current/voltage traces were recorded on an X-Y plotter.

Langmuir probes are usually biased over the potential range from below floating potential to beyond plasma potential in collecting a trace. However, Langmuir probes located in the high plasma density environment near the cathode orifice tended to melt at the higher potentials when this was done. To prevent this, they were biased from a potential in the region of ion saturation to one ~3 V beyond floating potential and the resulting probe current vs. voltage trace was then analyzed using the same procedure applied by Siegfried [4]. Electron temperature is determined in the conventional way using this

procedure, but plasma density is determined from the ion saturation current rather than the electron saturation current and plasma potential is estimated from the floating potential and the electron temperature measurements.

Measurement of the Spatial Distribution of High Energy Electrons

The Langmuir probe was also used to determine the spatial variation in high energy electron random current density in the region downstream of the hollow cathode. This was accomplished in several steps by recording the current to a probe held at a prescribed potential as a function of radial and axial position. Two sets of data, one with the probe biased at cathode potential and one with it biased 8 volts below cathode potential, were collected. By taking the difference in the two currents, measured at each location, data arrays describing the random current density of electrons with kinetic energies between the value associated with electron deceleration from plasma potential and the one 8 eV greater than this value were computed. For example, these arrays would have described the random current density of electrons with kinetic energies between 15 and 23 eV if the measurements were made in a plasma at a potential of 15 V. It is noted that this method yields valid results, only when the ion currents to the probe at a given location are the same at both probe potentials. Since the probe is biased significantly below plasma potential for both sweeps, it should draw the same ion current in both cases and this condition should be met.

Measurement of the Characteristics of Ions

A retarding potential analyzer (RPA) [17], positioned on the cathode centerline downstream of the hollow cathode as suggested in Fig. 2, was used to measure the distribution function of ions coming from the vicinity of the cathode. The design details of this probe, which was generally positioned 8.9 cm from the cathode, are shown in Fig. 4. Because this probe must operate in a relatively high plasma density environment, special attention had to be paid to shielding the ion collector from plasma electrons. This was accomplished by carefully sealing joints in the probe and by erecting barriers to keep electrons from reaching the collector. The first barrier to electron leakage into the probe is the outer body (0.25 mm thick stainless steel) and screen 1 which is connected to it. The second barrier is the inner body and the two screens connected to it (screens 2 and 3). These body/screen pairs are isolated from each other using Kapton film and from the collector, which is mounted on an Iso-mica plate, so they can be biased relative to each other. Connections to the collector and the inner body are made using, respectively, the center and outer conductors of a coaxial cable. Careful attention was paid to obtain a tight fit at the point of cable entry into the device so plasma contact with either point of cable connection or with the collector would be prevented. The electromesh nickel screens used to cover the orifices in front of the collector have an 85% optical open area and square openings 0.24 mm on a side. Visual examination of the screens showed that they are not aligned and as a result, some ions impinge on each screen. They are held planar on 0.25 mm thick stainless steel support plates so uniform, axial electric fields can be maintained throughout the probe aperture region.

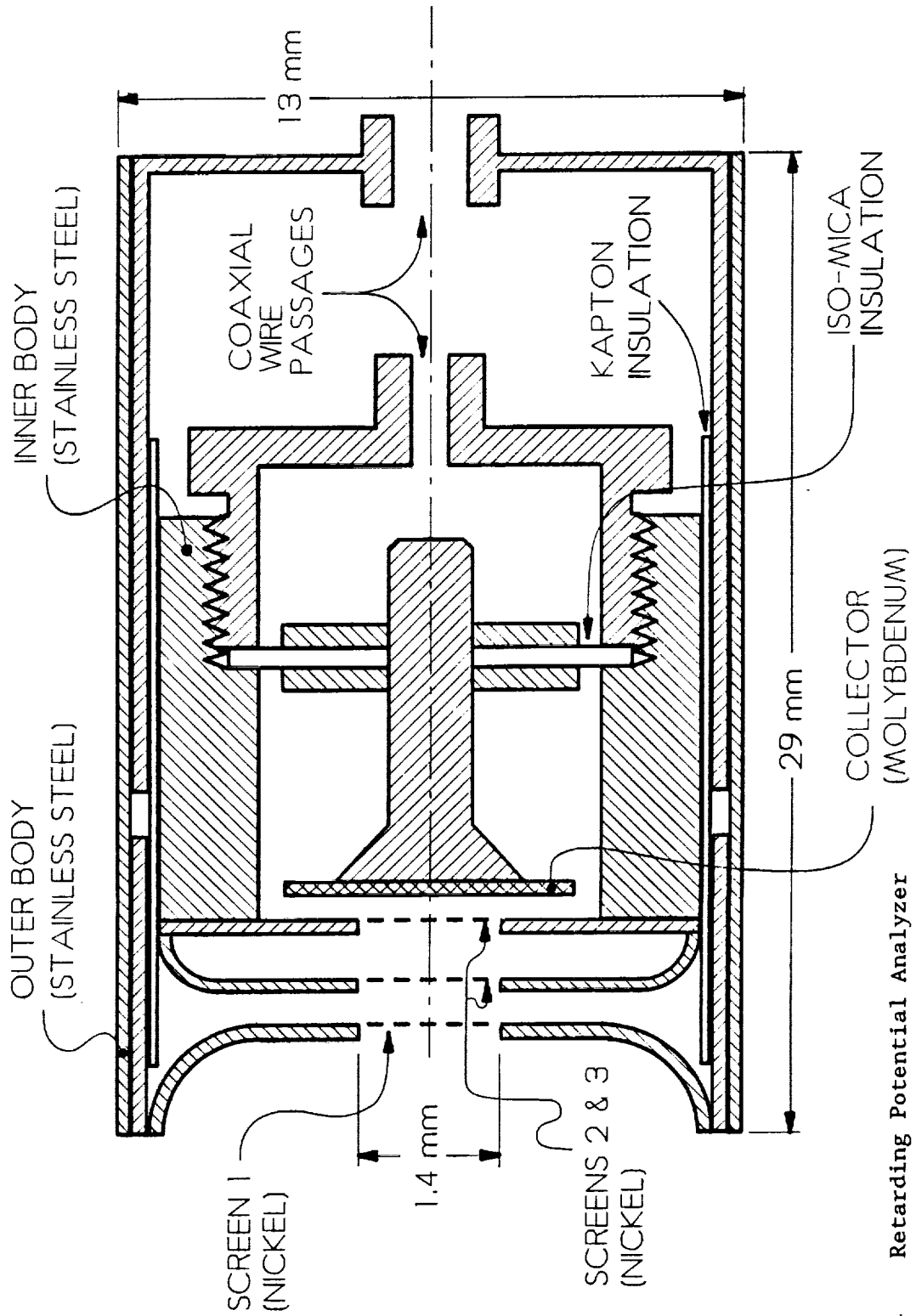


Fig. 4 Retarding Potential Analyzer

The voltages applied to the outer body, inner body and the collector were measured and designated respectively V_{OB} , V_{IB} and V_C . The current to the collector (J_C); which is equal to the product of the ion current density (j_C), the probe aperture area ($\pi[0.07]^2 \text{ cm}^2$) and the effective transparency of the three screen assembly ($\sim 0.85^3$); was also recorded. Experiments were usually conducted with the outer body held at cathode potential (0 V), screens 2 and 3 biased sufficiently negative to repel all electrons (about 32 V below cathode potential). The collector potential (V_C) was varied from cathode potential to a few tens of volts above it and collector current (J_C) was recorded as a function of this voltage on an X-Y plotter. A stainless steel shield ~ 13 mm in diameter was placed directly in front of the RPA and kept there until a trace was to be taken. When a trace was taken, the shield was removed only for the time needed to collect the data. This procedure was necessary to limit accumulation of an unknown contaminant that was observed on the collector plate after prolonged exposure to the cathode plasma.

Figure 5 is a typical plot of ion current density (j_C) versus ion collector potential. This particular example was measured with the probe aperture sighted on a cathode operating at a 40 A discharge current and a xenon flowrate of 280 mA eq. Since all voltages are measured relative to hollow cathode potential, zero collector potential on this plot corresponds to cathode potential. The structure of the trace in Fig. 5 reveals the characteristics of two groups of ions within the plasma at the probe (a lower energy [ambient] group and a higher energy [jet] group). The contributions of each of these groups to the RPA trace are identified on the figure. The ambient ions are all repelled at a collector bias of

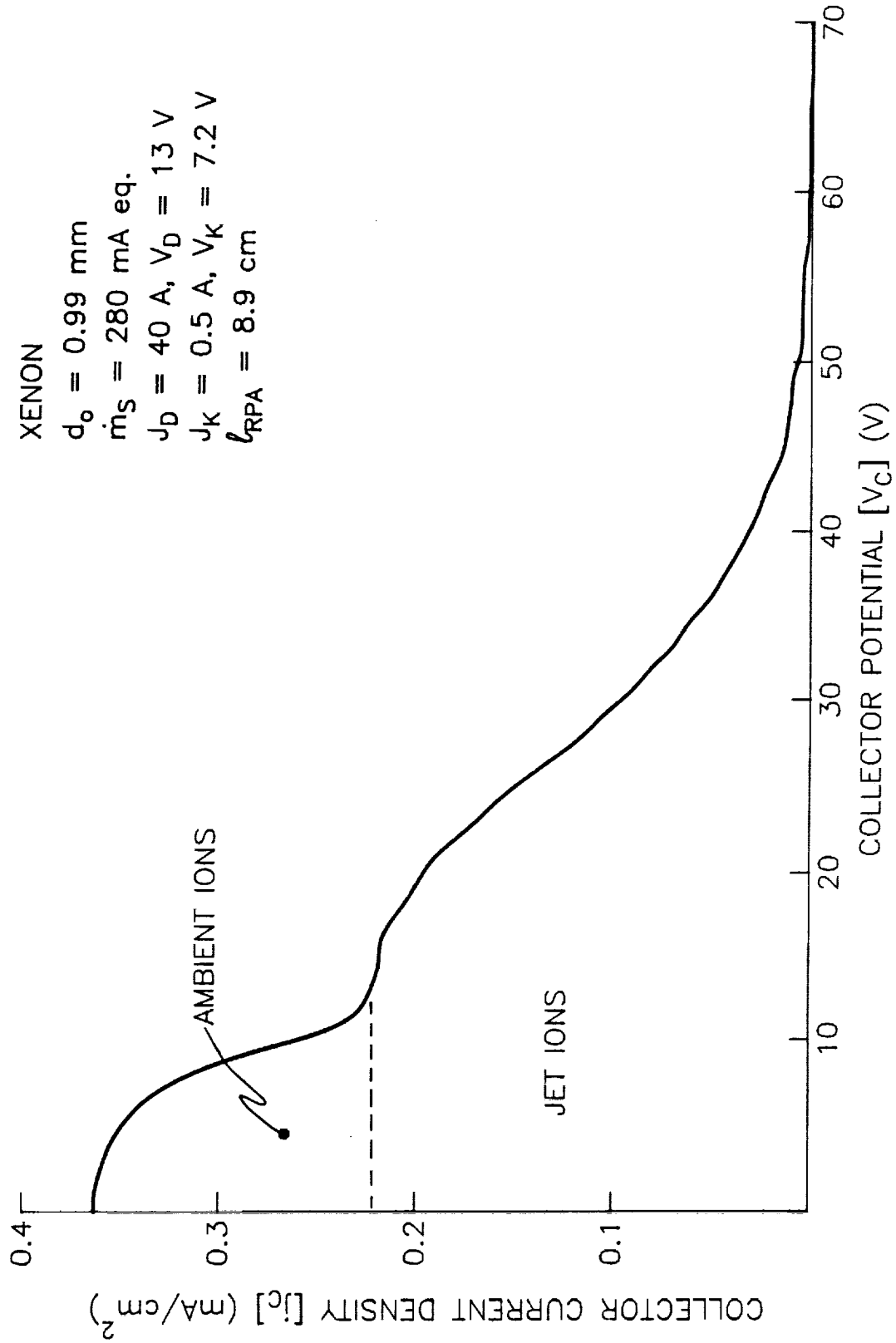


Fig. 5 Typical RPA Trace Sensed Downstream of a Hollow Cathode

-10 V while ~60 V is required to repel all of the jet ions. The high energy jet ions are of particular interest because they could induce substantial sputtering damage in thrusters. The current density of these ions for the case of Fig. 5 is seen to be 0.22 mA/cm^2 compared to 0.14 mA/cm^2 for the ambient ions.

Once the RPA data were recorded, they were digitized, fitted using a Fourier series and differentiated numerically using a procedure developed by Anderson [18]. The result of doing this with the data of Fig. 5 is shown in Fig. 6a. The distribution function describing a particular group of ions can be determined from data like those in Fig. 6a by applying the equation:

$$g(\epsilon) = -\sqrt{\frac{m_i}{2 e \epsilon}} \frac{1}{e} \frac{dj_C}{d\epsilon}; \quad (1)$$

where $g(\epsilon)$ is the ion energy distribution function, m_i is the ion mass, e is the electronic charge, ϵ is ion kinetic energy and j_C is ion current density to the collector. Details of the development of Eq. 1 which is based on the assumption that only singly-charged ions² comprise the beam are contained in Appendix A.

In order to determine the energy distribution of particles within the plasma at the probe aperture, the potential of this plasma V_{PL} must be known so the kinetic energy of the particles incident on the

²Multiply charged ions produced in a region of high potential would be stopped at the same potential as singly charged ones, so their presence would not affect the values of potentials inferred from RPA measurements. Any multiply charged ions produced would, however, approach a cathode potential surface at substantially higher energies and momenta than singly charged ones.

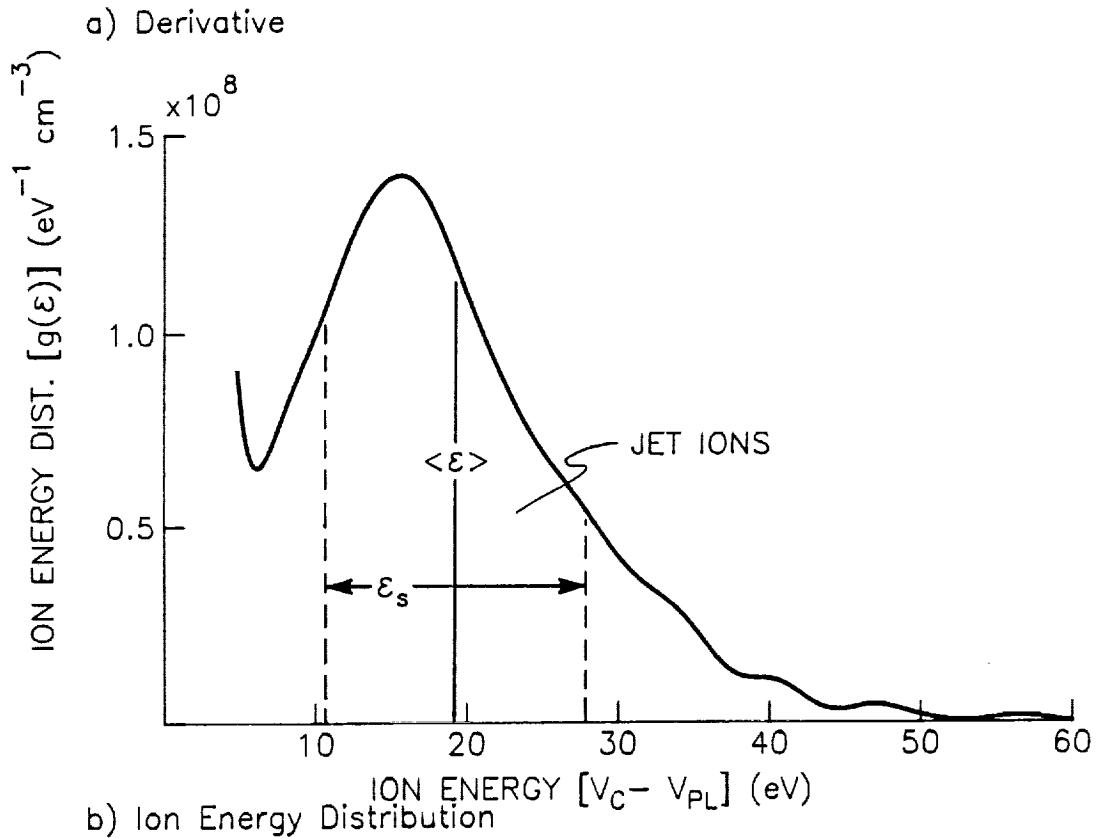
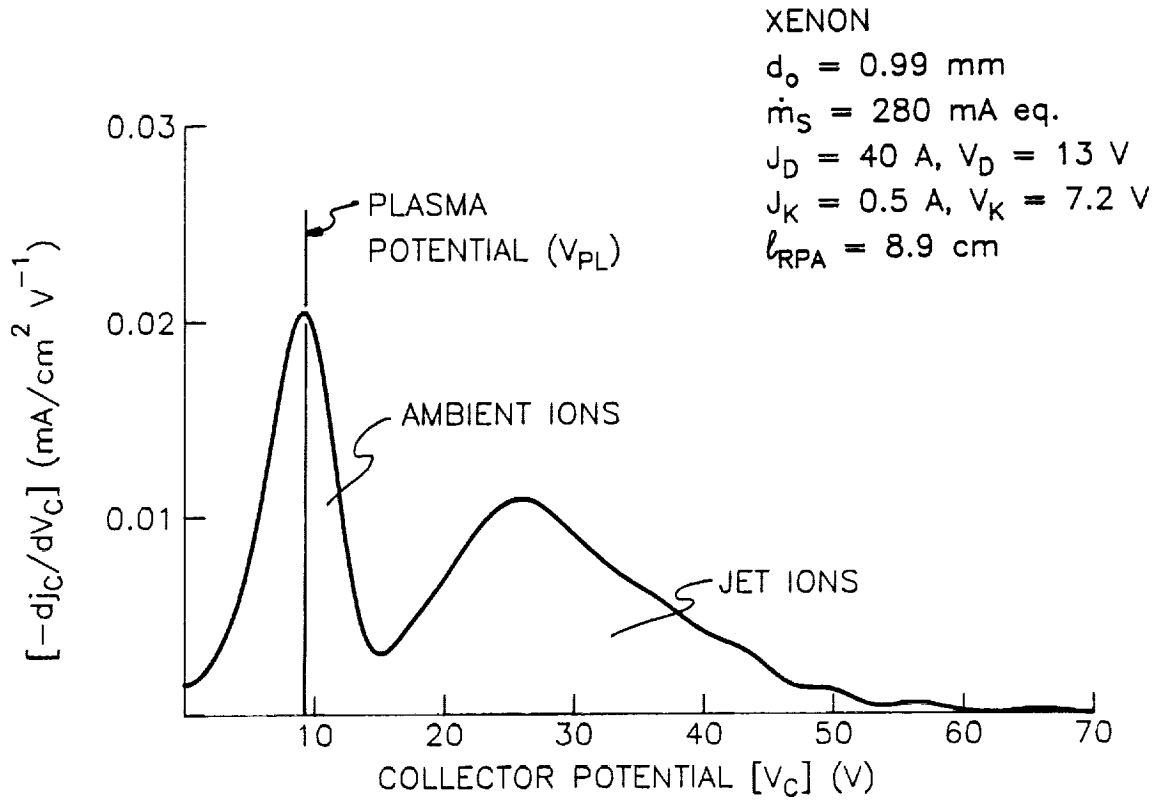


Fig. 6 Data from a Typical RPA Trace

probe can be determined. Once the plasma potential is known, particle kinetic energy (i.e. the retarding potential required to stop the particles) is given by

$$\epsilon = V_C - V_{PL}. \quad (2)$$

The plasma potential at the RPA, which is needed in Eq. 2, can be determined from Langmuir probe measurements, but it can also be estimated from the differentiated RPA probe trace. In this latter case, it is assumed that the majority of the ambient ions have energies centered around the potential of the plasma in the immediate vicinity of the probe. This implies a plasma potential (identified in Fig. 6a) located at the collector potential where the derivative associated with the ambient (lower energy) group is a maximum. The 9 V value associated with the data of Fig. 6a is close to the discharge voltage (13 V -- the estimated maximum potential of the plasma at the probing location). Ion kinetic energies calculated using these two values differ by ~6% at a collector potential of 40 V and the magnitude of this difference decreases as ions associated with higher collector potentials (higher kinetic energies) are considered. When this 9 V potential is used in Eq. 2 to compute ion energies and they are then used in Eq. 1 to compute the ion energy distribution function for the Fig. 6a results, the results shown in Fig. 6b are obtained. Regarding this curve it is noted that the ambient ion contribution (near zero potential) is large because its determination requires division by an energy that approaches zero at plasma potential. It is, however, the jet ions that are of principal

interest in this study, and their distribution function is well behaved.

The jet ion energy distribution curve shown in Fig. 6b, which is typical of those observed in the study, has a shape that approaches a gaussian one. In order to simplify data presentation, the jet ion distribution curves will be characterized by a mean ion energy ($\langle \epsilon \rangle$) and an ion energy spread (ϵ_s). Numerical values for these parameters, defined on Fig. 6b for the case being considered, are computed using the following equations:

$$\langle \epsilon \rangle = \frac{\int_{\epsilon_{\text{MIN}}}^{\infty} \epsilon g(\epsilon) d\epsilon}{\int_{\epsilon_{\text{MIN}}}^{\infty} g(\epsilon) d\epsilon} \quad (3)$$

and

$$\epsilon_s = 2 \sqrt{\langle \epsilon^2 \rangle - \langle \epsilon \rangle^2} \quad (4)$$

where

$$\langle \epsilon^2 \rangle = \frac{\int_{\epsilon_{\text{MIN}}}^{\infty} \epsilon^2 g(\epsilon) d\epsilon}{\int_{\epsilon_{\text{MIN}}}^{\infty} g(\epsilon) d\epsilon} \quad (5)$$

and ϵ_{MIN} is the minimum energy associated with the jet ions. For the example shown in Fig. 6b, ϵ_{MIN} was taken to be ~6 eV.

The energy spread parameter ϵ_s represents the energy band centered at the mean energy $\langle\epsilon\rangle$ that would include 69% of the jet ions incident on the collector surface if the ions had a gaussian distribution. Although the jet ions are not distributed in a true gaussian fashion, this interpretation is approximately correct.

Erosion Testing

Tests were performed to determine the erosion rate of materials located downstream of a hollow cathode. The tests involved the erosion of small copper targets at various axial distances from a hollow cathode operating a discharge current (J_D) of 60 A and a xenon flowrate (\dot{m}_G) of 280 mA eq. Three copper targets were used in these tests and they were prepared by polishing and then masking them with a 0.25 mm thick piece of tantalum that had a 1.7 mm dia aperture in it. The masked samples were exposed one at a time at different locations along the cathode centerline for prescribed times and then removed. The erosion rate was determined by dividing the depth of the eroded crater, measured using a surface profilometer, by the associated exposure time.

III. RESULTS

In order for the experiments being performed in this study to have application to thruster cathodes, it is important that they induce erosion rates similar to those observed in thruster and cathode life tests. Evidence of these high erosion rates was sought by placing a copper surface on the centerline downstream of a cathode operating at a 60 A discharge current. Three separate tests were conducted using targets at different axial locations and they yielded the erosion rate data shown in Fig. 7. The error bar on each data point defines the uncertainty in the rate associated with the variability in the erosion depth measured across the crater produced during exposure to the cathode plasma. The data of Fig. 7 show a $1/Z^2$ variation with axial position (Z). This spatial variation suggests the craters were sputter-eroded by a diverging beam of high energy ions that came from a point source near the cathode orifice. Further, the copper targets remained relatively cool during exposure and the craters that were produced had the appearance of sputter-eroded surfaces rather than ones that had been produced by some melting process (i.e. the craters exhibited steep boundaries at the edges of the mask).

Additional support for the theory that high energy ions coming from a source near the cathode orifice sputter erode downstream structure comes from a life test conducted on a 30 cm thruster [19]. In this 10,000 hr test, the severely eroded baffle developed a "spoke-like" pattern and each of the four protruding spokes were located such

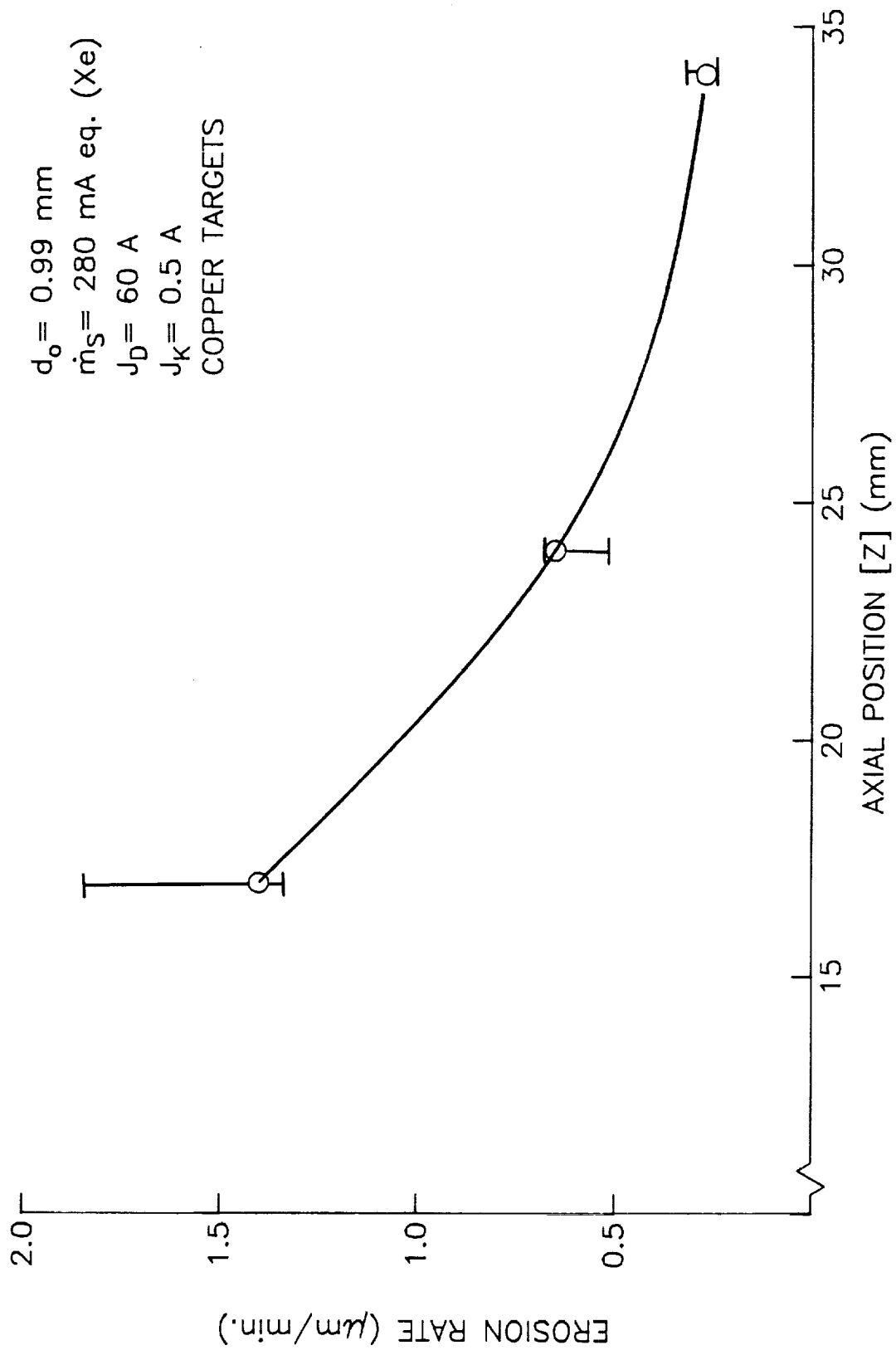


Fig. 7 Centerline Erosion Rate Profile

that the four baffle support legs would have shielded them from a source of high energy ions emanating from a point near the cathode orifice.

If sputtering is presumed to be the erosion mechanism in the present tests, the data of Fig. 7 can be used to infer the erosion rates of other materials (by multiplying by the ratio of the sputtering yield of the material of interest to that of copper and applying the $1/Z^2$ decay to account for variations in position). Recall that Rawlin [9] observed a sputter rate of $0.9 \mu\text{m/hr}$ on the tantalum baffle 5 cm downstream of a xenon hollow cathode operating at a 35 A discharge current in an ion thruster. On the basis of the data in Fig. 7 one would predict a rate of $\sim 2 \mu\text{m/hr}$ (this assumes 100 eV ions to calculate the ratio of tantalum to copper sputter yields) under the conditions associated with the Rawlin test. While the rate associated with the Fig. 7 data is greater than the value measured by Rawlin, probably because it is based on a cathode operating at a higher current, the two rates are comparable. Thus, it is argued that the same phenomena that induce baffle erosion in thrusters operating at high discharge current levels are active in the experimental apparatus being used in this study.

Basic Energy Considerations

In discharges of the type under consideration here, ions are generally produced by high energy electrons that are drawn from the cathode and bombard atoms. The resulting ions typically have low kinetic energies at the potential of the plasma in which they are produced. They acquire a kinetic energy equal to the plasma-to-cathode potential difference, however, as they fall through a sheath

and strike cathode potential surfaces like thruster baffles or the copper erosion surfaces associated with the tests of Fig. 7. Because bulk plasma-to-cathode potential differences are typically too low to accelerate ions to the energies required for substantial sputtering, the experimental data pose a dilemma. Collett et al. [19] pointed this out in discussing the 30 cm dia. thruster baffle erosion results. They observed that, "The generally accepted model of the discharge chamber plasma potential distribution would place the plasma potential within the cathode pole piece at approximately the keeper voltage. Thus, no doubly charged ions should be formed in the region and singly charged ions should not be capable of causing damage."

Typical discharge (anode) and keeper voltages (V_D and V_K respectively) measured using the 0.99 mm orifice diameter (d_o) cathode operating over a range of discharge currents (J_D) from 5 to 60 A and propellant supply rates (\dot{m}_S) from 180 to 460 mA eq are shown in Fig. 8. These voltages are modest (less than 15 V [discharge] and 10 V [keeper]) and relatively constant over these ranges of current and flowrate. The results of Fig. 9 show that changes in orifice, orifice plate and cathode tube diameters do not affect these voltages significantly. While the data in these figures do suggest that the discharge and keeper voltages (and therefore the bulk plasma potential) do increase slightly with discharge current, particularly at the lowest flowrate, the important point to notice is that the voltage magnitudes are low. Ions accelerated into a cathode potential surface from a bulk plasma at the most positive of these potentials would have energies below typical sputter yield threshold energies

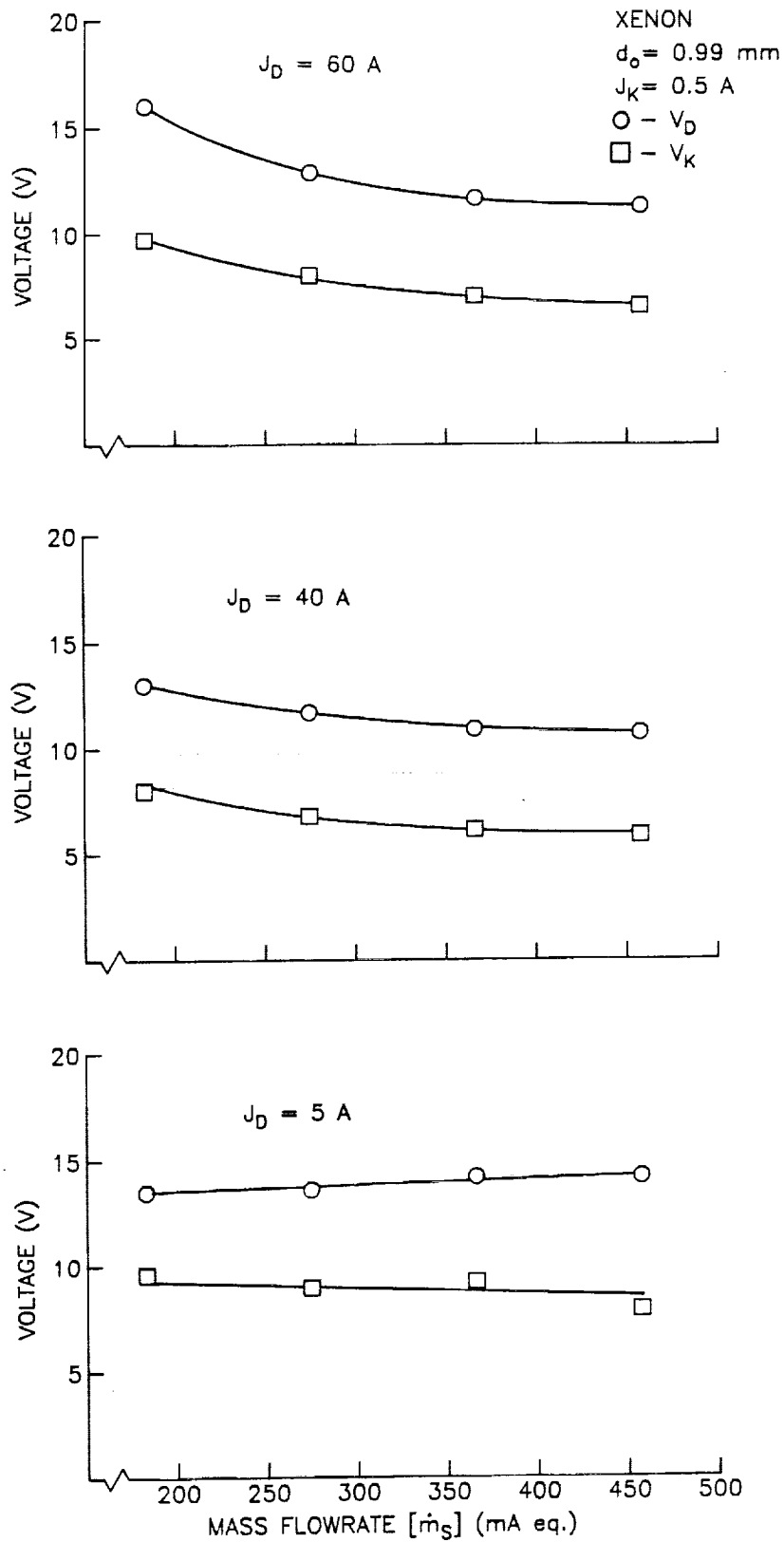


Fig. 8 Effect of Propellant Flowrate on Discharge and Keeper Voltages

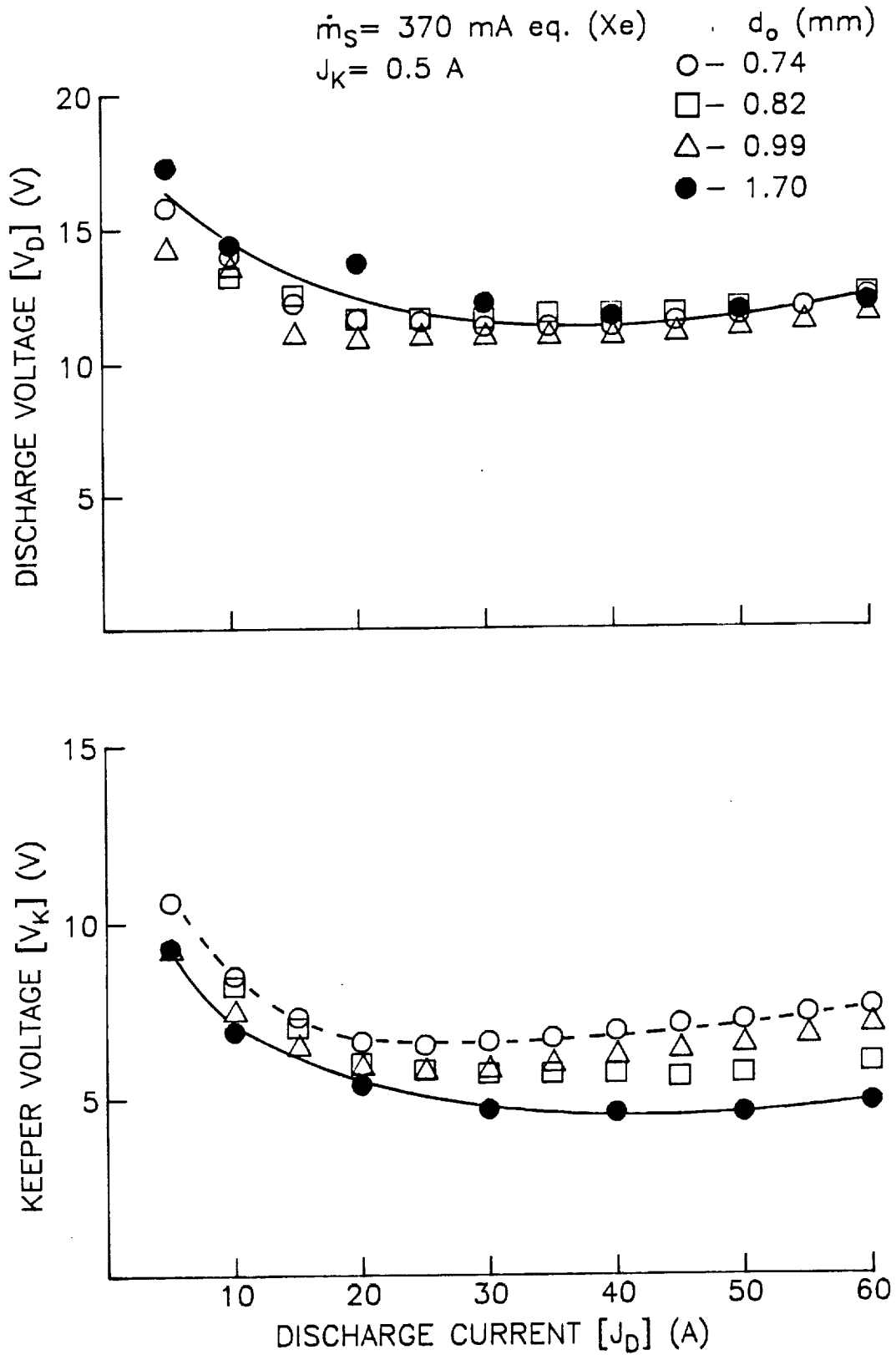


Fig. 9 Effect of Discharge Current on Discharge and Keeper Voltages with Orifice Diameter as a Parameter

[20]. Hence the data of Figs. 8 and 9 suggest that ambient ions produced in the bulk plasma downstream of the cathode are not inducing the sputtering that is observed.

It is noted that higher energy ions could be created if the plasma potential were fluctuating. In this case, ions created when the potential was a maximum would strike a cathode potential surface with the maximum plasma-to-cathode potential difference. In order to investigate this possibility, anode voltage fluctuations, which should couple to those of the plasma, were measured using an oscilloscope. The peak-to-peak anode voltage variation was found to be 1 V at 60 A and 5 V at 5 A discharge current, and these variations added to the steady voltage levels are still insufficient to induce the observed sputtering.

Visual and Random Electron Current Density Observations

Figure 10 is a photograph of a hollow cathode operating at 60 A discharge current in a nulled magnetic field environment. The particular cathode in this photograph was the one with the 0.99 mm orifice diameter, but cathodes with different orifice diameters operating at this same current looked the same. The intense, luminous jet emanating from the cathode can be seen because photons, resulting presumably from atomic and possibly ionic de-excitation reactions, are produced within the region occupied by the jet. Because the jet is so well confined, it seems obvious that the excitation reactions that precede these de-excitation events must be induced by a well-collimated jet of high energy electrons coming from the cathode. At this point, it should be noted that these jet electrons may or may not be tied to or located near the jet ions suggested previously. The

ORIGINAL PAGE
BLACK AND WHITE PHOTOGRAPH

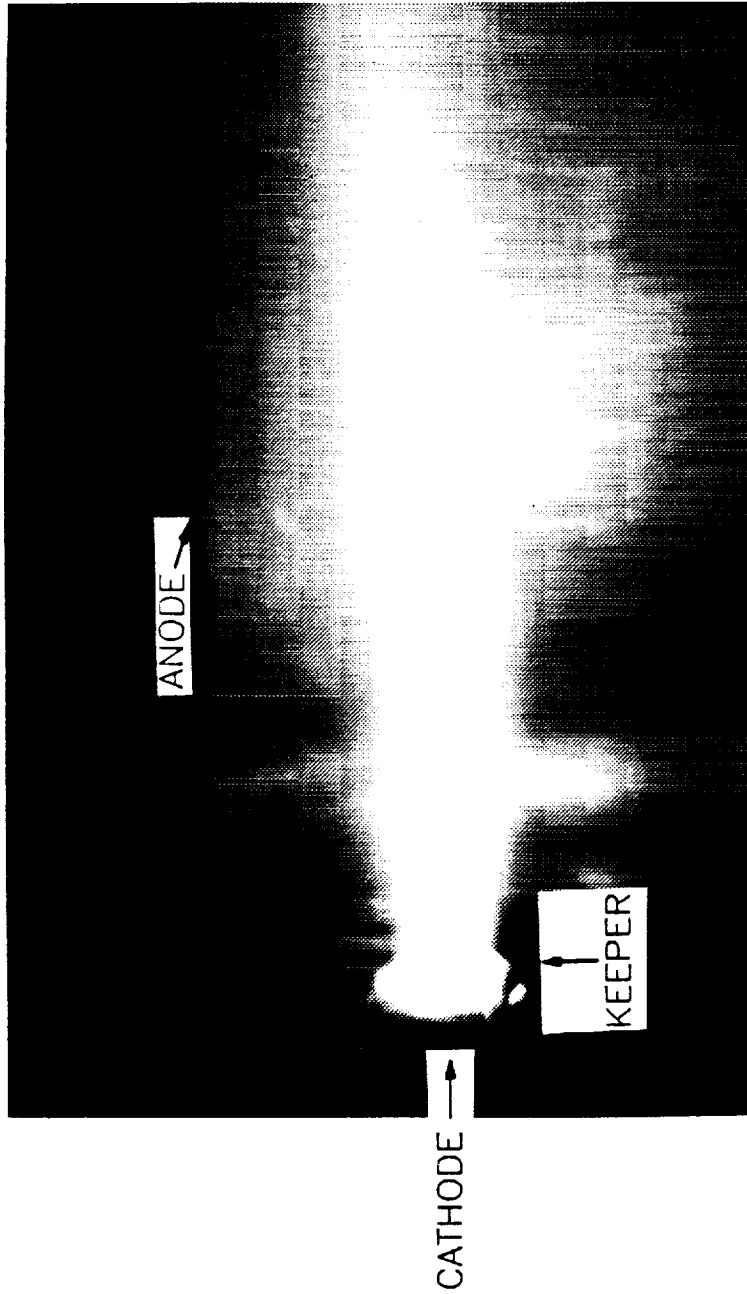


Fig. 10 Hollow Cathode Operating at 60 A Discharge Current in Nulled
Magnetic Field Environment

atoms being excited by the jet electrons could be either the ambient ones or those being supplied through the cathode orifice. Those flowing through the orifice would be expected to expand in a spherical segment extending from the orifice and exhibit a $1/Z^2$ density decay within this segment.

When an axial magnetic field was applied to the hollow cathode, it looked the same as the one shown operating with a nulled magnetic field in Fig. 10. With the "60 gauss" axial field (see Fig. 3) applied to a cathode operating at a 60 A discharge current, the random current densities of high energy electrons (those with energies between 12 and 20 eV) were measured. A plot of constant current density contours measured at this operating condition is shown as Fig. 11. This figure shows that the high energy electron current density is highest near the cathode, that these current densities drop off axially and that the shape of the constant current density contours is similar to that of the visible jet.

When only the natural, transverse 0.4 gauss magnetic field was present rather than the axial or null fields that yielded jets like the one shown in Fig. 10, the luminous jet was observed to curve upward until it contacted the anode in the manner shown in Fig. 12a. High energy electron current densities were measured in a plane that passed through the centerline and was perpendicular to the plane of Fig. 12a and the constant current density plot of Fig. 12b was obtained. Comparison of the data of Figs. 11 and 12b confirms the fact, suggested by the photographs (Figs. 10 and 12a), that the transverse magnetic field causes the high energy electrons to curve upward because of the $\mathbf{v} \times \mathbf{B}$ force it imposes on them. The cyclotron radius associated with this motion (determined from Fig. 12a) can be

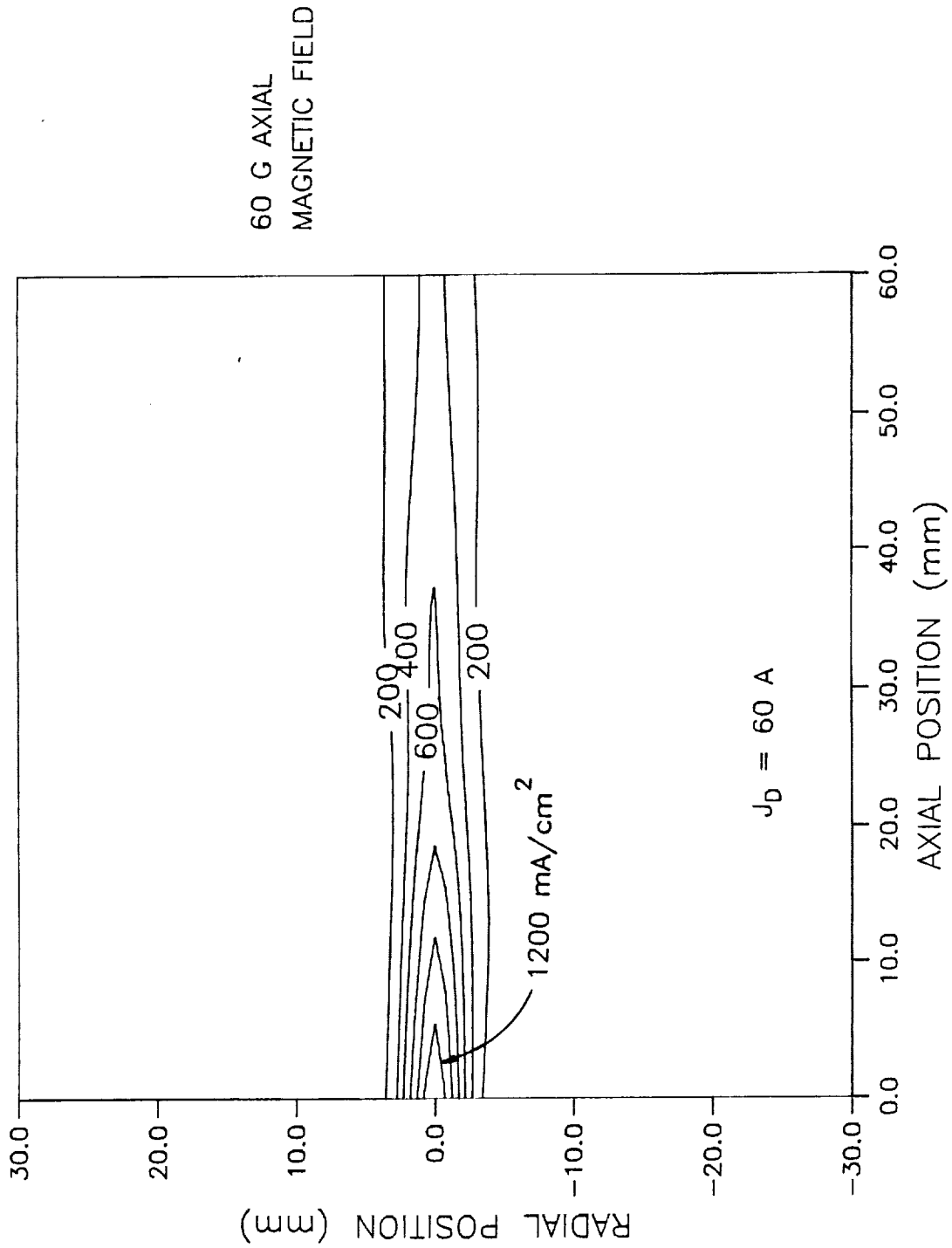
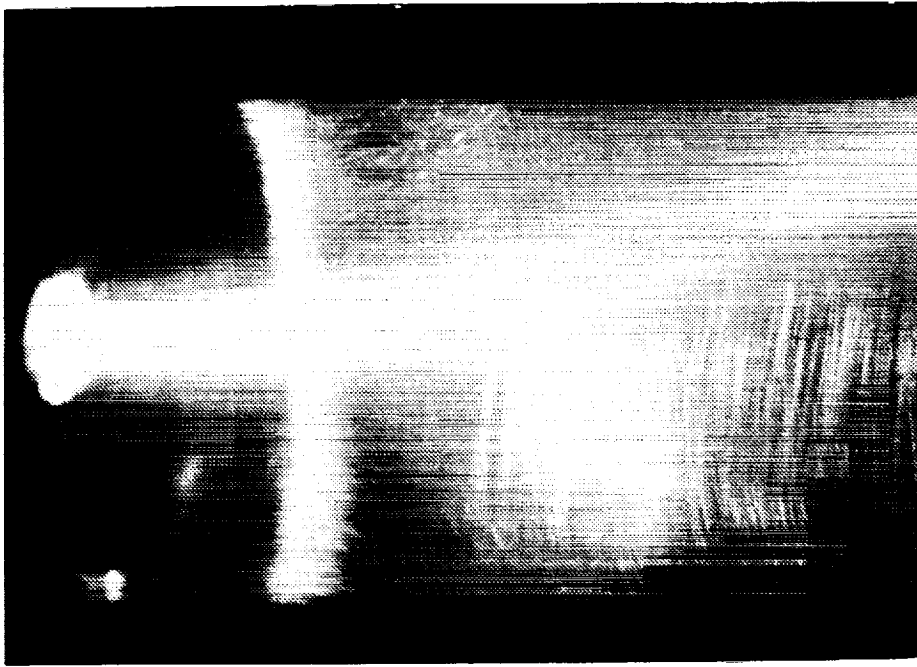


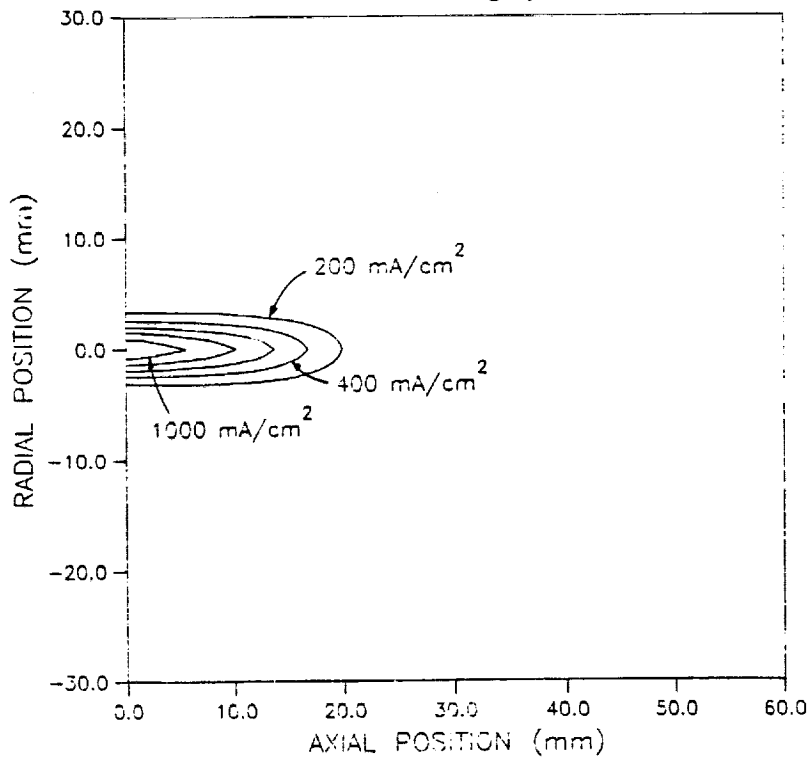
Fig. 11 Constant Current Density Contours Associated with High Energy Electrons at 60 A Discharge Current

ORIGINAL PAGE
BLACK AND WHITE PHOTOGRAPH



$J_D = 60 \text{ A}$
0.4 G

a) Physical Appearance (Magnetic Field Direction out of Page)



b) Constant Current Density Contours

Fig. 12 High Discharge Current Electron Jet in 0.4 G Transverse Magnetic Field

used with the magnitude of the transverse magnetic field to estimate the energy of the jet electrons. The resulting energy (~ 10 eV) is in good agreement with both the magnitude of the discharge voltage, which would be expected to determine the electron energy, and the Langmuir probe bias potentials used to obtain the high energy electron current density plots (Figs. 11 and 12b).

The current density of the high energy electrons varies as the discharge current is changed. The extent of this change can be seen in Fig. 13 where constant current density plots pertaining to 20 and 60 A discharge currents are compared for the case where the 60 gauss axial magnetic field was being applied. These data show the current density levels are higher for the 60 A case, as expected. In addition, they suggest a more constricted jet extending further downstream at the higher discharge current. This observation is consistent with visual observations of the luminous jet extending only ~ 20 mm downstream at a 20 A discharge current, while it extended about an order of magnitude further when it was operating at a 60 A discharge current. It is noted that both sets of data in Fig. 13 were obtained at a 370 mA eq. flowrate but, over the range investigated, flowrate affected neither the current density profiles nor the physical appearance of the jets significantly.

Downstream Plasma Properties

Plasma property profiles measured downstream of the hollow cathode with the 0.99 mm dia. orifice operating at a flowrate of 370 mA eq. and discharge currents of 20, 40 and 60 A are shown in Fig. 14. These profiles are typical; similar profiles were observed at other flowrates and with other cathodes. They show that discharge plasma

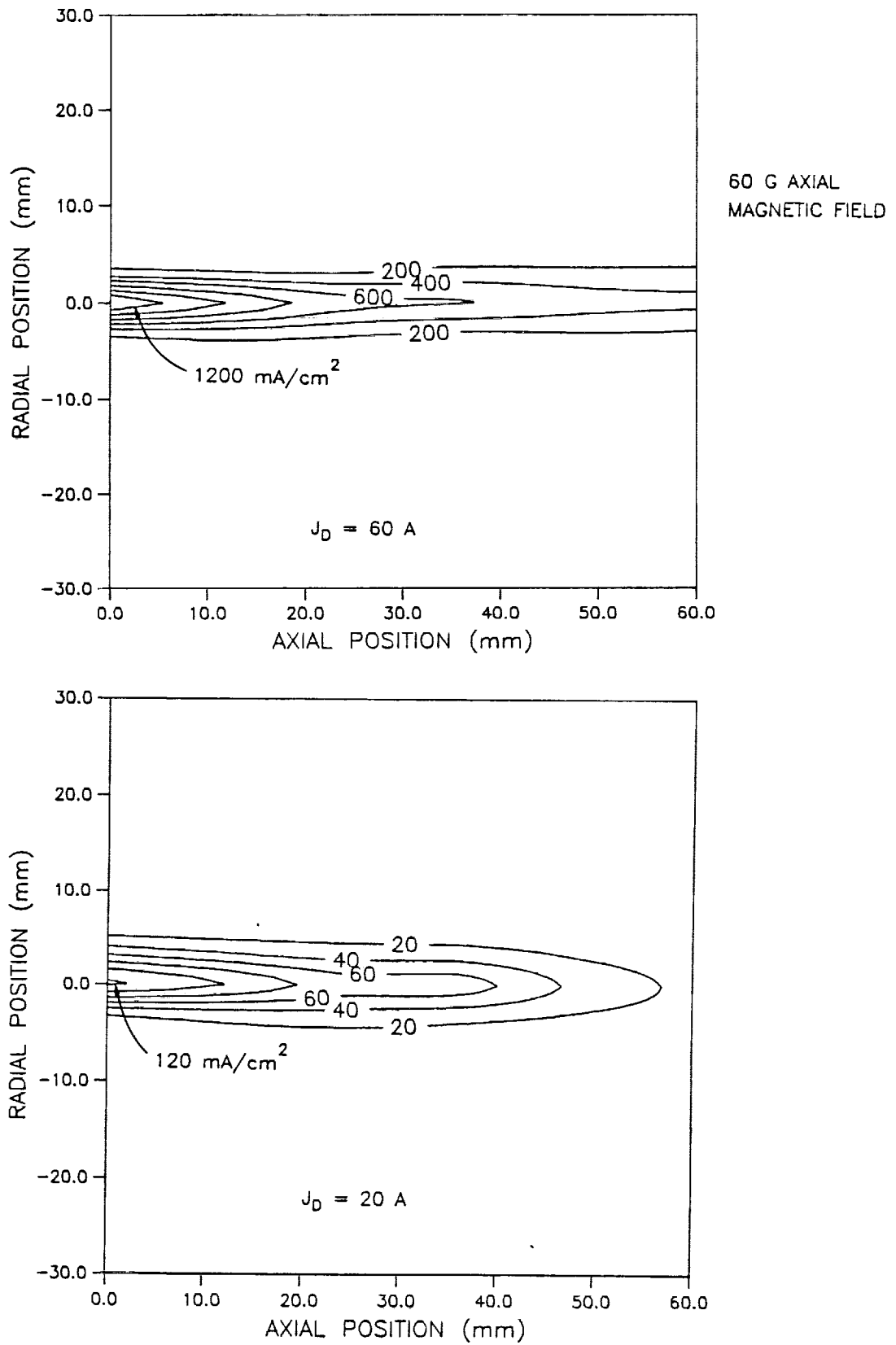
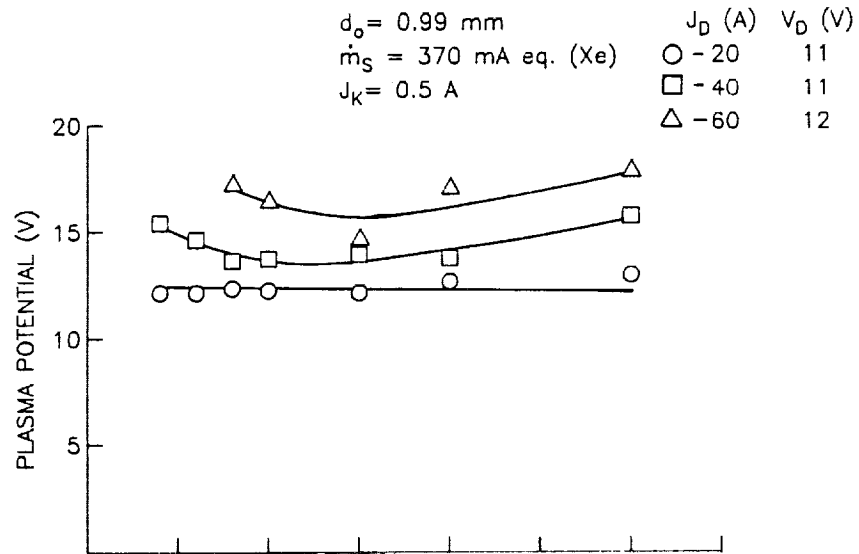
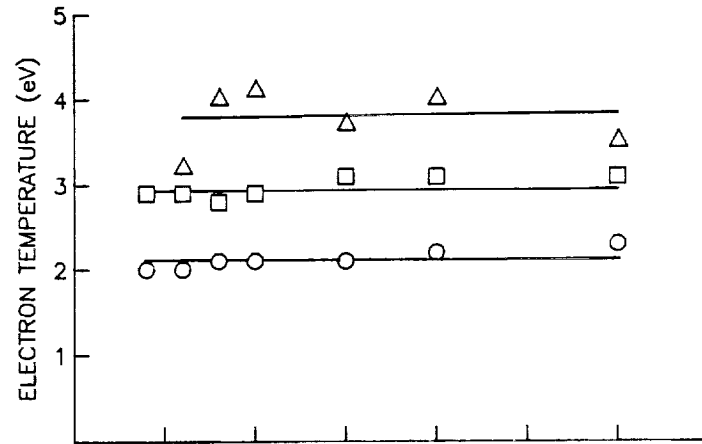


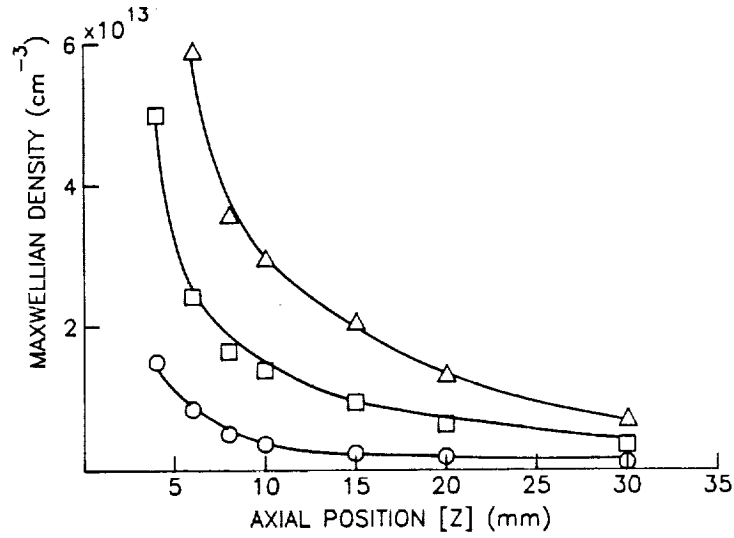
Fig. 13 Effect of Discharge Current on Constant Current Density Contours Associated with High Energy Electrons



a) Plasma Potential



b) Electron Temperature



c) Maxwellian Electron Density

Fig. 14 Effect of Discharge Current on Centerline Plasma Property Profiles

potentials are relatively uniform and that they are only a few volts positive of the discharge (anode) voltages. As suggested previously, these potentials are generally insufficient to accelerate ambient ions into surfaces at the kinetic energies needed to induce substantial sputter erosion.

Two trends reflected in these plots are noteworthy and will be used later to support a model that describes the characteristics of high current hollow cathodes. First, there is a trend for the general level of the plasma potentials to increase with increases in discharge current faster than the discharge voltage does. Second, there is a tendency for the plasma potentials to rise in the region close to the cathode (i.e. as $Z \rightarrow 0$) that becomes greater as the discharge current is increased. In order to investigate the peak potentials achieved close to the cathode, it would be desirable to probe closer to the cathode orifice plate plane. Unfortunately, this could not be done because close probing perturbed the cathode operating conditions and frequently resulted in probe destruction in the hostile plasma environment there.

Langmuir probe measurements revealed a plasma that is nearly Maxwellian and has temperature profiles shown in Fig. 14b to be axially uniform that rise to higher values as discharge current is increased. Evidence that the plasma environment near the cathode orifice becomes increasingly hostile as the discharge current is increased is given in Fig. 14c. This plot shows that the electrons are at density levels that approach 10^{14} cm^{-3} under the test conditions. As with the plasma potential data, the data of Fig. 14b and c are typical. Increases in propellant flowrate and changes to

other cathode configurations did not change the magnitudes or trends indicated in this figure significantly.

Direct Measurements of Ion Energy Characteristics

In order to determine if high energy ions that could induce observed sputter erosion rates were present, the energy distribution of ions in the plasma were measured using the retarding potential analyzer (RPA). Figure 15 presents typical RPA traces measured at discharge currents ranging from 10 to 60 A when the analyzer was located at a distance (l_{RPA}) 8.9 cm downstream of the cathode orifice on the cathode centerline and sighted on the orifice. All of the RPA traces shown in this figure suggest there are two groups of ions being collected by the probe. The low energy (ambient) group would be produced in a plasma having a potential about equal to that at the RPA but the high energy (jet) group would have to be produced at some location where the plasma potential is considerably greater. The jet ion contribution to total ion current density is seen to vary from a small fraction at the lowest discharge current ($J_D = 10$ A) to the dominant fraction at $J_D = 60$ A. These plots also show that the maximum energy of the jet ions increases with discharge current (note the scales change on both axes). For example, a 20 V collector potential is sufficient to repel essentially all jet ions at a 10 A discharge current while over 100 V is required to repel them at $J_D = 60$ A. These results are important because they provide evidence that ions with energies sufficient to induce sputtering are produced in a cathode discharge and that the energies and current densities associated with

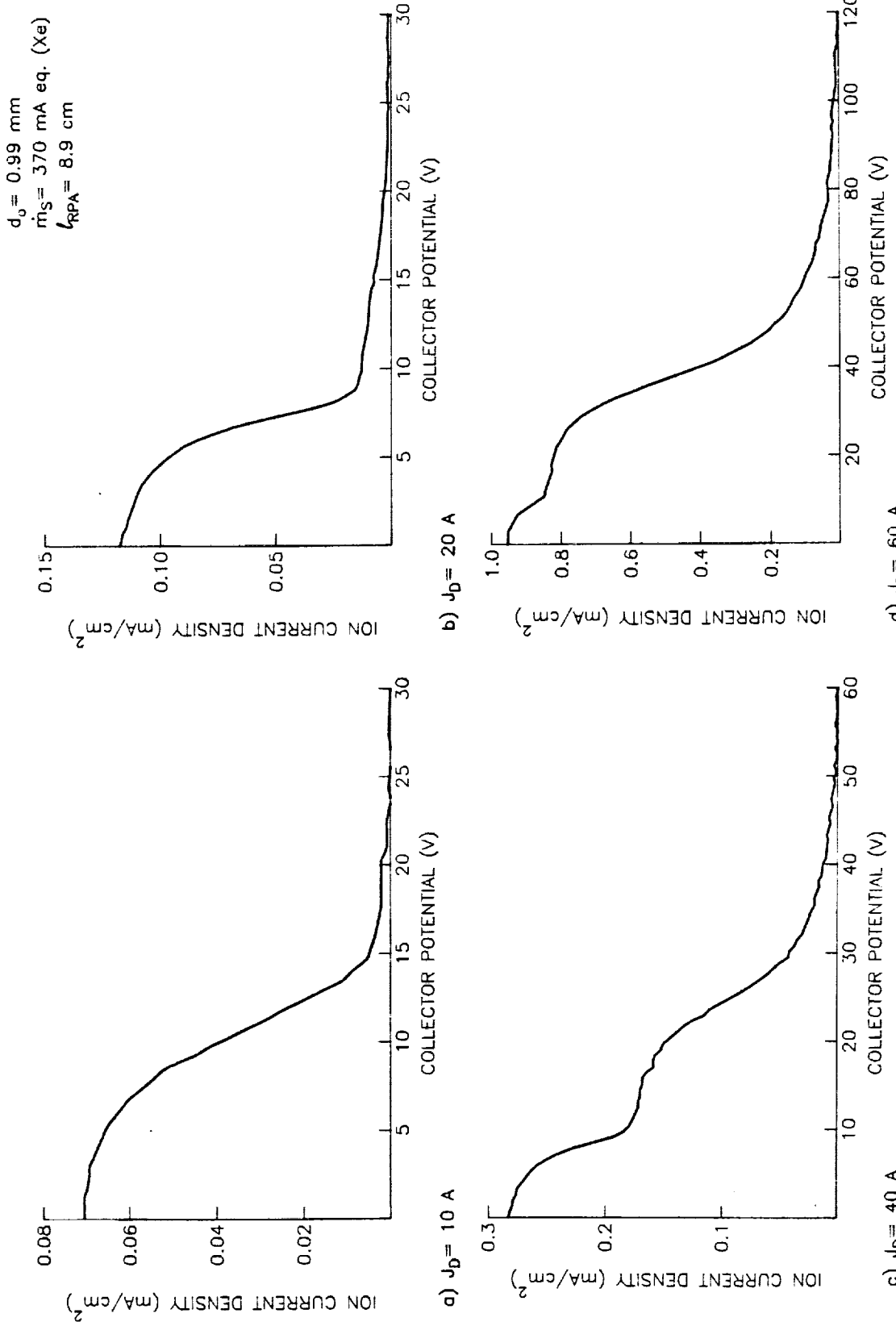
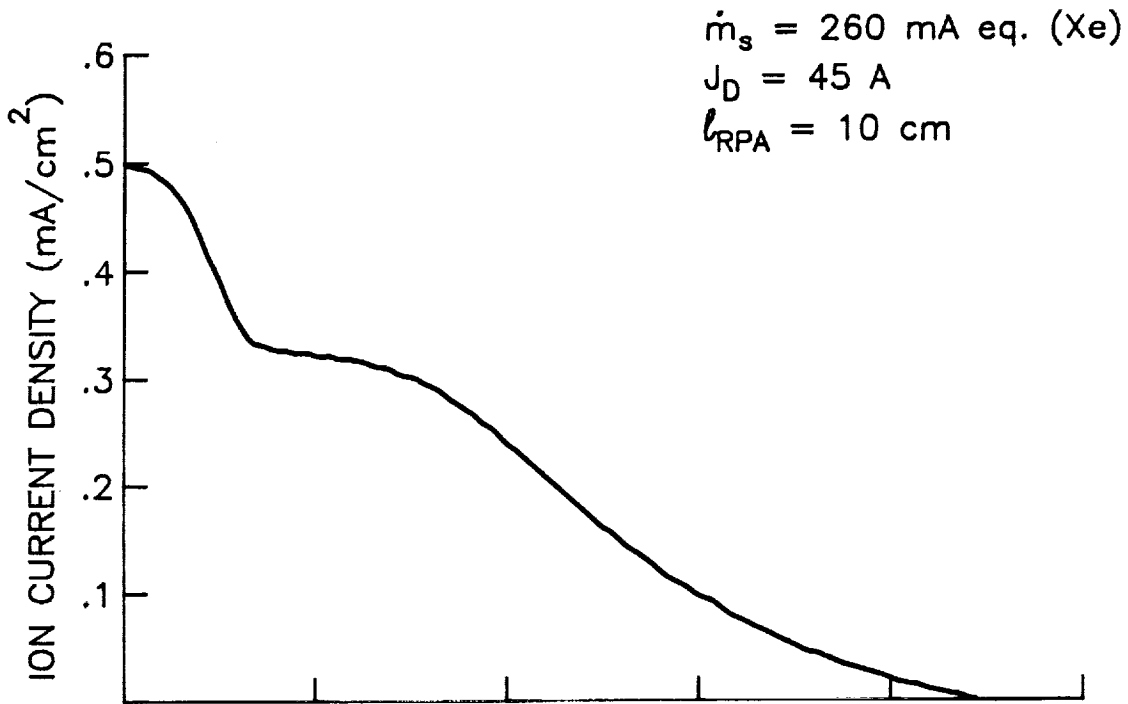


Fig. 15 Effect of Discharge Current on Centerline RPA Data

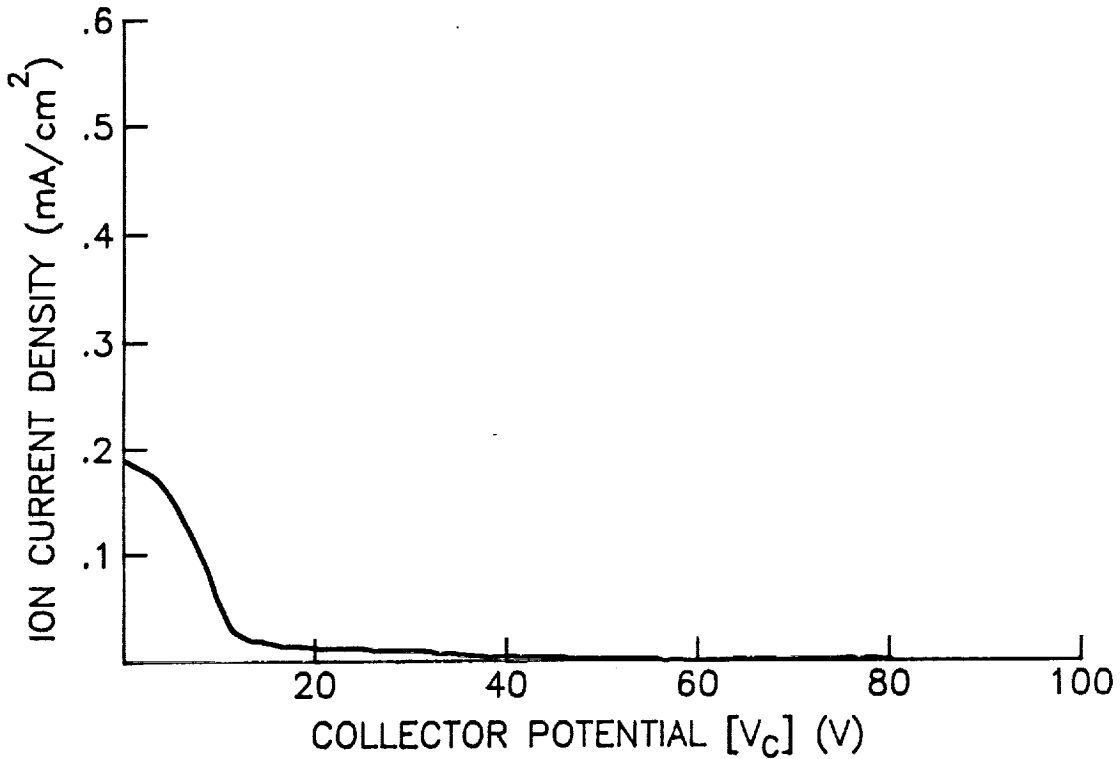
these high energy, jet ions increase with discharge current. These results are, therefore, consistent with the erosion trends observed by Rawlin [9] and by Brophy and Garner [13].

Evidence that the jet ions come from the immediate vicinity of the cathode orifice is shown in Figs. 16 and 17. Figure 16 presents results of a simple experiment in which the energy characteristics of the ions in the plasma downstream of a cathode operating at a 45 A discharge current were first measured in the conventional way (Fig. 16a). Then the 1.3 cm diameter stainless steel shield was positioned about 2.5 cm from the cathode so it would intercept ions passing in a straight line from the cathode orifice to the probe and the measurement was repeated (Fig. 16b). Comparison of Figs. 16a and b demonstrates very clearly that the shield stopped the jet ions from entering the probe but did not affect the ambient ions. This result shows that the jet ions are produced within 2.5 cm of the cathode orifice.

The data of Fig. 17 illustrate the changes in data measured by the RPA when it was moved from a position 7 cm downstream of a cathode operating at a 40 A discharge current to one 10 cm from it. Accepting the previously postulated $1/Z^2$ decay in ion current density, the ratio of the jet ion current densities (designated j_j) at these two locations ($0.35/0.15 \text{ mA/cm}^2 = 2.3$) suggests the source of the ions lies within about 1 cm of the cathode orifice (because $[10-1]^2/[7-1]^2 = 2.3$). Since the sputtering rate of a surface is directly proportional to the current density of the sputtering ions incident on it, this result is also consistent with the $1/Z^2$ dependence of sputtering rate observed previously in the data of Fig. 7. The data of Fig. 17 also indicate that while the current densities sensed by



a. Orifice Visible from RPA



b. Orifice Obscured from RPA

Fig. 16 The Effect of a Shield Obscuring the Orifice of an Operating Hollow Cathode from the RPA

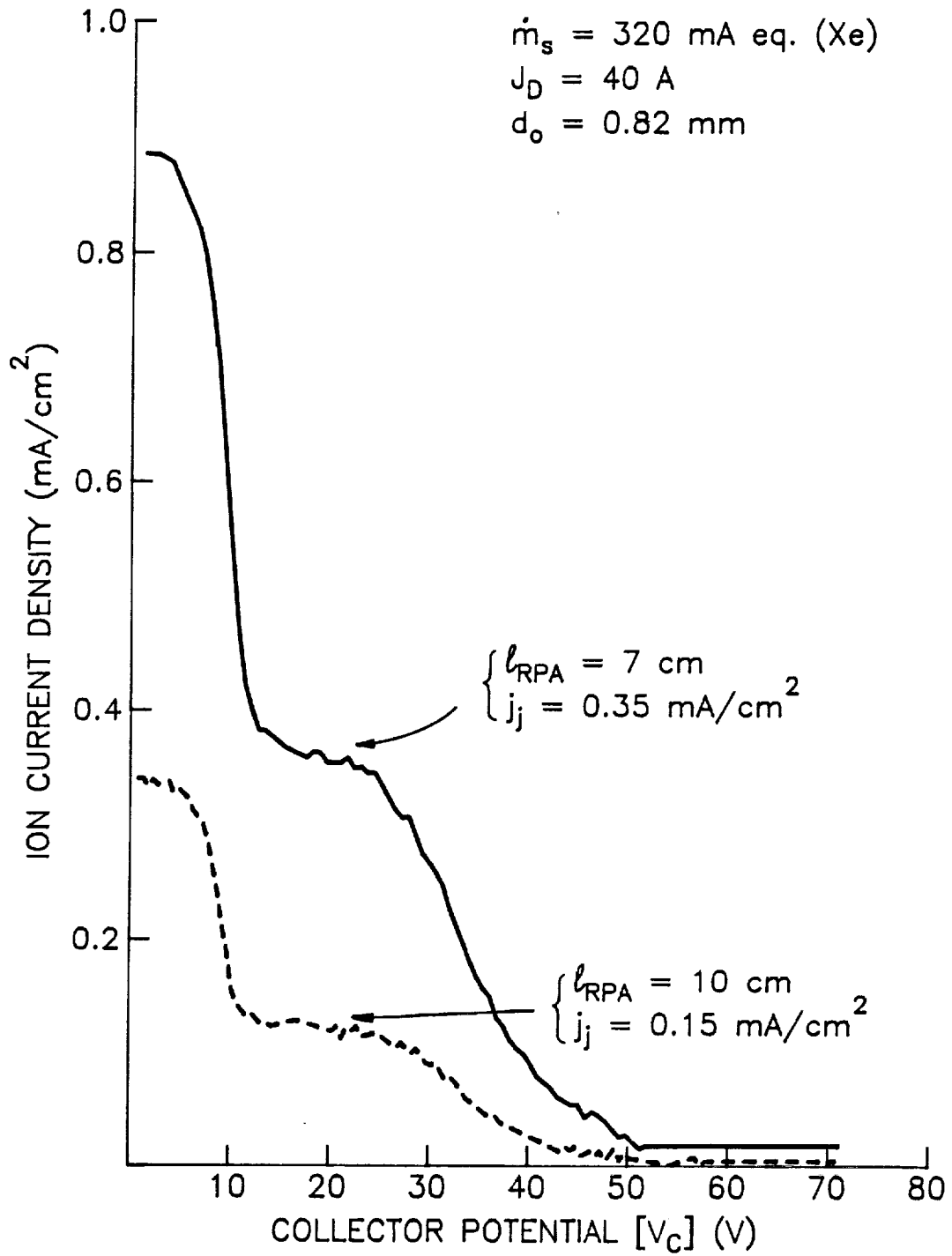


Fig. 17 Effect of RPA Axial Position on its Output Trace

the probe vary as a function of its axial position, the relative energy distribution of these ions does not.

The effects of discharge current, propellant flowrate and cathode geometrical factors on the energy characteristics of jet ions produced near a hollow cathode can be presented more concisely in terms the mean energy ($\langle \epsilon \rangle$) and energy spread (ϵ_s) parameters defined in the Procedure Section of this thesis. When the mean energy and energy spread of the ions are plotted as functions of discharge current and flowrate, results like those shown in Fig. 18 are obtained. They show that increases in discharge current and decreases in flowrate cause both the mean energy and energy spread of the jet ions to increase. In Fig. 19, the effect of flowrate on jet ion current density is shown to be small, but an increase in discharge current is shown to cause this current density to increase dramatically above a threshold level that appears to be between 10 and 20 A.

The effect of flowrate on the mean energy and energy spread of the jet ions is shown in Fig. 20 for three different orifice diameters. The effect of flowrate on both parameters is similar, namely the lower the flowrate through the cathode, the higher the mean jet ion energy and the greater the energy spread. Increases in flowrate appear to cause both parameters to decrease to values that are determined by the orifice diameter. If one assumes that high energy ions are being produced just downstream of the cathode orifice, then it would be reasonable to assume further that these ions leave the region of creation in all directions. If this is the case, then the data of Fig. 20 would also suggest that cathode and keeper erosion

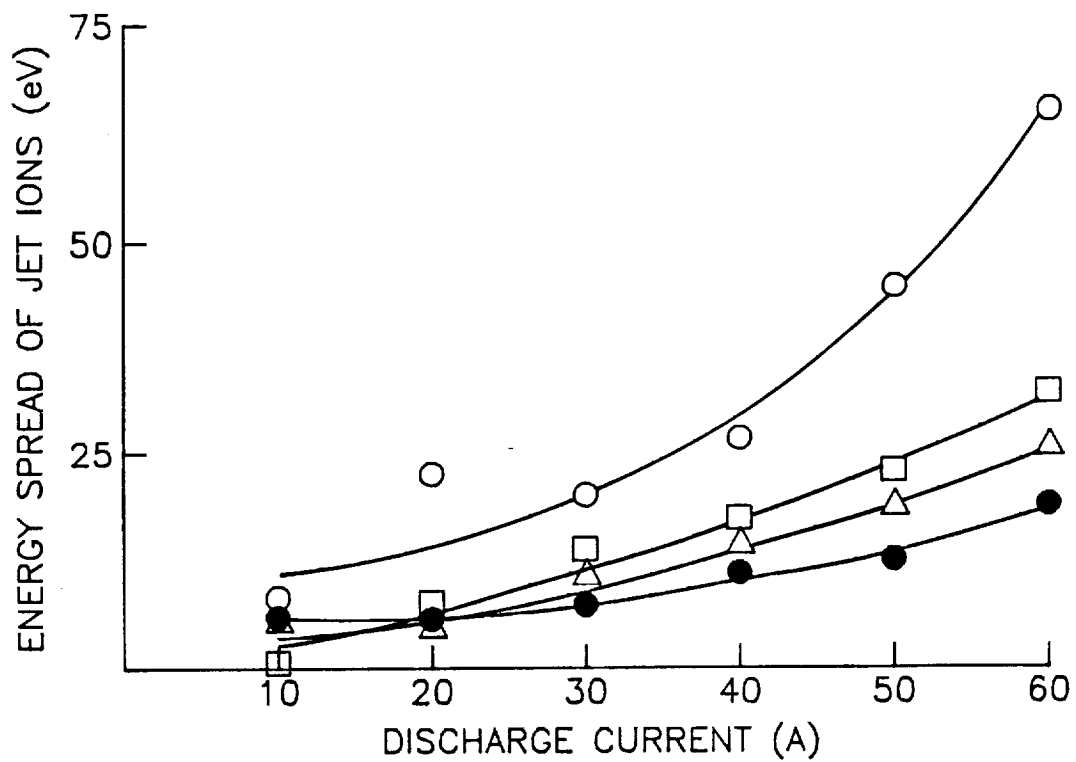
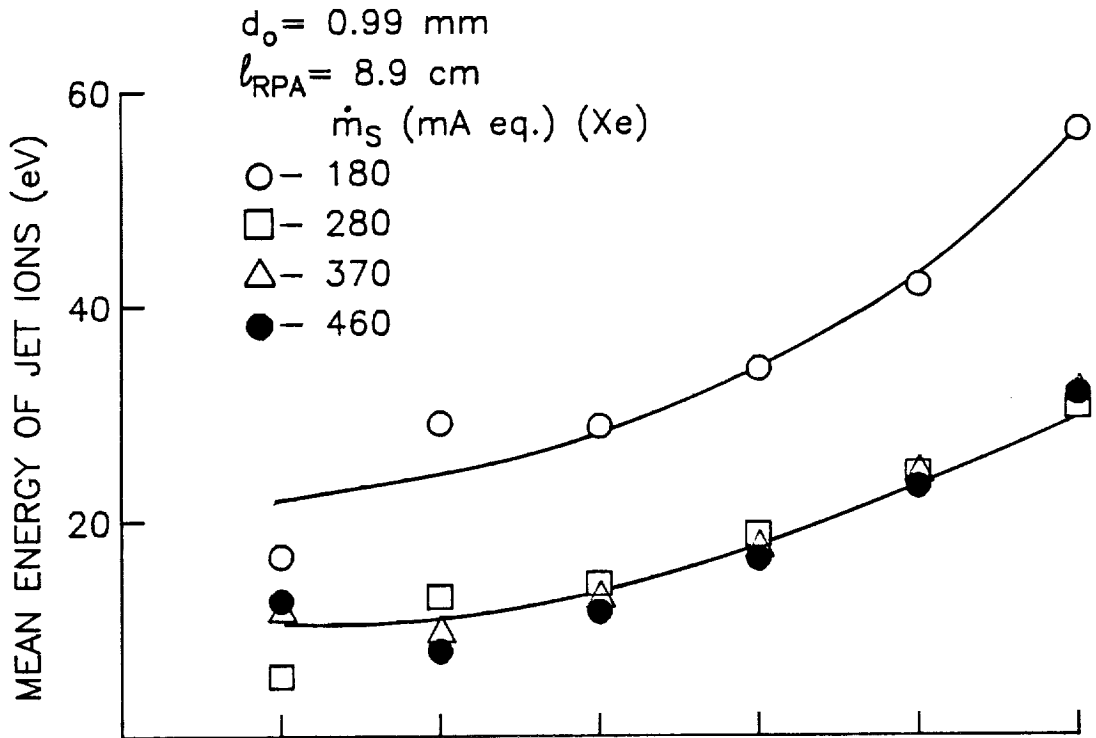


Fig. 18 Effects of Discharge Current and Flowrate on the Energy Characteristics of Jet Ions

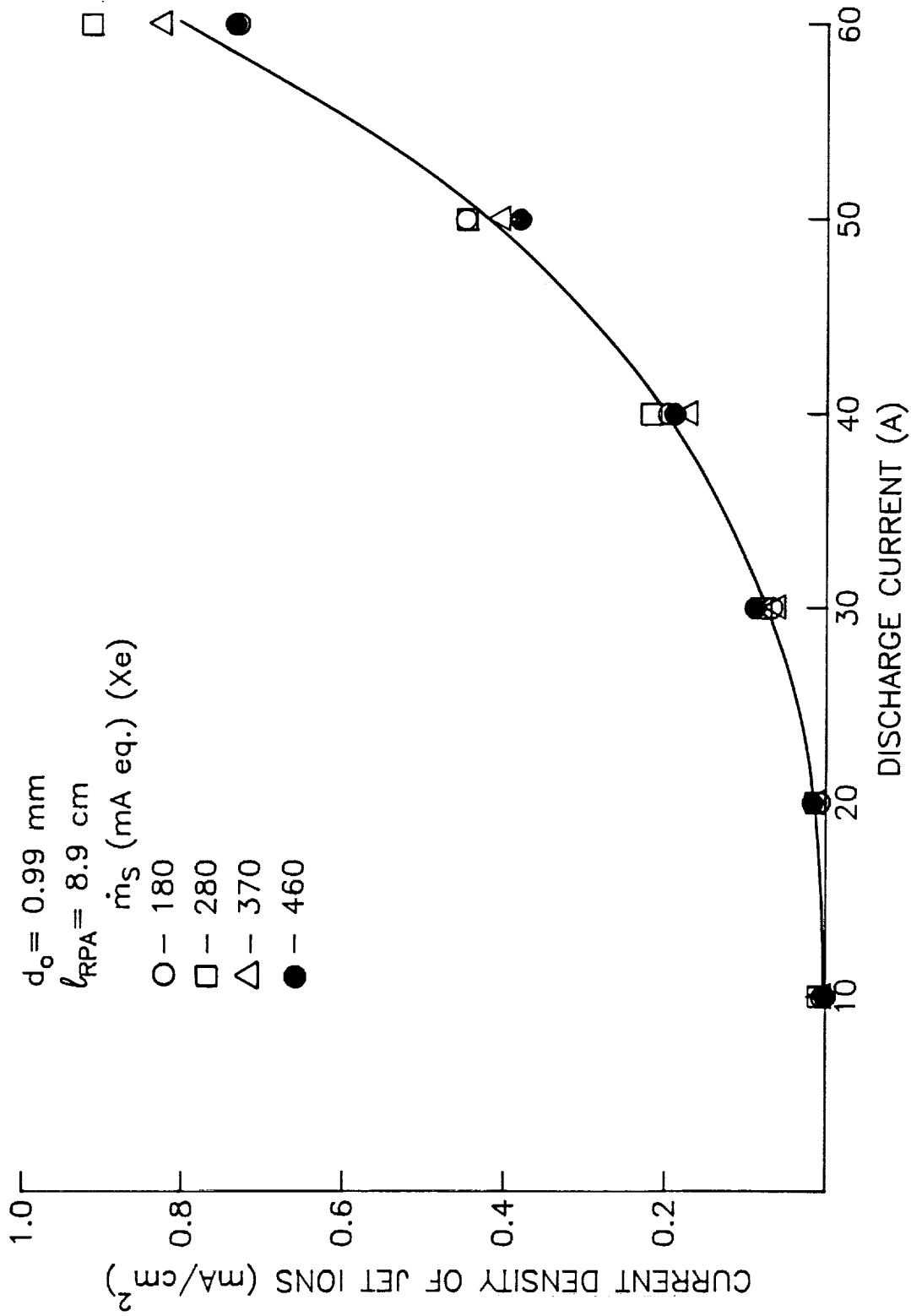


Fig. 19 Effects of Discharge Current and Flowrate on the Current Density of Jet Ions

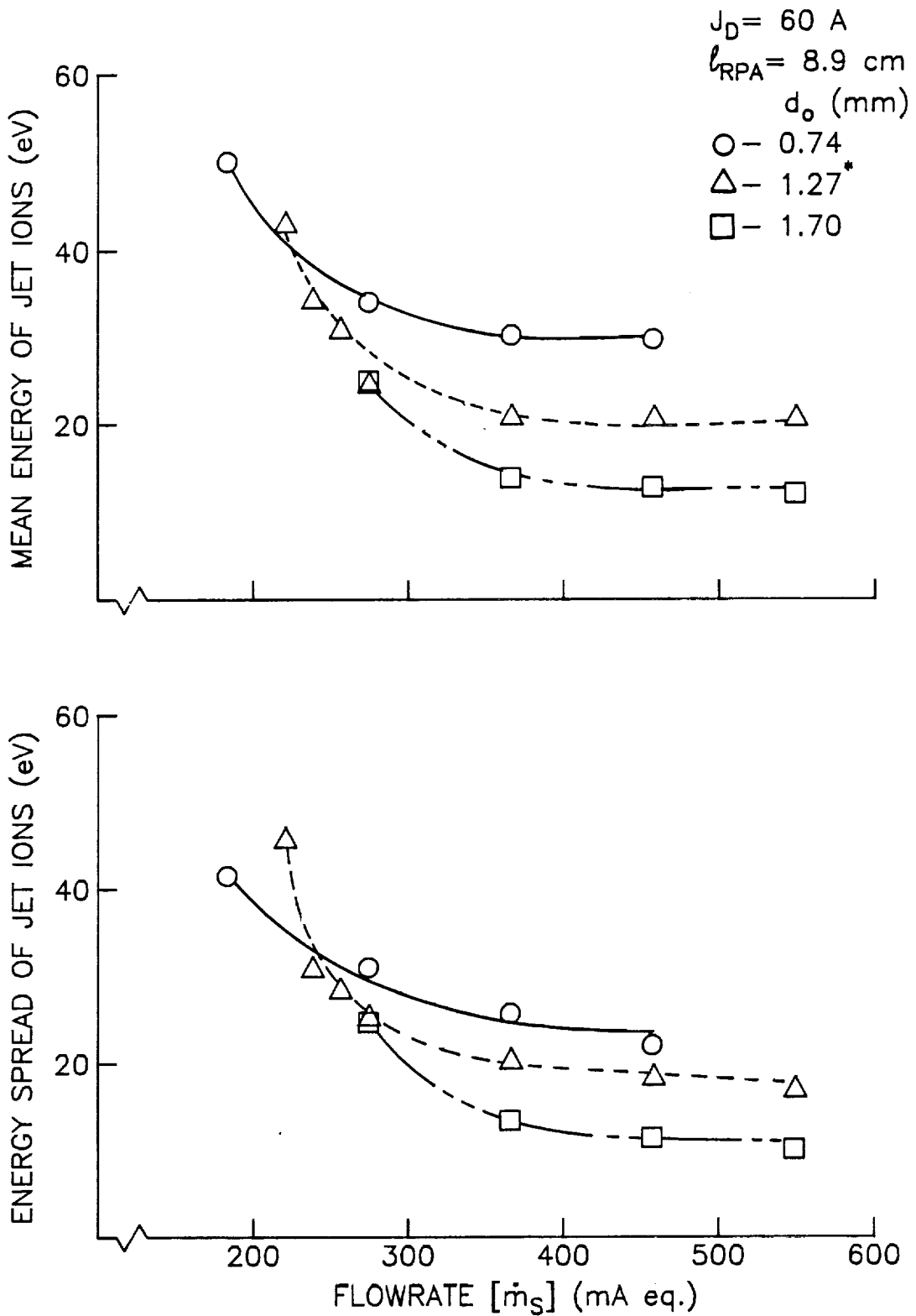


Fig. 20 Effects of Flowrate and Orifice Diameter on the Energy Characteristics of Jet Ions (* designates cathode with 12.8 mm tube diameter)

should increase as cathode flowrate is reduced below a threshold value. Kaufman [21] has suggested that this trend is observed in a substantial body of experimental data.

At a given discharge current, the jet ion current density was observed to remain relatively constant over the ranges of flowrate and orifice diameter indicated in Fig. 20. It is also noteworthy that increasing the cathode tube diameter from 6.4 mm to 12.8 mm (the $d_o = 1.27$ mm data) does not appear to affect the energy characteristics of the jet ions.

Taken together, the results of Figs. 15 through 20 show that high energy (jet) ions are produced in hollow cathode discharges, that the energies of these ions, which are assumed singly charged, are sufficient to induce sputter erosion at an appreciable rate and that both the current densities and energies of these ions increase dramatically with discharge current. The energy characteristics of the jet ions are dependent on the flowrate and orifice diameter. In these tests, the jet ion measurements were made only on the cathode centerline so the extent to which these ions diverge is not certain. On the basis of erosion patterns observed by other researchers conducting life tests [12,19], however, it is argued that the jet of ions is, in contrast to the well-collimated electron jet, very divergent (expansion through 2π steradians is, in fact, considered likely).

In another series of tests, the keeper was modified so it could be moved axially while the cathode was being operated. These tests showed that axial movement of the keeper did not affect the energy distribution of the jet ions, but it did affect their current densities on centerline. This latter effect is illustrated by the

data of Fig. 21 which show that progressively higher current densities were measured on the cathode centerline as the keeper was moved further from the cathode and that they were a maximum when the keeper was removed. These data are interesting because they suggest that jet ion current densities can be influenced by the keeper. This in turn suggests that it might be possible to limit sputter erosion effects by positioning and operating it properly. It could be, however, that changing the keeper position simply causes a fraction of the ions that were being focused along the centerline to be redirected along other paths.

Effect of the Cathode Insert

The cathodes used in the experiments described thus far contained rolled tantalum foil inserts. Typical ion thruster hollow cathodes, on the other hand, utilize impregnated, sintered tungsten inserts. The effect of changing the insert on the experimental data was investigated in a series of comparative tests conducted using the hollow cathode with the 0.82 mm orifice diameter and radiation fin. The effect of this change on discharge and keeper voltages measured as a function of discharge current is shown in Fig. 22. These data indicate the rolled foil insert may cause the discharge voltages to be slightly lower but this change is probably within the range of scatter associated with the exchange of inserts of like kind. Figure 23 shows that the insert change did not induce any significant change in the centerline plasma properties. Finally, the effects of changing the insert on the characteristics of the jet ions are shown in Figs. 24 and 25. While these data do show differences in the results obtained with the two inserts, they are generally small and they are also

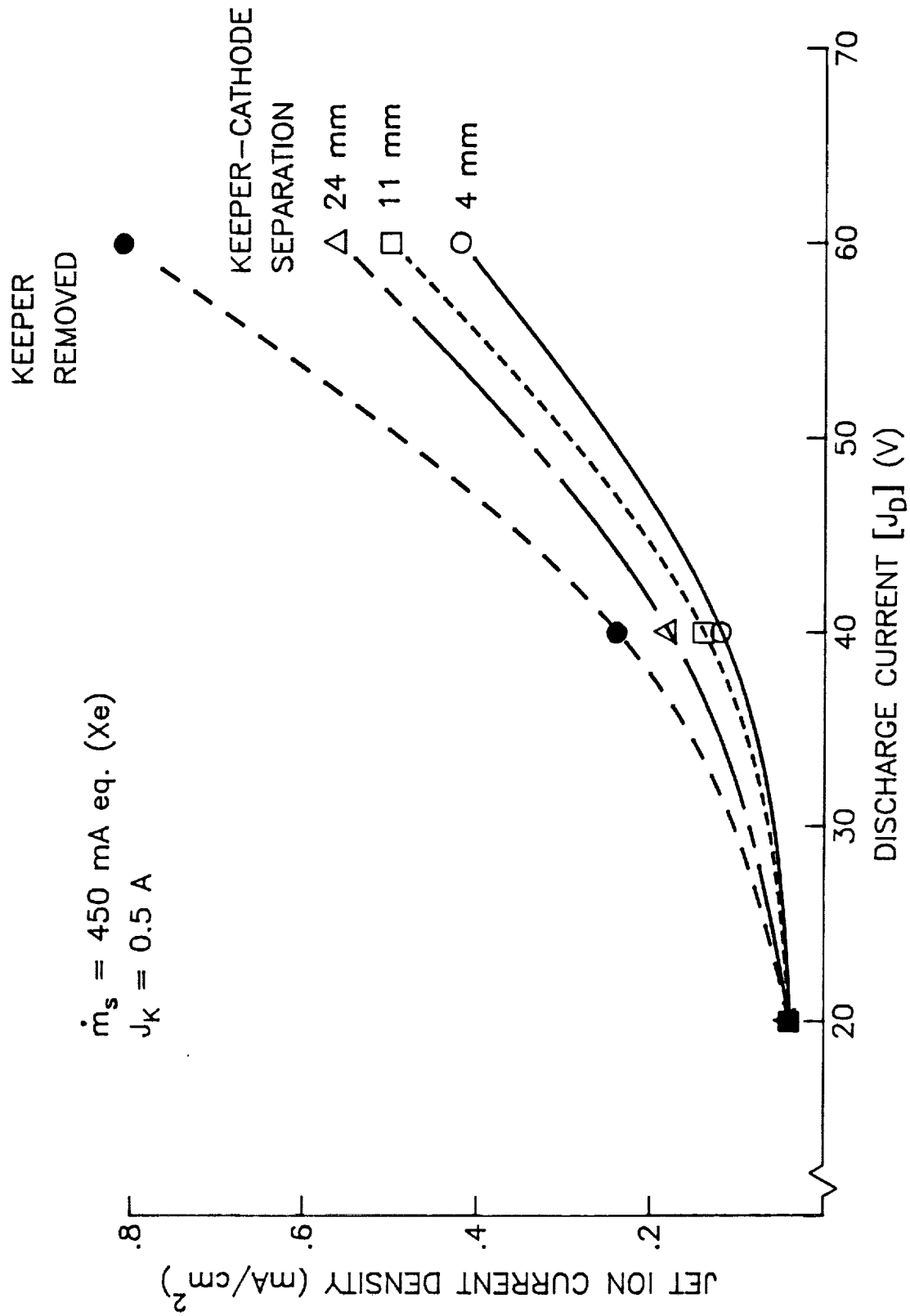


Fig. 21 Effect of Keeper Position on Jet Ion Current Density

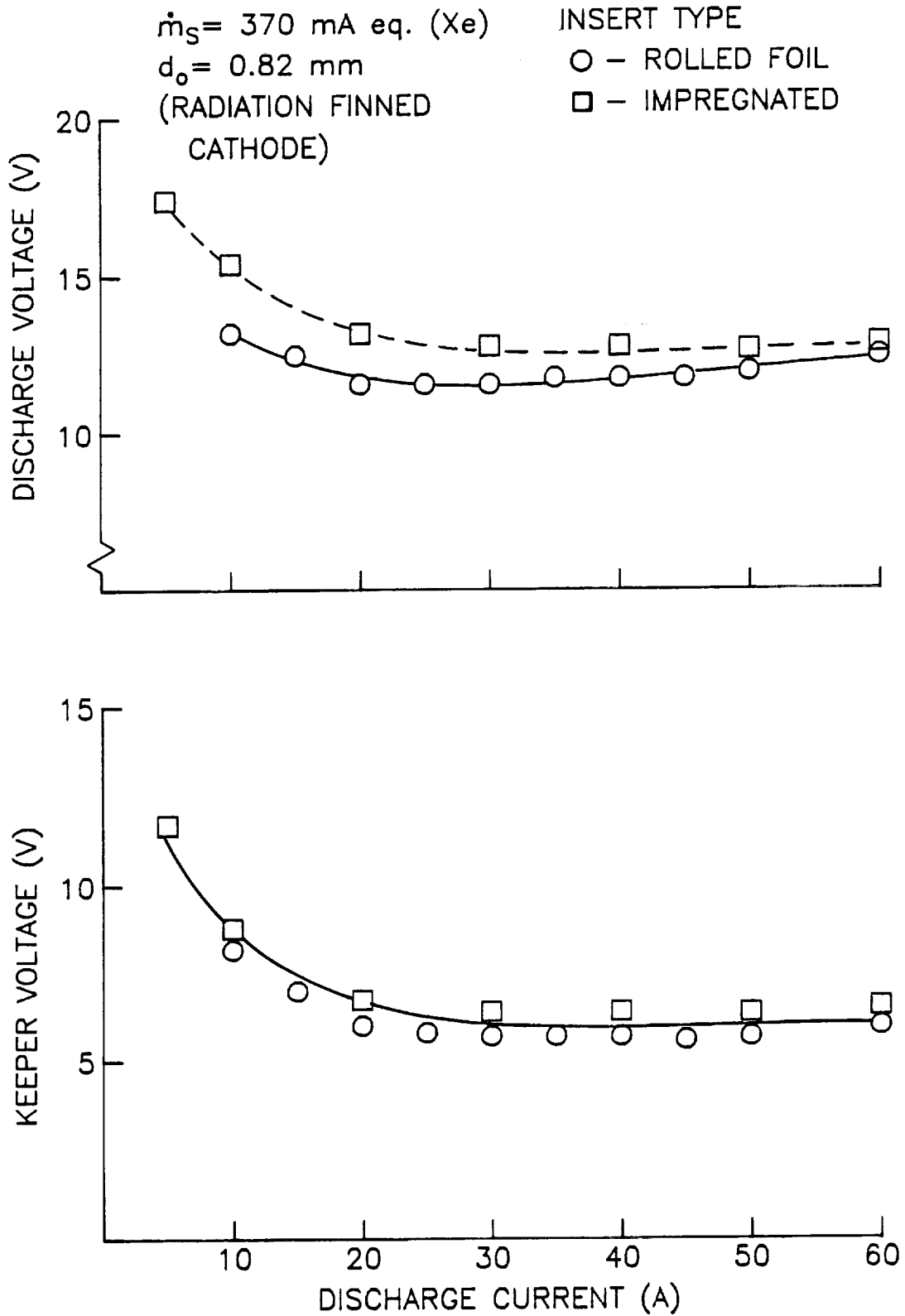


Fig. 22 Effect of Insert Type on Current Voltage Characteristics

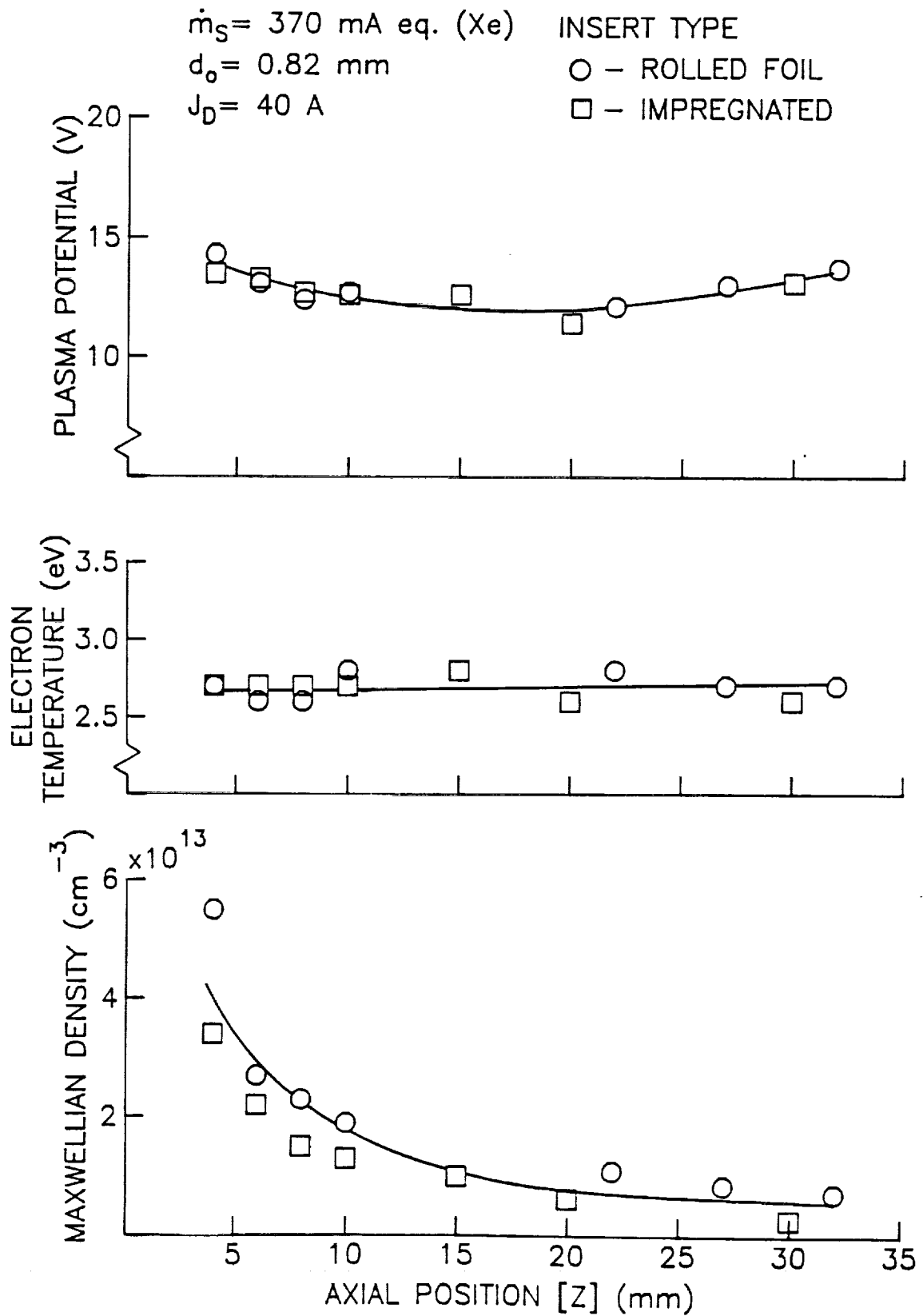


Fig. 23 Effect of Insert Type on Plasma Property Profiles

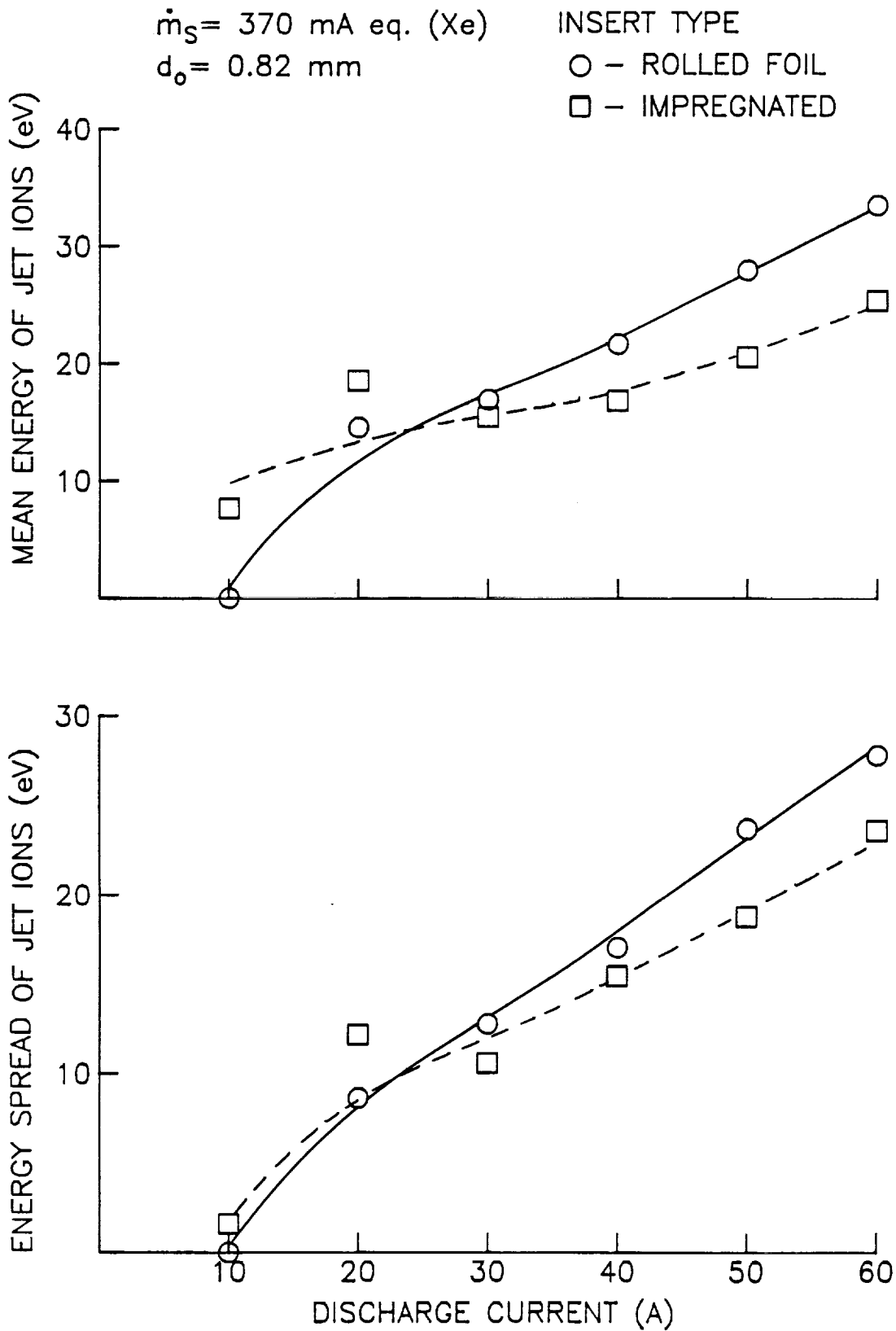


Fig. 24 Effect of Insert Type on the Energy Characteristics of Jet Ions

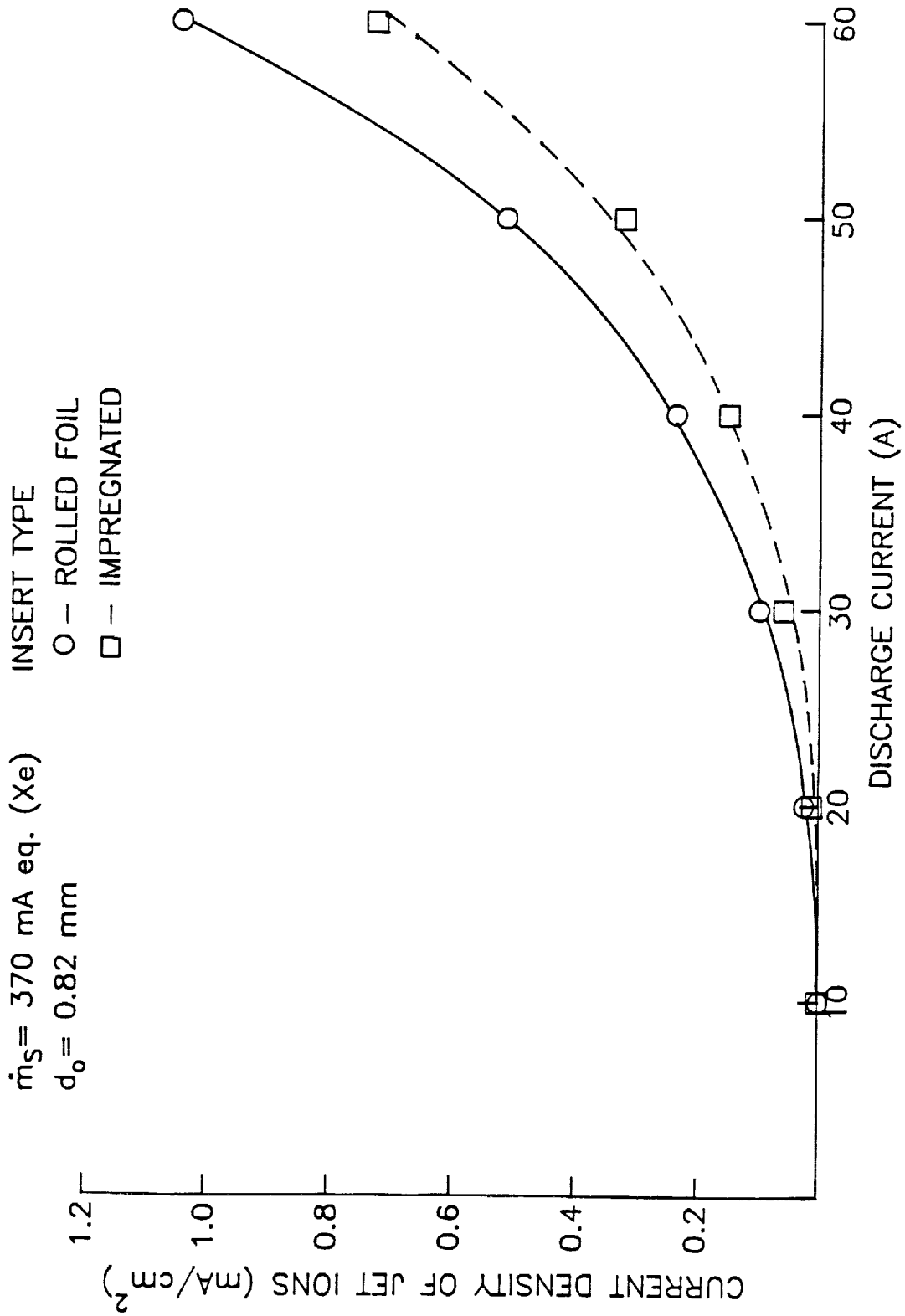


Fig. 25 Effect of Insert Type on Jet Ion Current Density Data

considered to be within the limits of experimental error. If there is a trend, it is for the jet ion energies and current densities to be slightly lower when the impregnated insert is used.

Effects of the Ambient Magnetic Field

The data concerned with the characteristics of the jet ions presented to this point in the thesis were all collected in the natural 0.4 gauss transverse magnetic field environment because it was experimentally convenient. Because the hollow cathode is in an axial magnetic field environment in a typical ion thruster, however, it is important to demonstrate the effect of an axial field on the experimental results. The tests designed to investigate this effect were conducted on the cathode with 0.82 mm diameter orifice operating with an impregnated, sintered tungsten insert. They involved changing from the 0.4 gauss transverse to the 30 and 60 gauss axial magnetic field environments (see Fig. 3) and measuring the resulting changes in operating, ambient plasma and jet ion conditions. Since both magnetic field and discharge current could be changed and data could be collected rapidly, the comparative validity of the data is high.

Keeper and discharge voltage were observed to remain essentially unchanged when the ambient magnetic field environment was altered. On the other hand, the centerline plasma density (bottom plot of Fig. 26) typically increased with the axial magnetic field strength, while the electron temperature (middle plot of Fig. 26) and plasma potential (upper plot of Fig. 26) remained unchanged.

Changes in the ambient magnetic field induced negligible changes in the various parameters that characterize the jet ions. This observation is demonstrated by the close proximity of the data points

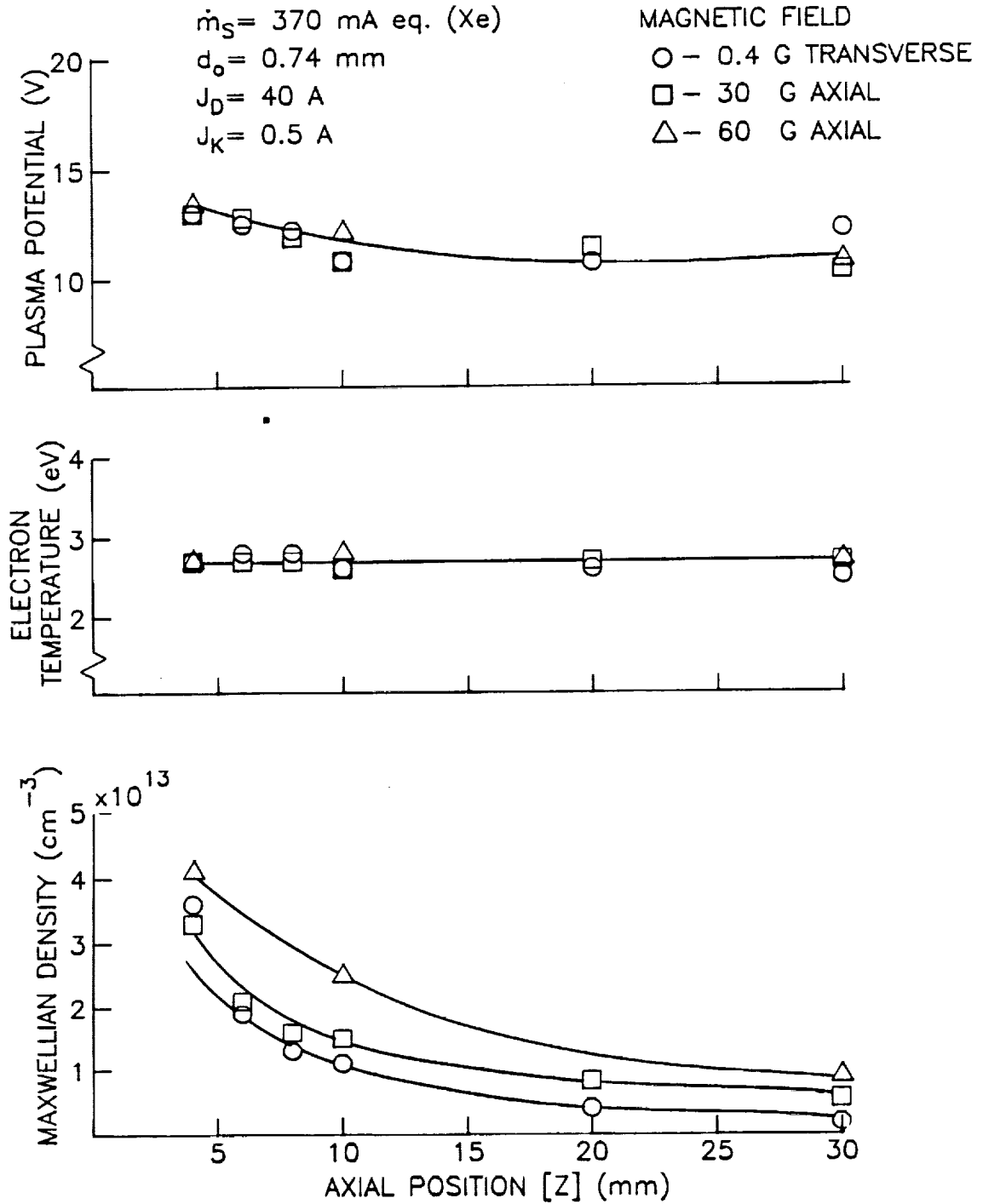


Fig. 26 Effect of Magnetic Field Environment on the Properties of the Plasma Downstream of a Cathode

associated with each discharge current in Figs. 27 and 28. The fact that the jet ion current density is not affected by changing the magnetic environment from a 0.4 gauss transverse to 30 and 60 gauss axial is initially quite surprising in view of the fact that such changes cause the high current density electron jet (as detected from luminosity and Langmuir probe measurements) to change from one of upward curvature to one coincident with the centerline (compare Figs. 10 and 12a). Taken together these observations lead one to conclude that there are two jets; one that is luminous and well-collimated contains the high energy electrons and the other that is neither luminous nor well-collimated contains the high energy ions. When the null or axial fields are applied, both have a common centerline. When the 0.4 gauss transverse magnetic field is applied, the luminous electron jet curves but the divergent trajectories of the more massive ions are not affected significantly.

Figure 29 shows that increases in the axial magnetic flux density cause the ratio of jet-to-total ion current density to decrease. Since the jet ion current density does not change (Fig. 28), this implies the ambient ion current density increases with magnetic flux density. This result is consistent with the idea that the 0.4 gauss transverse field causes the luminous electron jet (in which the ambient plasma density is higher) to curve while the ion jet remains essentially unchanged. It is noted that application of the axial magnetic field caused the collimated electron jet to be focused onto the RPA aperture and this in turn caused it to indicate inaccurate ion collection currents. This occurred because excessive numbers of jet electrons began to penetrate the Faraday screens on the RPA, to reach

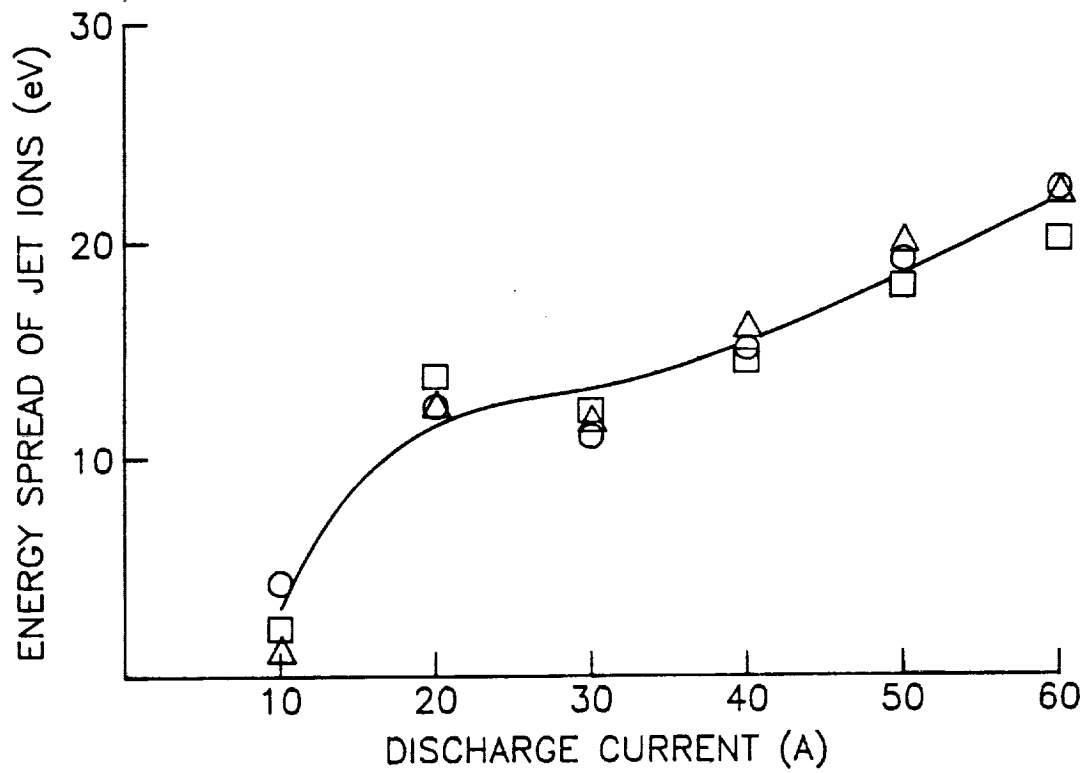
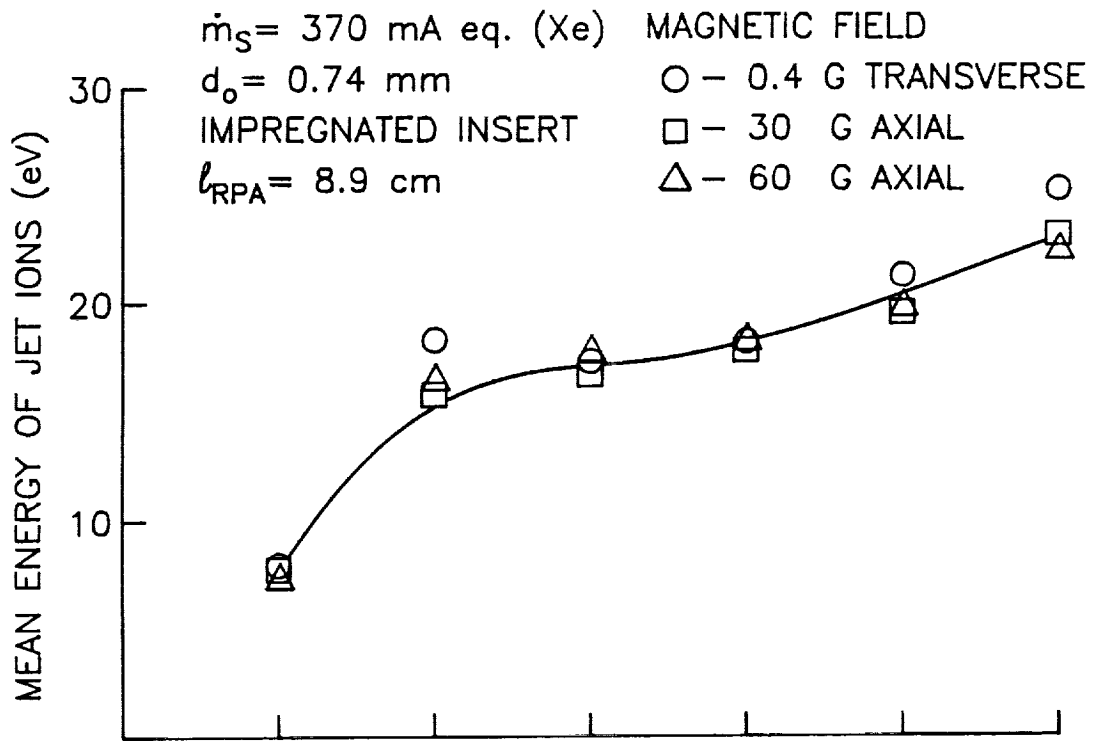


Fig. 27 Effect of Magnetic Field Environment on the Energy Characteristics of the Jet Ions

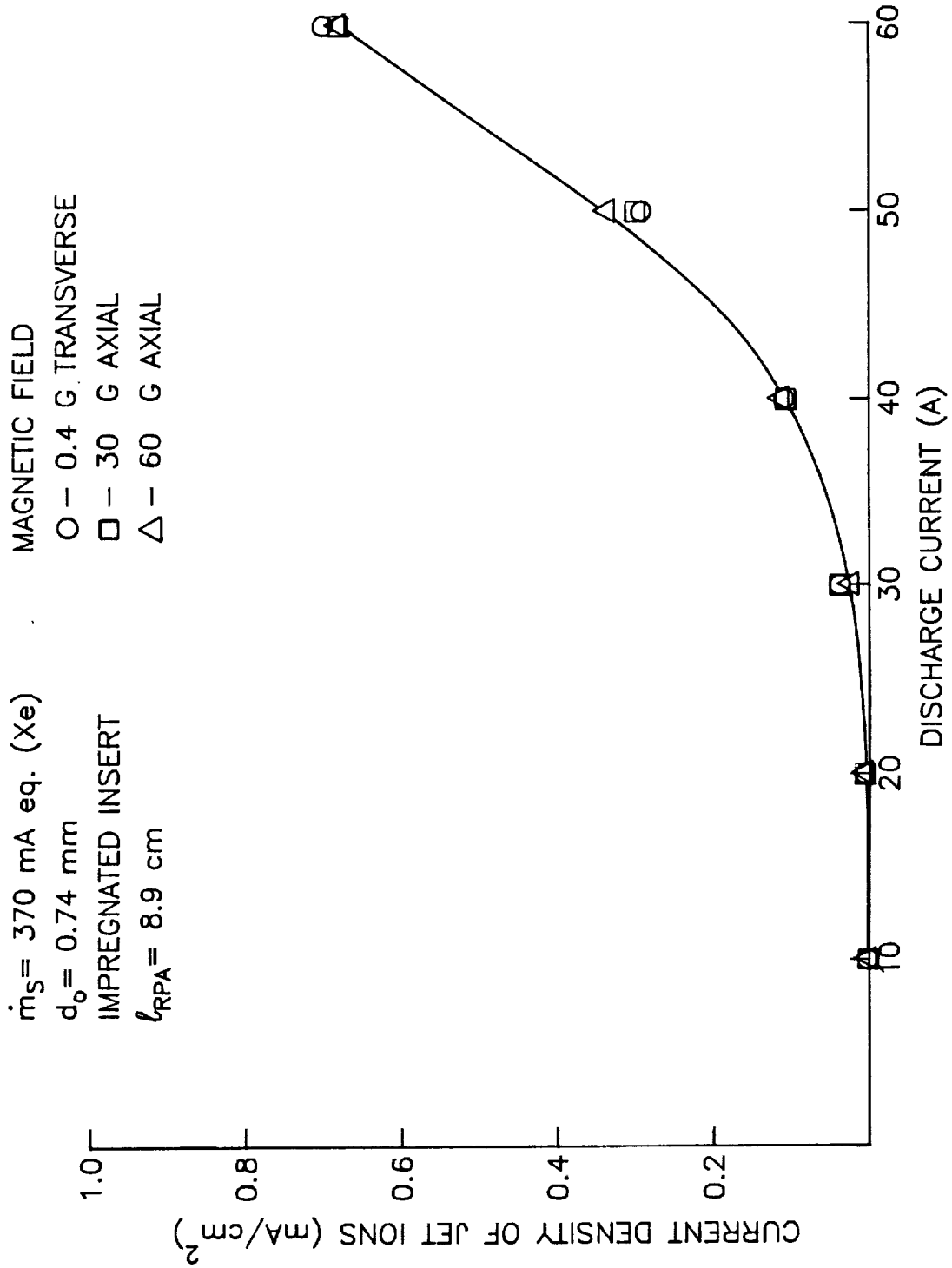


Fig. 28 Effect of Magnetic Field Environment on Jet Ion Current Density Data

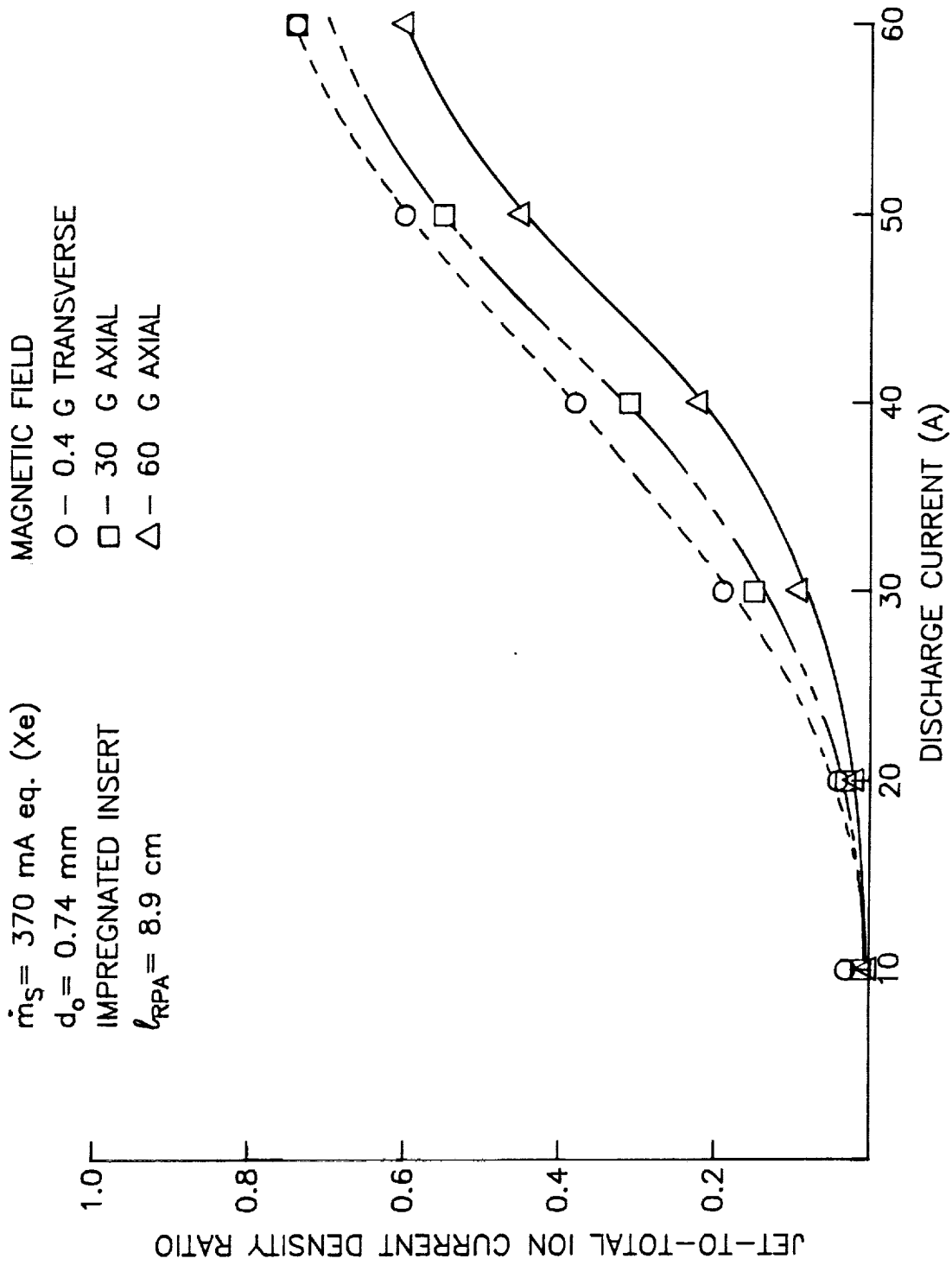


Fig. 29 Effect of Magnetic Field Environment on the Jet-to-Total Ion Current Density Ratio

the collector and to thereby introduce errors. In order to prevent this problem, the RPA had to be positioned off-centerline so the luminous jet would strike it at least a few millimeters from the aperture when the cathode was being operated at high discharge currents.

Plasma Noise Considerations

Data presented in preceding sections show that high energy ions are present in the plasma downstream of the cathode and it has been suggested that they could be produced in a region of high positive potential located near the cathode orifice. This could be either a region of steady, high positive potential, or one in which the potential oscillates periodically to high values. If the mechanism of production involved potential oscillation and the amplitudes of the oscillations close to the cathode were sufficient to produce ions with the high energies that have been observed, then it is considered likely that significant noise would be observed in the ambient plasma downstream of the cathode. The plasma noise was measured using a Langmuir probe biased near plasma potential and located a few centimeters from the cathode orifice. The ratio of the rms probe current fluctuation to the mean probe current was measured using an oscilloscope (0 - 5 MHz bandwidth) and was found typically to be less than 10%. Probe current fluctuation ratios of this magnitude observed by other researchers near a region of potential variation in a plasma have been related to the occurrence of the ion-acoustic instability [22] and it may be this instability that is inducing the noise that is measured. Since the ratio of the turbulent energy in the plasma to its total internal energy is approximately equal to the square of the

probe current fluctuation ratio (i.e. ~1%), it is argued that the plasma is relatively quiescent [23] (i.e. potential fluctuations with amplitudes no more than a few volts are occurring). Because of this, it is considered unlikely that a region exists in which plasma potentials fluctuate with sufficient amplitude to induce the high energies that have been observed in the jet ions.

Temperature Effects

As the discharge current being extracted from a hollow cathode is increased the current of ions striking the cathode insert and orifice plate surfaces also increases and as a result the input thermal powers and temperatures associated with these surfaces increases. These temperatures should be close to that at the interface between the cathode tube and orifice plate (the cathode wall temperature). The experimentally measured increases in cathode wall temperature with discharge current for five different cathodes are shown in Fig. 30. Changes in cathode flowrate induced no measurable changes in the temperatures, so the each data point shown corresponds to the average of temperatures measured at flowrates over a range from 180 to 550 mA eq. In general the curves show the expected trends; they all tend to level off at the higher discharge currents where radiative heat transfer from the orifice plate becomes substantial. The two higher curves suggest that an increase in orifice diameter may induce a slight decrease in cathode wall temperature. The lower curve shows the benefit of using a cathode with an oversized orifice plate and larger cathode diameter from which heat can be radiated to reduce the temperature. Also, in this same operating temperature range is the cathode with the largest orifice diameter. Figure 31 shows the effect

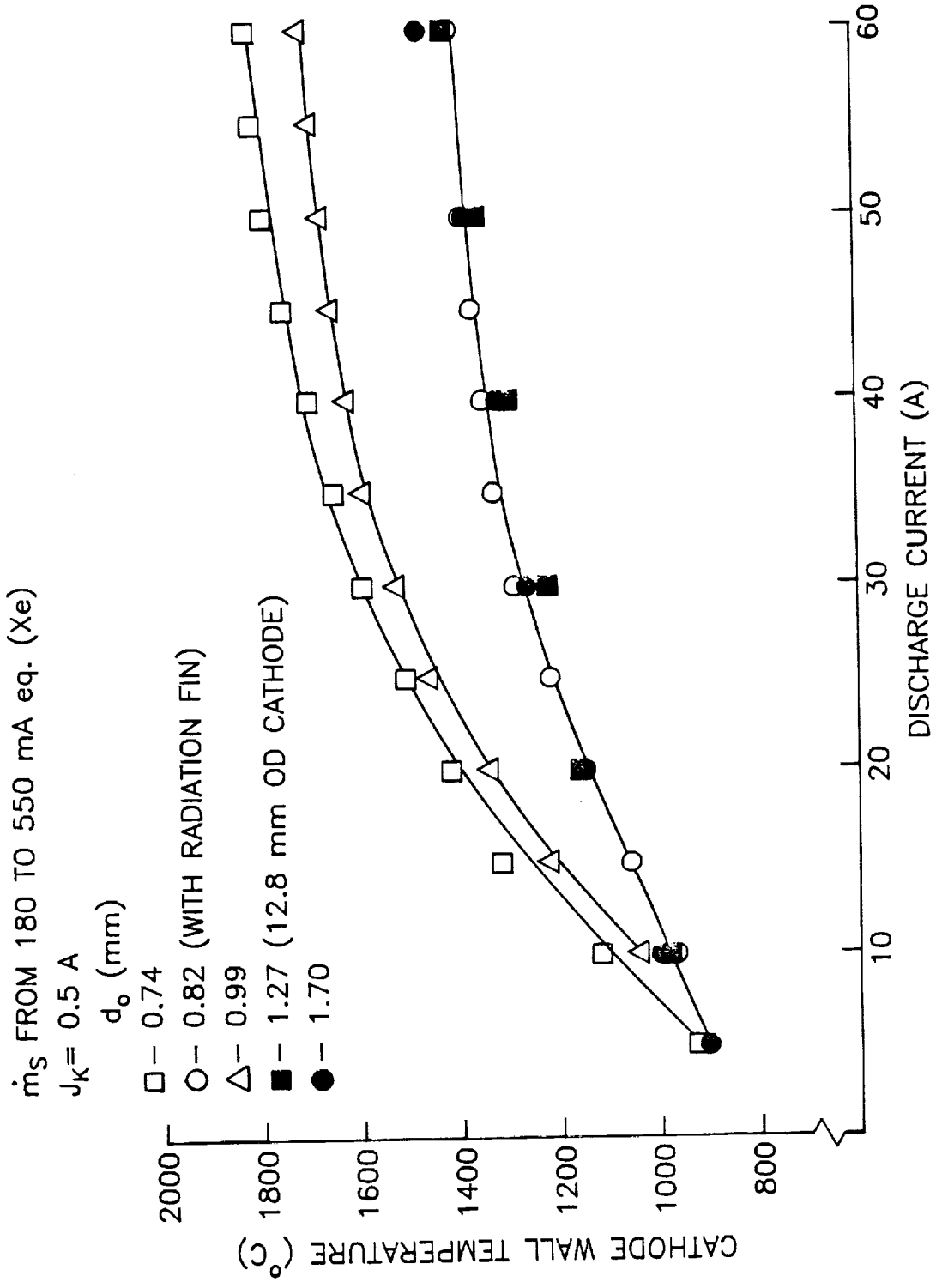


Fig. 30 Effects of Discharge Current and Cathode Configuration on Cathode Wall Temperature

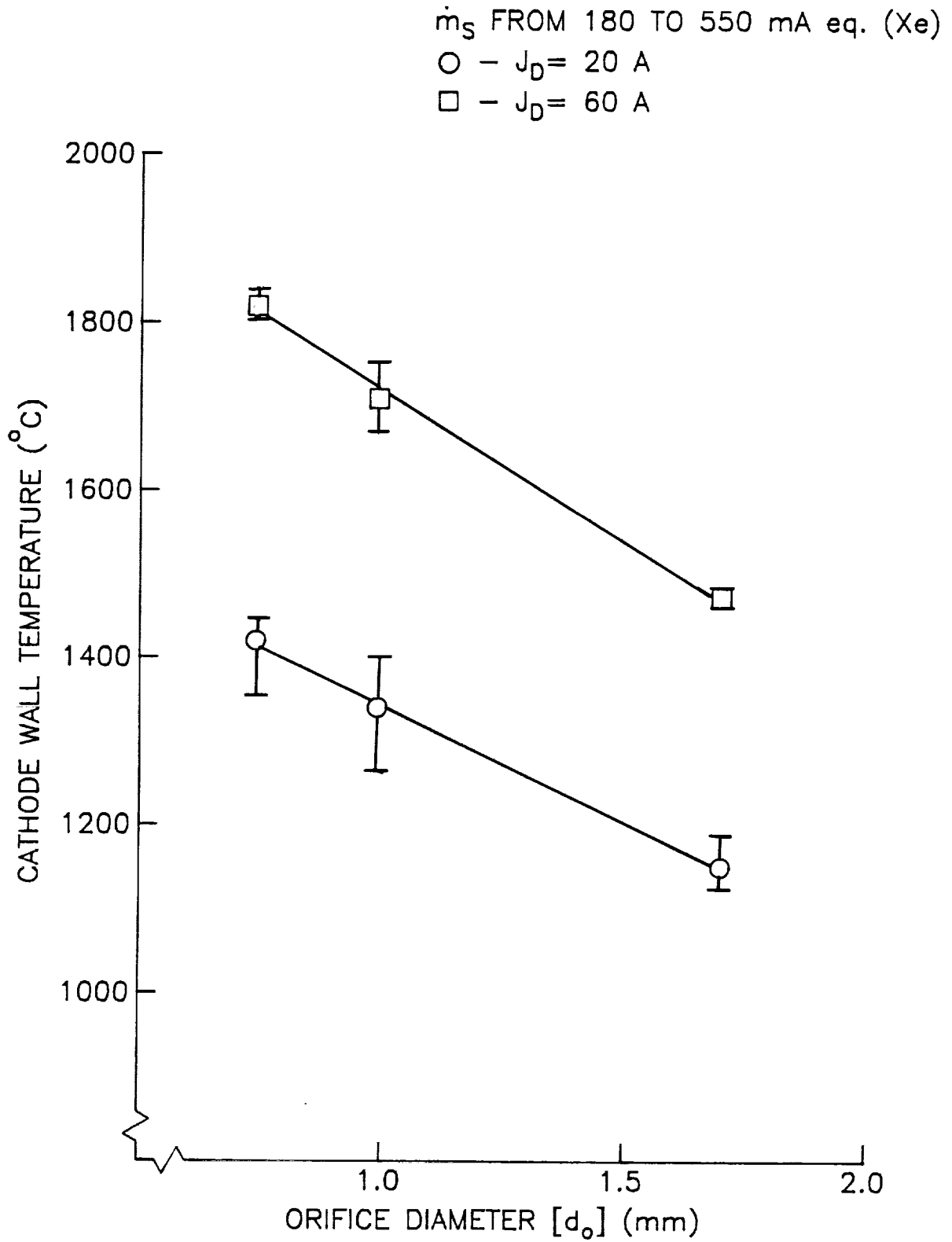


Fig. 31 Effect of Orifice Diameter on Cathode Wall Temperature

of orifice diameter on cathode wall temperature for two different discharge currents. The data in the figure are for cathodes with a common tube diameter (6.4 mm) and with no radiation fin. They clearly show a linear decrease in cathode temperature with increases in orifice diameter.

The magnitudes of the temperatures reached at discharge currents above about 10 A in Fig. 30 are considered excessive because they would induce rapid, low work-function material migration from the insert [14]. This would be expected to result in turn, in relatively rapid degradation of the insert and a short cathode lifetime. It is noted, however, that these temperatures could be reduced by redesigning the cathode to enhance radiative and conductive heat transfer from the insert and orifice plate where most of the heat is deposited. Accomplishing this is considered to be a straightforward thermal design problem.

A test was conducted in which the insert was changed from the rolled foil to the impregnated design to determine if this change would influence the cathode temperature. As the data of Fig. 32 suggest, it did not. Similarly, changes in the ambient magnetic field environment did not affect cathode temperatures significantly.

Flowrate/Pressure Correlation Study

A designer that can predict the pressure within a hollow cathode will be able to ensure it is in a range where emission from a small zone, attendant localized insert overheating and a shortened cathode lifetime are unlikely. Typical cathode internal pressures measured as a function of discharge current and propellant supply rate (\dot{m}_G) are shown in Fig. 33a for the cathode with the 0.74 mm dia orifice. As

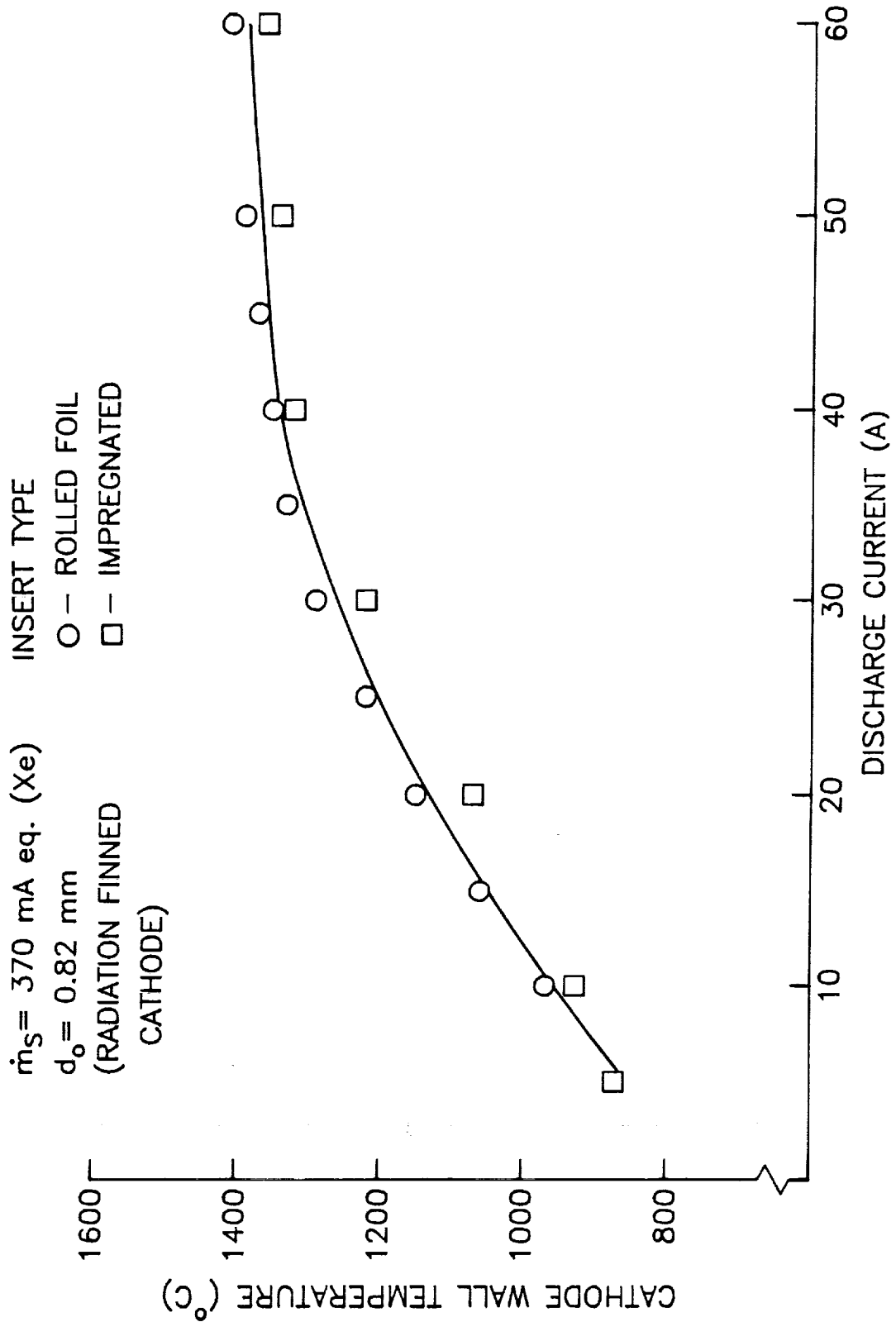


Fig. 32 Effect of Insert Type on Cathode Wall Temperature

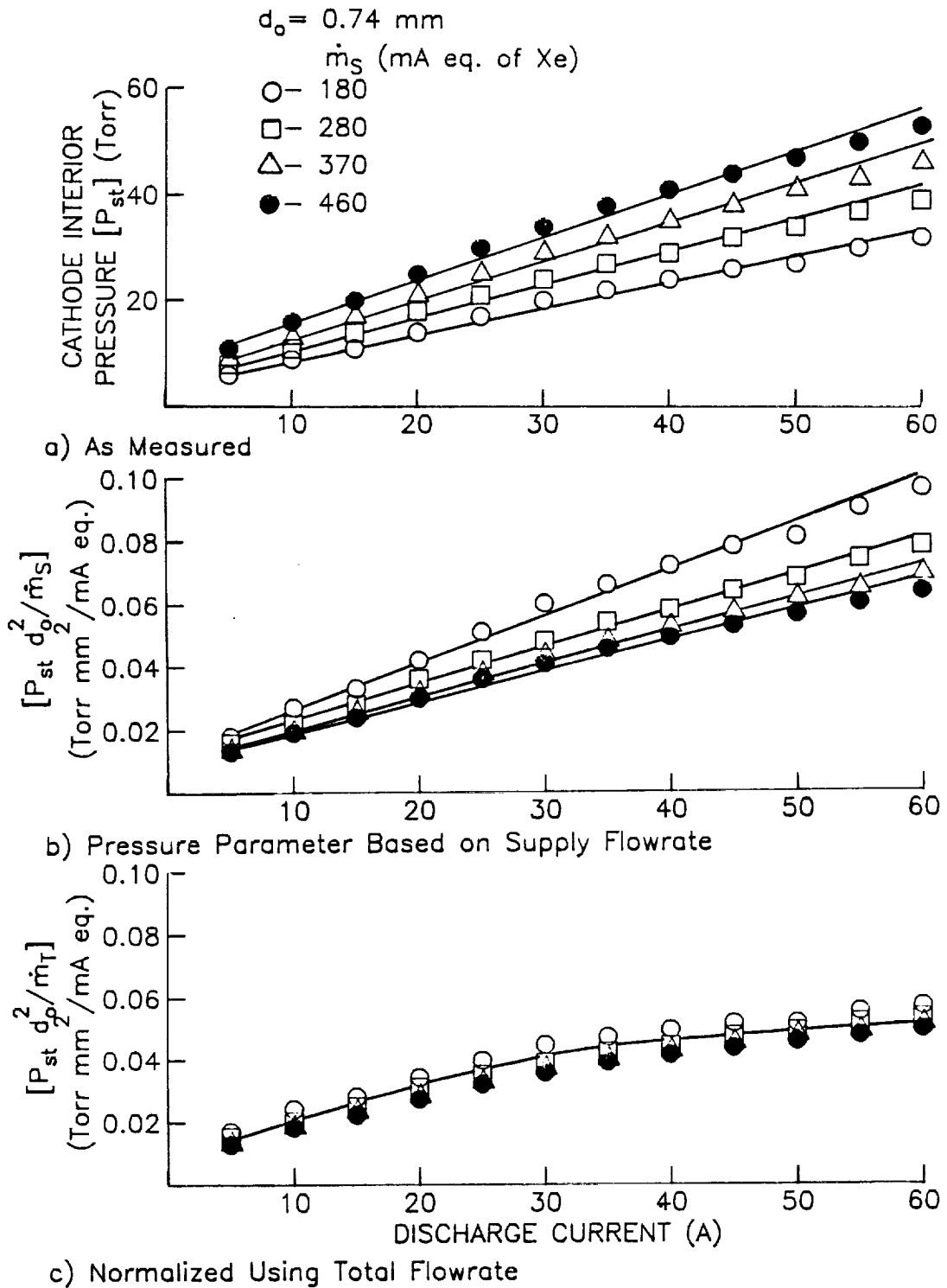


Fig. 33 Effects of Discharge Current and Propellant Flowrate on Cathode Internal Pressure

these data suggest, the pressure increases in approximately direct proportion to both the discharge current and flowrate. The data in this figure are striking because they suggest that pressures within this particular cathode reach 50 Torr at high currents and flowrates when values below 20 Torr are preferred. The calculated length of the electron emission region at 50 Torr is only a few tenths of a millimeter [6].

Siegfried [4] has pointed out that the stagnation pressure within the cathode (P_{st}) should be related to the cathode flowrate and orifice diameter by the equation:

$$P_{st} = \frac{C' \dot{m}_T \sqrt{T_{ni}}}{d_o^2} \approx \frac{C \dot{m}_T}{d_o^2} \quad (6)$$

where \dot{m}_T is the total flowrate of propellant through the orifice, d_o is the orifice diameter, T_{ni} is the temperature of the neutral atoms inside the cathode and C' and C are constants determined by the extent to which the flow is free molecular or continuum. A test was performed in which the cathode wall temperature of an operating hollow cathode was increased by 300 °C using the cathode heater and no change in cathode pressure was observed. Hence, it is argued that the temperature appearing in Eq. 6 has a modest effect, that it can be neglected in this analysis and that the approximate form of the equation can be used.

If one treats the supply rate of propellant into the cathode (\dot{m}_S) as the total flowrate of propellant through the orifice, Eq. 6 suggests the cathode interior pressure could be normalized to account for the effects of flowrate and orifice diameter using the parameter

$P_{st} d_o^2 / \dot{m}_S$. When this correlating parameter is applied to the data of Fig. 33a, the correlations shown in Fig. 33b are obtained. If this were a good pressure/flowrate correlating parameter, all of the data would be scattered about a common line. Because they are not, it is apparent that some correction, reflecting a physical effect that is being neglected, is needed. The correction needed can be understood if it is recognized that there is a flowrate associated with ions that are drawn backward through the orifice by the electric field that draws electrons forward through it. These backstreaming ions, which flow into the cathode interior at a rate \dot{m}_i must eventually leave as neutral atoms thereby contributing to the total flowrate through the orifice. Considering this correction, the total flowrate through the orifice becomes:

$$\dot{m}_T = \dot{m}_S + \dot{m}_i \quad (7)$$

The rate of ion backstreaming into the cathode, can be related to the total electron current flowing through the orifice (i.e. discharge plus keeper currents or emission current [J_e]) if it is assumed that the cathode is operating at the doubly space-charge limited condition [24]. At this condition, the current of backstreaming ions (J_i) is given by:

$$J_i = J_e \sqrt{\frac{m_e}{m_i}} \quad (8)$$

In this equation m_e and m_i are the electron and propellant ion masses, respectively. At each discharge current condition, the ion current

given by Eq. 8 is multiplied by 1000 so both the backstreaming ion flow and the supply flowrate will be in the same units (mA eq.) and they can be added to determine the total flowrate. When this total flowrate is used in place of the propellant supply rate to compute the correlating parameter, the data plotted in Fig. 33c are obtained. This plot shows reasonable scatter about a common line and this suggests that the dominant flowrate effects are now reflected properly in the pressure normalizing parameter.

When similar tests were conducted using cathodes having different orifice diameters, the data shown in Fig. 34 were obtained. In this figure each data point represents the average of pressure correlating parameters measured at the four flowrates indicated on the data in Fig. 33. These data are also considered to show a reasonable scatter about the mean line that has been drawn. This indicates that the pressure parameter also reflects the effect of orifice diameter properly. Additional tests were conducted at various ambient magnetic field conditions and with different cathode inserts. These changes did not influence the pressures or the pressure correlation results.

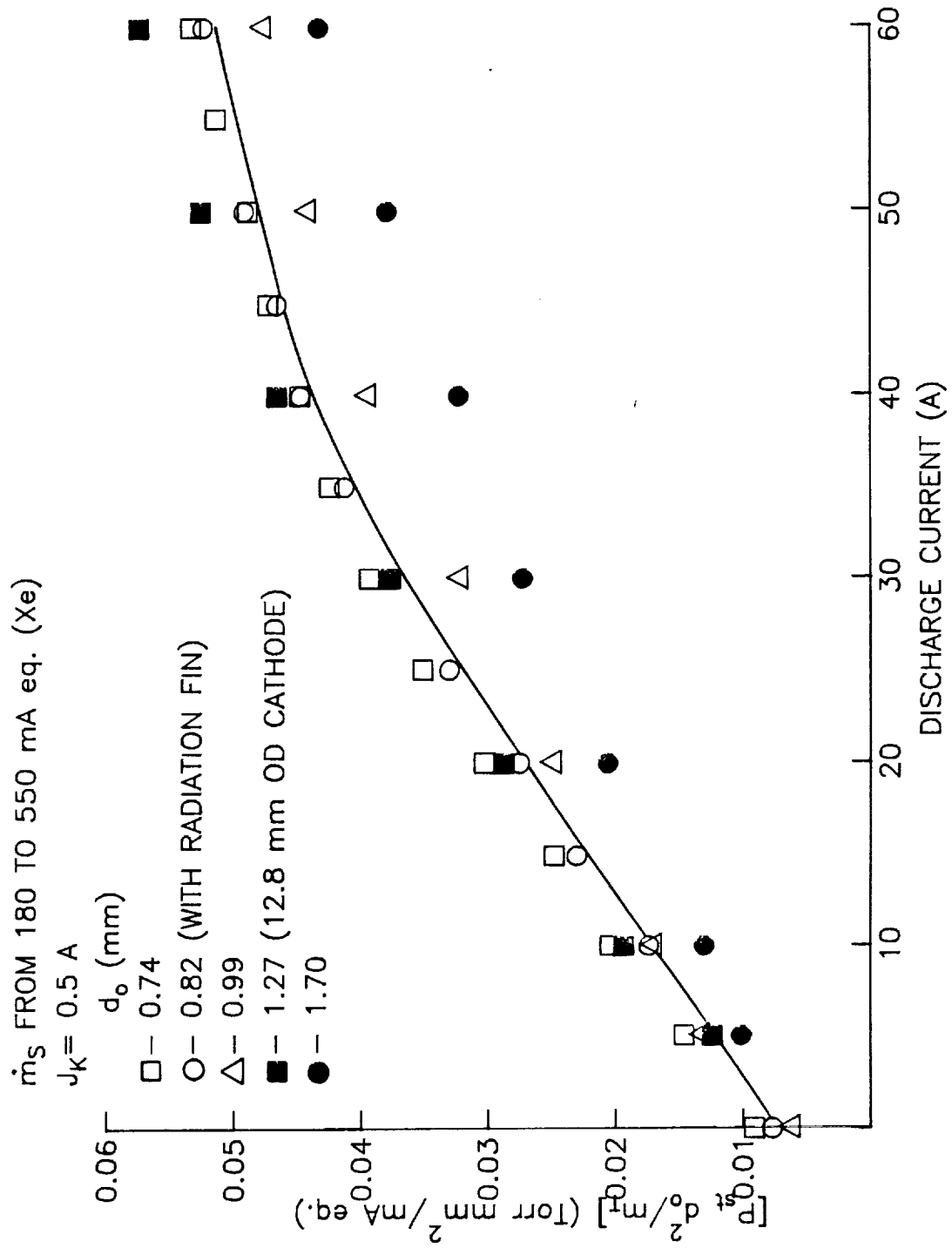


Fig. 34 Effect of Cathode Orifice Diameter on Normalized Pressure Parameter Data

IV. THEORY

A Model of High Energy Ion Creation

The data presented in this thesis have shown that ions with energies sufficient to induce substantial sputtering are produced in a hollow cathode discharge. A mechanism by which they could be produced has, however, not been suggested. The jet ion current data of Fig. 18 and 19, high erosion rates of the copper targets, and the evidence of rapid baffle erosion observed at high hollow cathode current levels suggest the existence of a population of ions with energies and current densities that increase with cathode current. It is not obvious, however, how such ions could be created in plasma environment where the maximum potentials measured in the plasma and on the anode are about 15 V. It would be expected that singly charged ions created in this environment would achieve a maximum kinetic energy of 15 eV as they were accelerated to a cathode potential surface and that doubly charged ones would reach 30 eV. Higher ion kinetic energies could develop only if the ions were created at a location where the plasma potential was substantially greater than the discharge voltage.

If a plasma potential profile like the one shown in Fig. 35 existed downstream of the cathode, it could explain the observed high energy ions and high sputter erosion rates. The potential would rise to maximum value near the cathode (the Langmuir probe data of Fig. 14a indicate it would be within 4 mm of it) before it dropped to a relatively constant downstream value. Langmuir has pointed out that such a potential hill can develop when high energy electrons are

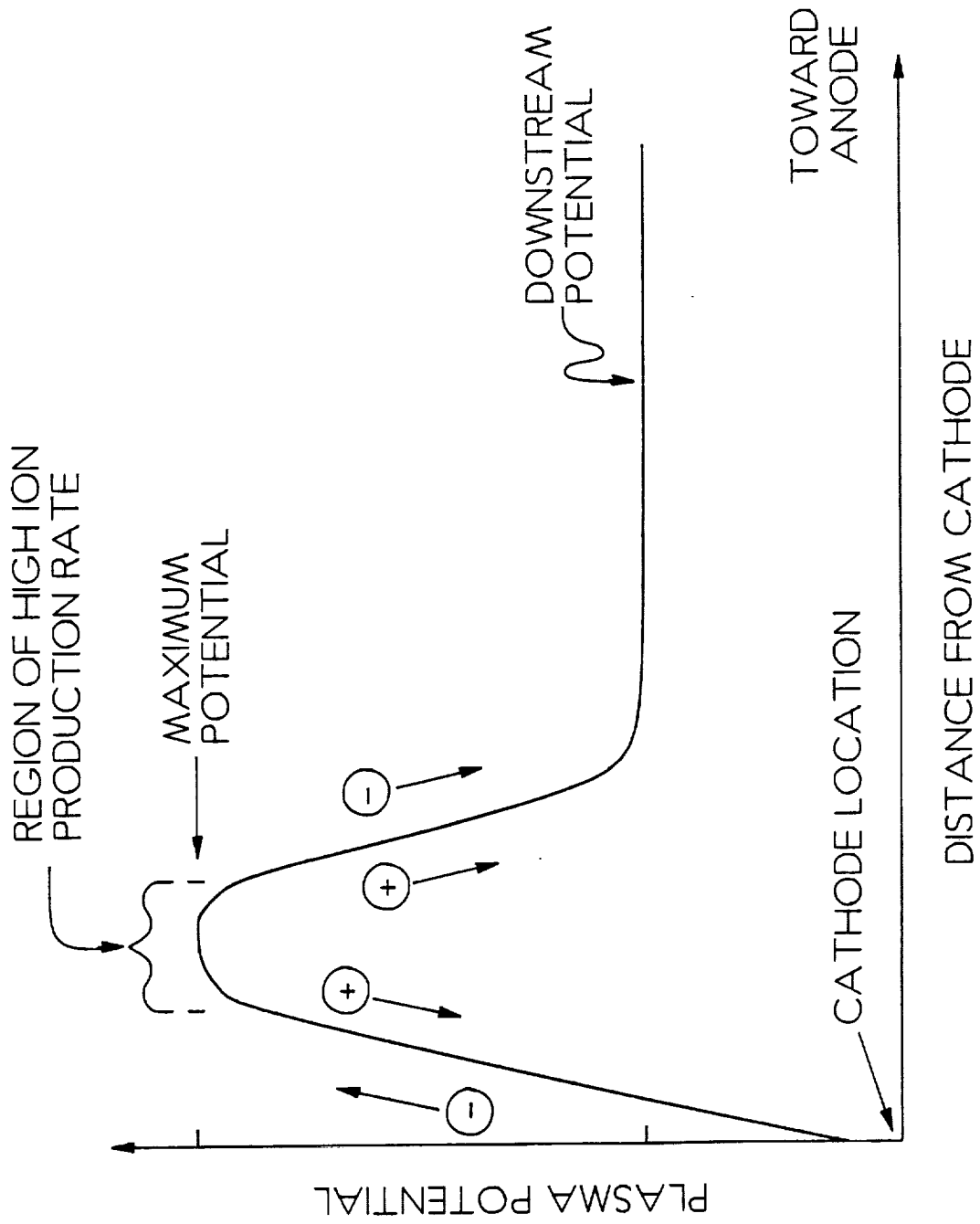


Fig. 35 Theoretical Plasma Potential Downstream of a Hollow Cathode

injected into neutral gas [24] as they are at a hollow cathode orifice. In fact Williams [25] has observed such a region of high potential immediately downstream of a hollow cathode emitting electrons in a hollow cathode plasma contactor experiment. The potential hill observed by Williams was measured at a low emission current (< 1 A) but the fact that it was observed at all demonstrates that potentials above anode potential can and do develop immediately downstream of a hollow cathode.

The physical mechanisms by which a region of high potential could develop can be understood by considering a jet of electrons being ejected out of a hollow cathode orifice through a plume of relatively high density neutral gas also coming through the orifice. It is postulated that electrons are accelerated to substantial kinetic energies as they pass through a double sheath [24] located at the downstream edge of the hollow cathode orifice. Evidence that such a sheath develops across the cathode orifice has been obtained at low discharge currents (< 10 A) where plasma property measurements could be made both upstream and downstream of it [16]. These data revealed that the substantial plasma potential, electron density and electron temperature differences suggestive of a double sheath do develop across the orifice.

Electrons accelerated through a double sheath could acquire the kinetic energy needed to ionize some of the neutral gas they pass through downstream of the double sheath. If one presumes the electrons gain kinetic energies significantly in excess of the ionization energy of the gas atoms, then the secondary and primary electrons coming out of the ionization event would also tend to have substantial kinetic energies. These electrons would therefore tend to

escape from the region rapidly, leaving behind the less-mobile ions that were a product of the ionization. The net result of this sequence of events would be the accumulation of net positive charge which would induce an increase in local plasma potential, i.e. in the height of the potential hill shown in Fig. 35. This potential hill would, in turn, provide the mechanism to accelerate electrons coming from the cathode, thereby enhancing the ion production rate further. It would also serve to accelerate ions both upstream and downstream of the peak potential (to the high energies observed using the RPA) and to decelerate electrons leaving the potential hill region. Both of these latter effects would tend to limit the height of the potential hill by limiting the net positive space charge there. The difference between the maximum and downstream potentials would determine the kinetic energy of the jet ions measured using the RPA.

The mechanistic description just outlined has also been proposed by others to describe potential hills observed at cathode emission spots [26], but it is not without flaws. For example, it does not include detailed mechanisms that would facilitate heating of the secondary electrons resulting from ionization events. If these electrons were not heated, they would become trapped and would neutralize the positive ion space charge that is an essential feature of the model. It appears that the only way this could be accomplished would be through elastic collisions between primary and secondary electrons.

Orifice Pressure Drop Considerations

The gas dynamic parameter used to correlate cathode interior pressure data in Figs. 33c and 34 appears to reflect the effects of

orifice diameter and flowrate properly. This suggests that simple gas dynamic phenomena determine the internal pressure at a given discharge current. These data also show that changes in discharge current induce changes in the internal pressure, and the mechanism by which this occurs is uncertain. Since the RPA data indicate high energy ions flow away from the cathode it is suggested that they also flow back toward it. As these ions flow through the orifice they could collide with the neutrals flowing forward and thereby induce a drag force. Such drag forces have been estimated by assuming the jet ions backflow through the orifice at the space-charge-limited current density level after having fallen from potentials associated with the jet ion energies measured in these experiments. The order of the forces computed in this way is sufficient to account for the observed pressure increase with discharge current. However, there are many other effects that could also contribute to or even dominate the observed pressure increases which need to be investigated. They include:

- gas dynamic losses related to heat addition,
- orifice wall friction,
- flow regime changes (e.g. from free molecular or transitional flow to continuum flow) and
- multiply charged ions (significant multiply-charged ion production is expected from primary electrons accelerated to the potentials associated with the energies of jet ions measured in these experiments).

V. CONCLUSIONS

High erosion rates observed on structures located downstream of hollow cathodes are caused by a divergent jet of high energy ions through the mechanism of sputter-erosion. The jet of ions originates at a small region located just downstream of the cathode orifice where high positive potentials are produced as a result of positive space charge accumulation induced by a high rate of ionization. This high rate of ionization is in turn a consequence of the high concentrations of neutral atoms and high energy electrons that are extracted through the cathode orifice.

The mean energy and energy spread of the jet ions both increase in approximately direct proportion to the electron discharge current being supplied from the cathode. A decrease in the cathode orifice diameter causes both of these energy parameters to increase. Reductions in the flowrate of propellant through the cathode below threshold levels associated with each cathode diameter also induces increases in the energies of the jet ions. Dramatic increases in the jet ion current density are induced by increases in discharge current above the 10 to 20 A range. The current density of these ions measured on centerline can be reduced by moving the keeper electrode closer to the cathode, but such movement may simply be inducing an azimuthal redistribution of the ions rather than any reduction in their production rate.

A well-collimated jet of high energy electrons also emanates from a small region close to the cathode orifice. This electron jet induces atomic excitation reactions that cause luminosity and make it visible. The electron jet trajectory is readily altered by changing the direction of a local magnetic field having a flux density that less than one gauss, but such field changes do not appear to alter the more divergent trajectories of the jet ions.

Most test results on which these conclusions are based were obtained in a 0.4 gauss transverse magnetic field environment using a hollow cathode equipped with a rolled tantalum foil insert. Changing test conditions to the axial magnetic field environments and impregnated inserts that are more typical of an ion thruster application do not alter these conclusions.

The temperature of the cathode wall increases with discharge current. Lower temperatures are best obtained by redesigning the cathode assembly to facilitate increased radiative and/or conductive heat transfer from it. The cathode wall temperature can also be reduced by increasing the cathode orifice diameter, but it is not affected significantly by altering the cathode flowrate.

Changes in the pressure measured within a hollow cathode that are induced by changes in propellant flowrate and orifice diameter can be described using traditional fluid mechanical models provided the effect of ion backflow through the cathode orifice is reflected in the flowrate.

REFERENCES

1. Rawlin, V.K. and W.R. Kerslake, "Durability of the SERT II Hollow Cathode and Future Applications of Hollow Cathodes," AIAA Paper 69-304, Williamsburg, VA, March 1969.
2. Williams, John D. and P.J. Wilbur, "Plasma Contacting--An Enabling Technology," AIAA Paper 89-0677, Reno, Nevada, January 1989.
3. Mirtich, M.J. and W.R. Kerslake, "Long Lifetime Hollow Cathodes for 30 cm Mercury Ion Thrusters," AIAA Paper 76-985, Key Biscayne, FL, Nov. 1976.
4. Siegfried, Daniel E., "A Phenomenological Model for Orificed Hollow Cathodes," NASA CR-168026, Dec. 1982.
5. Kerslake, W.R., Goldman, R., and Nieberding, R.G., "SERT II: Mission, Thruster Performance and In-Flight Thrust Measurements," J. Spacecraft and Rockets, v. 8, No. 3, pp. 213-224, 1971.
6. Siegfried, Daniel E., "Xenon and Argon Cathode Research," appears in NASA CR-168340, P.J. Wilbur, Ed., Jan. 1984, pp 76-121.
7. Rawlin, V.K., "Performance of Large Area Xenon Ion Thrusters for Orbit Transfer Missions," NASA TM 102049, JANNAF Propulsion Meeting, Cleveland, OH, May 1989.
8. Sponable, Jess M., Jay P. Penn, "Electric Propulsion for Orbit Transfer: A Case Study," J. Propulsion and Power, v. 5, No. 4, July-Aug. 1989, pp. 445-451
9. Rawlin, V.K., "Internal Erosion Rates for a 10 kW Xenon Ion Thruster," AIAA Paper 88-2912, Boston, Mass., July 1988.
10. Bechtel, R.T., G.E. Trump and E.J. James, "Results of the Mission Profile Life Test," AIAA Paper 82-1905, New Orleans, LA, Nov. 1982.
11. Collett, C.R. and R.L. Poeschel, "A 10,000 Hour Endurance Test of a 700 Series 30-cm Engineering Model Thruster," AIAA Paper 76-1019, Key Biscayne, FL, Nov. 1976.
12. Nakanishi, S. and R.C. Finke, "9700-Hour Durability Test of a Five Centimeter Diameter Ion Thruster," Journal of Spacecraft and Rockets, v. 11, No. 8, Aug. 1974, pp 560-566.
13. Brophy, J.R. and C.E. Garner, "Tests of High Current Hollow Cathodes for Ion Engines," AIAA Paper 88-2913, Boston, Mass., July 1988.

14. Zuccaro, D., "Mercury Vapor Hollow Cathode Component Studies," AIAA Paper, 73-1141, Lake Tahoe, Nevada, Nov. 1973.
15. Siegfried, D.S., Private Communication,
16. Friedly, V.J., "High Current Hollow Cathode Research," appears in NASA CR-182254, P.J. Wilbur, ed., Feb. 1989, pp 3-38.
17. Simpson, Arol J., "Design of Retarding Analyzers," The Review of Scientific Instruments, v. 32, No. 12, Dec. 1961, pp. 1283-1293.
18. Anderson, J.R., "A Fourier Series Technique for Differentiating Experimental Data," Appendix C in NASA CR-182254, P.J. Wilbur, ed., Feb. 1989, pp 67-79.
19. Collett, C.R. et al., "Thruster Endurance Test," NASA CR-135011, May 1976, pp. 156-179.
20. Anonymous, "Sputter Yield Data in the 100-600 eV Energy Range," General Mills Report 2309, July 15, 1962
21. Kaufman, H.R., "Technology of Electron-Bombardment Ion Thrusters," Advances in Electronics and Electron Physics, v. 36, L. Marton, ed., Academic Press, Inc., New York, 1974, p. 358.
22. Guyot, M. and Ch. Hollenstein, Experiments on potential gradients in a current-carrying plasma. I. Potential structures," Phys. Fluids, v. 26, No. 6, June 1983, pp. 1596-1605.
23. Gekelman, W. and R.L. Stenzel, "Ion Sound Turbulence in a Magnetoplasma," Phys. Fluids, v. 21, 1978, pp. 2014-2023.
24. Langmuir, I. , "The Interaction of Electron and Positive Ion Space Charges in Cathode Sheaths, " Phys. Rev., v. 33, No. 6, June 1929, pp. 954-989.
25. Williams, J.D. and P.J. Wilbur, "Ground-Based Tests of Hollow Cathode Plasma Contactors," Proceedings of the Third International Conference on Tethers in Space, San Francisco, May 1989, pp
26. Davis, William D. and H. Craig Miller, "Analysis of the Electrode Products Emitted by dc Arcs in a Vacuum Ambient," J. Appl. Phys., v. 40, No. 5, April 1969, pp. 2212-2221.

APPENDIX A

Analysis of Retarding Potential Analyzer Data

The current density, j , of charged particles that reach a planar surface with no retarding potential is given by

$$j = e \int_0^{\infty} \int_{-\infty}^{\infty} \int_{-\infty}^{\infty} v \, d^3n \quad (A1)$$

where e is the electronic charge and v is the charged particle velocity component normal to the probe. The velocity space differential volume d^3n is defined by

$$d^3n = f(u,v,w) \, du \, dv \, dw ; \quad (A2)$$

where $f(u,v,w)$ is the velocity distribution function for the particles and du , dv , and dw are differential velocities in the x , y and z directions, respectively. If the ion velocity is one dimensional, (the velocity in one direction is much greater than it is in the other two directions) the velocity distribution function $f(u, v, w)$ can be written

$$f(u,v,w) = \delta(u) f(v) \delta(w) \quad (A3)$$

where $\delta(u)$ and $\delta(w)$ describe particles that have zero velocity components in the directions perpendicular to the probe and $f(v)$

describes the velocity distribution normal to the probe surface. By definition, the total particle density n_t in physical space is given by

$$n_t = \int_0^{\infty} \int_{-\infty}^{\infty} \int_{-\infty}^{\infty} d^3n = \int_0^{\infty} \int_{-\infty}^{\infty} \int_{-\infty}^{\infty} \delta(u) f(v) \delta(w) du dw dv . \quad (\text{A4a})$$

Integration of Eq. A4a over u and w yields the following equation

$$n_t = \int_0^{\infty} f(v) dv . \quad (\text{A4b})$$

Substituting Eq. A3 into Eq. A2 and the putting this result into Eq. A1 yields

$$j = e \int_0^{\infty} \int_{-\infty}^{\infty} \int_{-\infty}^{\infty} v \delta(u) f(v) \delta(w) du dw dv ,$$

or

$$j = e \int_0^{\infty} v f(v) dv . \quad (\text{A5})$$

Frequently it is preferable to express the distribution of particles in terms of their energies ϵ (in eV) rather than their velocities. The energy distribution function $g(\epsilon)$ can be obtained by recognizing the kinetic energy of a charged particle is equal to the potential required to prevent it from reaching the probe. For the case being considered here the ions have a one-dimensional velocity so

$$e\epsilon = 1/2 mv^2 \quad (\text{A6})$$

where ϵ is the kinetic energy of the particle in units of eV, m is the particle mass and v is again the particle velocity. Solving Eq. A6 for v and then differentiating one obtains

$$dv = \sqrt{\frac{e}{2 m \epsilon}} d\epsilon \quad . \quad (A7)$$

Since by definition

$$dn = g(\epsilon) d\epsilon = f(v) dv \quad (A8)$$

one obtains

$$f(v) = g(\epsilon) \sqrt{\frac{2 m e}{e}} \quad (A9)$$

from Eqs. A7 and A8. Substituting Eqs. A6, A7, and A9 into Eq. A5 one obtains

$$j = e \int_0^{\infty} \sqrt{\frac{2 e \epsilon}{m}} g(\epsilon) d\epsilon \quad . \quad (A10)$$

The current density given by Eq. A10 is arriving at a surface with no retarding potential applied to it. If the the planar surface had a retarding potential ϕ applied to it, then only those particles with kinetic energy equal to or greater than ϕ would reach it and the current density to it would be given by

$$j = e \int_{\phi}^{\infty} \sqrt{\frac{2 e \epsilon}{m}} g(\epsilon) d\epsilon . \quad (\text{A11})$$

Differentiating Eq. A11 with respect to ϵ yields

$$\frac{dj}{d\epsilon} = -e \sqrt{\frac{2 e \epsilon}{m}} g(\epsilon) . \quad (\text{A12})$$

To get the energy distribution of the particles one must solve Eq. A12 for $g(\epsilon)$.

$$g(\epsilon) = - \frac{dj}{d\epsilon} \frac{1}{e} \sqrt{\frac{m}{2 e \epsilon}} \quad (\text{A13})$$

If the probe current (J) is given rather than the current density, then the energy distribution is given by

$$g(\epsilon) = - \frac{dJ}{d\epsilon} \frac{1}{e A} \sqrt{\frac{m}{2 e \epsilon}} \quad (\text{A14})$$

where A is the probe area, ϵ is the kinetic energy of the particle, m is the particle mass, and e is the electronic charge.

Equation A14 is valid for analysis of particles with a one dimensional velocity component normal to the probe surface. In applying it in this study it has been assumed that only singly-charged ions approach the probe. Also, the energy ϵ used in Eq. A14 is the kinetic energy the particles have at a reference potential (generally

the potential of the plasma at the probe) and thus the energy distribution given by it is that which would be measured in the plasma immediately adjacent to the probe.

